UNIVERSITY OF SOUTHAMPTON

FACULTY OF ENGINEERING AND PHYSICAL SCIENCE

National Centre for Advanced Tribology

Investigation of Ni-MoS_2 self-lubricating composite coating via electrodeposition as a potential alternative for Ni-PTFE coating

by

Nan Zhou

Thesis

for the degree of Master of Philosophy

Southampton, United Kingdom

February 2024

UNIVERSITY OF SOUTHAMPTON

ABSTRACT

FACULTY OF ENGINEERING AND PHYSICAL SCIENCE

National Centre for Advanced Tribology, nCATS

Thesis for the degree of Master of Philosophy

Investigation of Ni-MoS_2 self-lubricating composite coating via electrodeposition as a potential alternative for Ni-PTFE coating

by

Nan Zhou

Nickel-molybdenum disulphide (Ni-MoS_2) composite coating is studied in this work via electrodeposition from a Watts nickel bath as an alternative to the widely applied Nickel-Polytetrafluoroethylene (Ni-PTFE) coating for self-lubrication surface treatment. The toxicity of fluorinated surfactants involved in PTFE synthesis raises problems of severe long term environmental pollution and debilitating health issues resulting in adverse publicity and tougher industrial regulation. This study considers MoS_2 as an alternative solid lubricant, which is a naturally occurring material produced in more eco-friendly processes. Compared to inert PTFE particles, the hydrophobic and electrically conductive MoS_2 particles are found to induce the early onset of non-uniform coating growth which could result in extensive porous and rough surface features rather than a compact coating structure. This study is focused on the effects of electroplating process parameters on the composition, texture and the tribological performances of Ni-MoS_2 composite coatings. Due to varying tribology test conditions in reported COF values, the findings are compared against a Ni-PTFE coating produced under similar conditions in order to draw both quantitative and qualitative analysis on the self-lubrication performances of the Ni-MoS_2 coating. A dry COF as low as 0.07 is found for Ni-MoS_2 coating against steel in this work, which is superior to a value of 0.1 for the Ni-PTFE coating comparison and significantly lower than values of 0.2 – 0.4 reported in literature. The low COF of the Ni-MoS_2 coating against steel is attributed to following points:

1. Highly effective particle dispersion prior to the electroplating process via high-shear mixing resulting in narrow particle size distribution with mean diameters of 1 micron from the original 10 micron in magnetic stirring.

2. The addition of wetting surfactant CTAB to stabilise particle suspension before and during electroplating,

3. Low particle concentration in bath (1 – 2 g L^{-1}) and constant mechanical agitation during electroplating to avoid particle agglomeration on the coating surface,

4. The addition of the brightener Saccharin reduced surface roughness of the coating via grain refinement and levelling effect to produce a more compact composite coating structure.

Furthermore, a concept of gradient layer composite coating with increasing particle content towards the surface is investigated due to concern that a high solid lubricant content in the composite coating could compromise its mechanical property e.g., hardness, and adhesion, hence limiting the tribological performance. The Ni-MoS_2 composite coating is produced via stepped bath agitation speeds during one-hour electroplating and show enhanced load bearing capability with lower COF compared to a single layer coating with high particle content. The facile one-pot process with agitation control could be adapted for manual or automated industrial plating.

Although it show promise, the Ni-MoS_2 composite electrodeposition process in this study still provided challenges in achieving a fully compact and smooth structure while maintaining high particle content for low COF solid lubrication. Future R & D is proposed, based on findings in this work and the literature.

Keywords: composite coating, electrodeposition, tribology, nickel, molybdenum disulphide

Table of Contents

Table of Contents ..... **i**
List of Tables ..... **v**
List of Figures ..... **vii**
Declaration of authorship ..... **xv**
Acknowledgements ..... **xvii**
Definitions ..... **xix**
Abbreviations ..... **xx**
Chapter 1 Introduction **23**
1.1 Tribology and self-lubricating surface treatment 23
1.2 Self-lubricating coatings 23
1.3 Self-lubricating nickel composite coating using PTFE 24
1.4 Molybdenum disulphide as an alternative solid lubricant in self-lubricating nickel composite coating 25
1.5 Research aim and objectives 26
1.6 Outline of the research 26
1.7 Research highlights 27
Chapter 2 Literature review **28**
2.1 Overview of surface finishing industry in the UK 28
2.2 Electrodeposition for tribological applications 29
2.3 Electrodeposition from a Watts nickel bath 30
2.4 Composite electrodeposition of suspended particles into a metal matrix 33
2.4.1 Mechanism for the particle codeposition process 35
2.4.2 Particle material for nickel composite electrodeposition 40
2.4.3 Effect of particle bath concentrations 43
2.4.4 Effect of bath agitation 43
2.4.5 Effect of surfactant 45
2.4.6 Effect of current density 47
2.5 Solid lubricant materials and their tribological functions 48
2.5.1 Operating environment of solid lubricant 50
2.5.2 Mechanisms of solid lubrication 51
2.5.3 Self-lubricating coatings with solid lubricant material 52

2.6 Nickel based composite materials for solid lubrication 52

2.6.1 Ni-PTFE composite deposits by electro-codeposition 53

2.6.2 Ni-MoS_2 self-lubricating coatings by electrodeposition 57

2.6.3 Effect of tribology test parameter on Ni-MoS_2 friction coefficient ... 63

2.6.4 Summary for Ni-MoS_2 composite coating via electrodeposition..... 65

Chapter 3 Experimental Methodologies 67

3.1 Overview and approach 67

3.2 Modified Watts nickel bath for composite electrodeposition..... 68

3.3 Substrate preparation 70

3.4 Vickers hardness test 71

3.5 SEM and EDS analysis..... 72

3.6 Surface profiles by optical microscopy 74

3.7 Friction and Wear Test 75

Chapter 4 The effect of MoS_2 particles on electrodeposition of Ni-MoS_2 composite coating 77

4.1 Ni-MoS_2 composite growth as a function of electrodeposition time 77

4.2 Effect of current density on Ni-MoS_2 composite coating 79

4.3 Effect of wetting additive on Ni-MoS_2 composite coating 80

4.4 Particle conductivity and Ni-MoS_2 composite coating growth 82

Chapter 5 Process control of saccharin as a brightener 85

5.1 Effect of saccharin on coating composition and structure..... 85

5.2 Effect of saccharin on coating tribological performance 89

5.3 Summary and comments 92

Chapter 6 Process control of MoS_2 bath concentration 93

6.1 Effect of MoS_2 bath concentration on Ni-MoS_2 coating composition 93

6.2 Friction and wear of Ni-MoS_2 coatings..... 98

6.3 Effect of PTFE bath concentration on Ni – PTFE composite coating 105

6.4 Friction and wear of Ni-PTFE coating 108

6.5 Summary and comments 111

Chapter 7 Process control of bath agitation..... 113

7.1 Effect of bath agitation on Ni-MoS_2 coating composition and structure 113

7.2 Effect of bath agitation on friction and wear of Ni-MoS_2 coatings 117
7.3 Development of gradient composite deposits via agitation control 119
7.3.1 Gradient Ni-MoS_2 composite coating via agitation control 119

Chapter 8 Process control of MoS_2 Particle dispersion in bath preparation before electrodeposition 123

8.1 Introduction 123
8.1.1 Mechanism of high Shear mixing 125
8.2 Experimental details 126
8.3 Visual appearance of particle dispersions 127
8.4 Particle size distribution and zeta potential in dispersions 127
8.5 Structure and surface morphology of Ni-MoS_2 composite coatings 131
8.6 Non-lubricated wear tests of Ni-MoS_2 composite coatings 135
8.7 Comparison with Güler's study on Ni-MoS_2 coatings 138
8.8 Summary and comments 139

Chapter 9 Conclusions 140
Chapter 10 Future work 142
List of publications 143
List of References 144

List of Tables

Table 2.1 Typical Watts type bath composition and plating conditions 31

Table 2.2 Effect of particle conductivity on surface roughness for codeposited copper composites (current density 6 A dm^{-2}, particle concentration 60 g L^{-1}, stirring speed 600 rpm in an acid copper sulphate bath)[109].....41

Table 2.3 Typical solid lubricant and friction coefficient range[26] 48

Table 2.4 Common solid lubricants and environmental parameters for their application[161] 50

Table 2.5 Effect of particle types on microhardness of electroless Ni-P composite deposits.....55

Table 2.6 Effect of Al_2O_3/PTFE bath concentration ratio on friction and wear behaviour of composite deposits.....56

Table 2.7 Process parameters studied in the electrolytic codeposition of Ni-MoS_2 composite by Chang[171] 58

Table 2.8 Surfactant types and their effect on Ni-MoS_2 codeposition studied by Wang[172] 61

Table 3.1 Composition of the modified Watts nickel electrolyte 68

Table 3.2 Operational conditions used for electrodeposition.....69

Table 6.1 Effect of bath concentrations on wear depth of Ni-MoS_2 coatings by cross section profile 102

Table 7.1 Effect of bath agitation speed on wear depth (cross section profile) of Ni-MoS_2 deposits 118

Table 8.1 Summary of the Ni-MoS_2 composite coatings from literature.....124

List of Figures

Figure 2.1 Industry sector market value for surface coating in 2015[36] 28

Figure 2.2 Surface treatment process market share by value in 2015[36] 28

Figure 2.3 Schematic of a nickel electroplating cell 31

Figure 2.4 Influence of process parameters on deposit properties and performances 34

Figure 2.5 Schematic of a five-stage (1-5) process for particle transfer to cathode and incorporation into the metal matrix[83] 37

Figure 2.6 Adsorption isotherm of CTAB (crosses) and CTA^+ (circles) at the silica–aqueous interface[145] (b) CTAB molecule (c) SDS molecule 45

Figure 2.7 Lamellar molecular structure of MoS_2 and Graphite[162] 51

Figure 2.8 N-[3-(perfluorooctanesulfonamide)propyl]-N,N,N-trimethylammonium iodide molecular structure[163] 54

Figure 2.9 Contact angle images of Ni-PTFE composite deposits: (a) 28.0 vol%, (b) 47.4 vol%[163] 54

Figure 2.10 Effect of particle types on friction coefficient of electroless Ni-P composite deposits56

Figure 2.11 Effect of MoS_2 bath concentrations on porosity and friction of Ni-W-MoS_2 deposits[121] 60

Figure 2.12 Zeta potential of MoS_2 diagram after BAS surfactant addition[172] 61

Figure 2.13 SEM images of (a) pristine MoS_2 powder; (b) 5 wt.% Al_2O_3 coated MoS_2 powders[173]. 62

Figure 3.1 (a) cross-section and (b) top plan view of the electrodeposition set-up: 1) cathode, 2) anode, 3) Watts bath, 4) Water bath, 5) magnetic stir bar, 6) magnetic stirrer.69

Figure 3.2 (a) Precision saw, (b) Lapping machine, (c) Polishing plate 70

Figure 3.3 Vickers hardness indenter (Matsuzawa) 71

Figure 3.4 Scanning Electron Microscope (SEM, JEOL – JSM6500F) 73

Figure 3.5 Plate degasser, Edwards PD3 73

List of figures

Figure 3.6 Optical microscopy for surface profiles (Surface 3D profile)..... 74

Figure 3.7 TE – 77 Tribometer and schematic of the testing platform..... 75

Figure 4.1 Surface 3D morphology of Ni-MoS_2 composite coating after different duration of electrodeposition 77

Figure 4.2 Surface roughness measurement of Ni-MoS_2 coating as a function of deposition time78

Figure 4.3 SEM images of hull cell panel for Ni-MoS_2 electrodeposition at reference distances for varying current densities 79

Figure 4.4 Comparison of Ni-MoS_2 coatings from baths with / without wetting additive..... 80

Figure 4.5 Effect of CTAB addition on particle surface zetapotential in bath 81

Figure 4.6 Effect of wetting additive on MoS_2 particle codeposition (MoS_2 particle concentration in bath: 2 g L^{-1})..... 81

Figure 4.7 Ni-MoS_2 coating cross sections with changing MoS_2 bath concentrations..... 82

Figure 4.8 Ni-PTFE coating cross sections with varying PTFE contents..... 82

Figure 5.1 Effect of saccharin on Ni-MoS_2 composite coating surface roughness..... 85

Figure 5.2 Cross section and 3D morphology of Ni-MoS_2 composite coatings with different saccharin concentrations in bath..... 86

Figure 5.3 Effect of saccharin bath concentration on compact coating structure..... 86

Figure 5.4 SEM surface characterisation of Ni-MoS_2 coatings with changing saccharin concentrations in bath..... 87

Figure 5.5 Effect of saccharin bath concentration on particle content in Ni-MoS_2 coating 88

Figure 5.6 Coefficient of friction of Ni-MoS_2 composite coatings with saccharin concentration in bath at (a) 1 g L^{-1}, (b) 4 g L^{-1} and (c) 8 g L^{-1}. 89

Figure 5.7 Before and after wear: Surface 3D morphology of Ni-MoS_2 composite coatings with saccharin concentration in bath at (a) 1 g L^{-1}, (b) 4 g L^{-1} and (c) 8 g L^{-1}. 89

Figure 5.8 Effect of saccharin addition on coating composition and coefficient of friction for Ni-MoS_2 coatings with 2 g L^{-1} particle in bath..... 90

Figure 5.9 Effect of saccharin addition on coating composition and coefficient of friction for Ni-MoS_2 coatings with 1 g L^{-1} particle in bath..... 91

Figure 5.10 Effect of particle content and surface roughness on friction of Ni-MoS_2 coatings ..92

Figure 6.1 Effect of MoS_2 bath concentrations on MoS_2 content in composite deposits: (a) present results; (b) previous work by Yang *et al.*[186].....93

Figure 6.2 Effect of bath concentrations on MoS_2 content in the deposit.....94

Figure 6.3 (a, c, e) SEM scan and (b, d, f) surface profiles of Ni-MoS_2 deposits with MoS_2 bath concentrations indicated for bath agitation speed at 600 rpm.....95

Figure 6.4 Influence of MoS_2 bath concentrations on average roughness (Ra) of Ni-MoS_2 deposits 95

Figure 6.5 Ni-MoS_2 coating cross sections with various MoS_2 concentrations in bath 96

Figure 6.6 Compact film thickness for Ni-MoS_2 deposits 97

Figure 6.7 EDX mapping of a nodular structure on Ni-MoS_2 deposits 98

Figure 6.8 Effect of MoS_2 bath concentrations on wear and friction coefficient of Ni-MoS_2 deposit, Load 20 N, frequency 1 Hz.....99

Figure 6.9 SEM images of Ni-MoS_2 coating before (a,c) and after (b,d) wear ([MoS_2] 0.5 g L^{-1}, bath agitation speed at 200 rpm).....100

Figure 6.10 EDS mapping of Ni-MoS_2 deposit before and after wear 101

Figure 6.11 EDS elemental mapping on sample roller counterpart after wear test 101

Figure 6.12 Wear track corss section profile of Ni-MoS_2 deposits ([MoS_2] 0.5 g L^{-1}, bath agitaion 200 rpm). 102

Figure 6.13 SEM scans of Ni-MoS_2 deposits before/after wear (agitation apeed 400 rpm).....103

Figure 6.14 Friction coefficient of Ni-MoS_2 deposits with extended test times and corresponding surface profiles 104

Figure 6.15 Back scattered image of Ni-PTFE deposits with specified PTFE bath concentrations 105

Figure 6.16 Ni-PTFE deposit cross sections with PTFE 2 g L^{-1} (a), 4 g L^{-1} (b) and 7 g L^{-1} (c).106

Figure 6.17 Surface 3D reconstruction via optical microscope scan of Ni-PTFE deposits 106

Figure 6.18 Effect of PTFE bath concentrations on surface roughness 107

Figure 6.19 Effect of PTFE bath concentrations on hardness of Ni-PTFE deposits.....107

List of figures

Figure 6.20 Effect of PTFE bath concentrations on coefficient of friction (20 N load, 1 Hz) .. 108

Figure 6.21 BSE image of Ni-PTFE composite wear track with specified PTFE bath concentrations 109

Figure 6.22 BSE image for magnified view of Ni-PTFE deposit wear track details..... 109

Figure 6.23 SEM on wear of Ni-PTFE: (a) [PTFE] 1 g L^{-1} in bath and (b) [PTFE] 2 g L^{-1} in bath109

Figure 6.24 Effect of PTFE content in Ni-PTFE deposit on wear depth..... 110

Figure 7.1 Effect of agitation speed on MoS_2 content in composite coating, MoS_2 2 g/L 114

Figure 7.2 Cross section images of coatings from selected bath agitation rates..... 114

Figure 7.3 Effect of agitation speed on MoS_2 content (wt.%) in Ni-MoS_2 coatings, MoS_2 0.5 – 2 g/L 115

Figure 7.4 (a, c, e) SEM scan and (b, d, f) optical microscope scan of Ni- MoS_2 coating surfaces with MoS_2 bath concentrationsof 2.00 g L^{-1} for agitation speeds at 200 – 600 rpm. 116

Figure 7.5 Influence of agitation speed on the average roughness (Ra) of Ni-MoS_2 coating surfaces 116

Figure 7.6 Effect of bath agitation speed on the wear and friction coefficient of Ni-MoS_2 deposits with selected particle bath concentrations (20 N, 1Hz)..... 117

Figure 7.7 SEM scans of Ni-MoS_2 deposit before/after wear with baht agitation variations.... 118

Figure 7.8 Process control for stepped agitation rate during Ni-MoS_2 composite electrodeposition 119

Figure 7.9 EDS mapping and SEM for cross section of gradient and single layer Ni-MoS_2 deposit 120

Figure 7.10 Coefficient of friction of Ni-MoS_2 deposits in load ramp test (load 20 – 100 N, 1 Hz) 121

Figure 8.1. (a) SEM image of the as-received MoS_2 particles, (b) high-shear mixer blade, (c) arrangement for high-shear mixing 126

Figure 8.2. MoS_2 particle dispersion in deionised water (a) shortly after mixing, (b) 8 h after mixing..... 127

Figure 8.3. MoS_2 particle Z-average size as a function of: (a) high-shear mixing speed for 1 h, and (b) high-shear mixing time at 8000 rev min^{-1} compared with magnetic stirring at 2000 rev min^{-1}; (c) effect of mixing time on particle zetapotential measurement 129

Figure 8.4. MoS_2 particle-size distribution in deionised water after: (a) magnetic stirring, 2000 rev min^{-1}, 3 h, and (b) high-shear mixing,8000 rev min^{-1}, 3 h. 130

Figure 8.5. Examples of (a) pure nickel, (b) Ni-MoS_2 coating via particle dispersion from high-shear mixing (8000 rev min^{-1}, 3 h) and (c) Ni-MoS_2 coating via particle dispersion from magnetic stirring (2000 rev min^{-1}, 3 h).....131

Figure 8.6 XRD patterns of: (a) MoS_2 powder, (b) pure Ni coating, (c) Ni-MoS_2 composite coating from particle dispersion via high-shear mixing and (d) Ni-MoS2 composite coating from particle dispersion via magnetically stirring. 131

Figure 8.7 SEM and 3D optical images of (a), (b): Ni-MoS_2 coating via particle dispersion from high-shear mixing; (c), (d): Ni-MoS_2 coating via particle dispersion from magnetic stirring. 133

Figure 8.8 EDX mapping of (a), (b) and (c): Ni-MoS_2 coating via particle dispersion from high-shear mixing; (c), (d) and (e): Ni-MoS_2 coating from a bath involving particle dispersion by magnetic stirring.....133

Figure 8.9 Cross-sectional BEI images of coatings on mild steel substrates: (a) Watts nickel coating, (b) Ni-MoS_2 coating via particle dispersion from high-shear mixing and (c) Ni-MoS_2 coating from a bath in which particle dispersion is achieved by magnetic stirring. 134

Figure 8.10 Coefficient of friction as a function of test time for Ni-MoS_2 composite coatings. (20 N, 1 Hz) 135

Figure 8.11 Wear track cross-sectional depth profile of (a) Ni-MoS_2 coating via particle dispersion from magnetic stirring and (b) Ni-MoS_2 coating via particle dispersion from high-shear mixing. 136

Figure 8.12. 3D optical scans and SEM images of (a), (b) and (c): wear track of Ni-MoS_2 coating via particle dispersion from high-shear mixing; (c), (d) and (e): wear track of Ni-MoS_2 coating from a bath in which particle dispersion is achieved by magnetic stirring.....136

Declaration of authorship

Print name: Nan Zhou

Title: **Investigation of Ni-MoS_2 self-lubricating composite coating via electrodeposition as a potential alternative for Ni-PTFE coating**

I declare that this thesis and the work presented in it are my own and has been generated by me as the result of my own original research.

I confirm that:

1. This work is done wholly or mainly while in candidature for a research degree at this University;
2. Where any part of this thesis has previously been submitted for a degree or any other qualification at this University or any other institution, this has been clearly stated;
3. Where I have consulted the published work of others, this is always clearly attributed;
4. Where I have quoted from the work of others, the source is always given. With the exception of such quotations, this thesis is entirely my own work;
5. I have acknowledged all main sources of help;
6. Where the thesis is based on work done by myself jointly with others, I have made clear exactly what is done by others and what I have contributed myself;

Signed:

Date:

Acknowledgements

The work included in this report is carried out under the kind and generous guidance from Prof. Frank C. Walsh and Dr. Shuncai Wang. I would also like to give my sincere gratitude to everyone in Electrochemical Engineering Group and Materials Engineering Group who has provided help in various forms. Dr. Pawee Kucita has generously provided help with substrate manufacturing and instrumentation training for sample analysis. Dr. Luis Fernando Arenas Martinez gave support for induction and training in the chemistry laboratory. I must record the gigantic if not tireless effort by Dr. Shuncai Wang in training me on SEM. The MPhil study is funded by a scholarship from Faculty of Engineering and Chinese Scholarship Council.

Last, but not least, I would like to extend my warmest feelings to my family, who have always understood, encouraged and supported me to follow my passion and pursue my studies abroad.

Definitions

n	amount of material
K	constant
I	current
ρ	density (of the metal)
q	electrical charge
F	Faraday constant
H	indentation hardness of the material
M	molar mass
M^{z+}	soluble metal ion
z	stoichiometric electron number
A	surface area
t	time (of electroplating)
Q	wear rate (total volume removed per unit sliding distance)

Abbreviations

Al_2O_3	Aluminium Oxide
B_2O_3	Boron Oxide
$CdCl_2$	Cadmium Chloride
CNT	Carbon Nanotube
CeF_3	Cerium Fluoride
CTAB	Cetyltrimethylammonium Bromide
CVD	Chemical Vapour Deposition
Co	Cobalt
CV	constant voltage
CA	Contact Angle
Cu	Copper
DC	direct current
deg	degree
EDS	Energy Dispersive Spectroscopy
Au	Gold
h-BN	Hexagonal Boron Nitride
In	Indium
Pb	Lead
PbI_2	Lead iodide
MoS_2	Molybdenum Disulphide
MoO_3	Molybdenum Trioxide
Ni	Nickel
PC	Pulsed current

PVD	Physical Vapour Deposition
PEG	Polyethylene Glycol
PTFE	Polytetrafluoroethylene
PV	pulse voltage
RPV	reverse pulse voltage
rpm	Revolutions per minute
SEM	Scanning Electron Microscopy
SiC	Silicon Carbide
Ag	Silver
Ag_2SO_4	Silver sulphate
$Na_2B_4O_7$	Sodium borate
Sn	Tin
Ti	Titanium
TiO_2	Titanium Dioxide (Titanate)
WC	Tungsten Carbide
WS_2	Tungsten disulphide
UV	Ultraviolet
V_2O_5	Vanadium Oxide
ZnO	Zinc Oxide

Chapter 1 Introduction

1.1 Tribology and self-lubricating surface treatment

The word tribology is defined as "the science and technology of interacting surface in relative motion, and of associated subjects and particles[1]." Tribology covers the scope of lubrication, adhesion, friction and wear of surface engineering by exploring the details and mechanisms of surface interactions which may lead to improvements in given applications. Numerous engineering systems such as instruments, vehicles, aircrafts, machines and engines depend on the process of motion[2]. The mechanical components such as bearings, gears, cams, cylinders, seals, joints include elements that move against each other via sliding, rolling or combination of various motions. Contact between the surfaces may cause high friction force with excessive loss of energy. In addition, direct contact of surfaces in relative motion may lead to wear damages which causes rapid failure of the mechanical component. Hence lubrication is essential for successful and long-lasting operation of mechanical systems. High repair cost and lost productivity will take place without lubrication or with inadequate lubrication. The consequent loss from the economic and social perspective is in terms of billions of dollars per year[3].

Apart from traditional liquid oil lubrication where a lubricant is supplied to the system, there are increasing applications that seek specific self-lubrication surface treatment. This could help reduce wear and enhance part life where the liquid lubricant film could sometimes be starved, or where the challenging environment of high contact pressure, extreme temperature, high vacuum and other high-performance requirements become unattainable for oil lubrications[4,5,6]. Various self-lubricating surface treatments are available depending on the substrate and operating conditions[26], and the author summarised two main criteria for self-lubricating surface treatment:

1. Facilitating the use of substrate materials made practical with such a surface treatment.

2. Allowing demanding usage conditions requiring less wear and lower friction.

In tribological terms, the self-lubricating surface treatment is often marked by a low surface friction for successful "dry" operation in the absence of a liquid lubricant, and the wear resistance imparted to the treated component for lasting operation life.

1.2 Self-lubricating coatings

Coatings containing solid lubricant materials could intrinsically reduce friction and wear in case of extreme deprivation of external lubricant, or even without[7]. These coatings are of particular

importance in tribological protection especially for moving parts in mechanical systems and are referred to as self-lubricating coatings. Due to the variation in composition and material type in coating research, there is no universal standard for self-lubricating coatings. However, most research would involve the following achievements: first, the successful incorporation of solid lubricant material into a coating matrix to form a composite layer; second, the successful demonstration of friction and wear reduction compared to the pure matrix layer before introducing the solid lubrican[8-9]. The presence of solid lubricant in coating at a detectable amount is a prerequisite for successful self-lubricating coating. Extremely low solid lubricant content in coating could lead to insufficient self-lubrication and high wear especially in dry wear conditions[10]. The solid lubricant content can be further fine-tuned in the coating to achieve the optimum balance between friction and wear resistance for the appropriate tribological applications.

1.3 Self-lubricating nickel composite coating using PTFE

Nickel electrodeposition has been a long-standing surface treatment for wear protection, corrosion resistance and bright surface finish. It is highly versatile, widely applicable, low cost, easy to scale up and quick to process[7]. Nickel-Polytetrafluoroethylene (Ni-PTFE) composite coating via electrodeposition has seen successful applications spanning across a wide range of industries to improve friction reduction, corrosion resistance and wear properties, including textile guides, aerospace connectors, hydraulic pistons, automobile piston rings, valves, injection nozzles, carburettors and oil pumps[8–24], all of which are produced in large quantities globally with a substantial demand for self-lubricating surface treatment. PTFE is an excellent solid lubricant material with ultra-low friction (COF 0.05 – 0.1) and non-stick property that could be mass produced in controlled shape and size. The inclusion of PTFE micro/nano particles into electroplated nickel coatings offered the combination of low surface friction, strong bonding of nickel with substrate, wear resistance and long coating life, which in turn improved part performance and reduced cost or downtime for repair and service.

However, the worldwide industrial chemical processes used perfluorooctanoic acid (PFOA) as a surfactant in emulsion polymerization of fluoropolymers. This surfactant has been classified as a Group 2B carcinogen that has shown toxicity towards liver, hormonal development, and immune systems[25]. Due to its high solubility in water and exceptional stability resisting natural degradation, it has become a significant source of global water body pollution with long-lasting environmental impacts. Class-action lawsuits against unregulated discharge brought negative publicity to major manufacturers such as 3M and DuPont, which are followed by fundamental reforms in environmental regulations. Although the use of PFOA is being gradually phased out, other polyfluorinated surfactants which may bear equivalent toxicity are still being developed and used as alternatives due

to the ever-increasing production of PTFE for popular commercial demand. From an environmental perspective in sourcing eco-friendly materials for surface treatment, there is a drive to find an alternative solid lubricant material to replace PTFE in electrodeposited nickel composite coating.

1.4 Molybdenum disulphide as an alternative solid lubricant in self-lubricating nickel composite coating

Another widely known solid lubricant material is Molybdenum Disulphide (MoS_2), which show excellent self-lubricating properties and robustness in ambient atmosphere[26–35]. According to the International Molybdenum Association, MoS_2 can be found in molybdenite, a naturally occurring mineral ore mined industrially as a primary source for marketable molybdenum products. The processing route for Molybdenite involves crushing, grinding, flotation, and leaching to obtain Molybdenite concentrate, followed by further processing to separate the impurities, and achieve high purity MoS_2. Technical grade Mo Oxide could also be obtained via roasting Molybdenite concentrate to produce Molybdenum, which is widely used as an alloying component in steel. Due to the large reserves of Molybdenite mines and extensive global production capacity, MoS_2 can be obtained at relatively low cost while avoiding potential environmental impact from chemical processing routes for fluoropolymer synthesis. However, MoS_2 has been much less used than PTFE in commercial composite electrodeposition for self-lubricating coating. Apart from both showing solid lubrication, MoS_2 has some distinctive properties that distinguish itself from PTFE. In terms of electrical property, bulk MoS_2 presents semiconductor properties similar to silicon, making it a conductive material compared against the electrically insulating PTFE. In terms of molecular structure, MoS_2 has a layered structure with weak interlayer van der Waals interactions, whilst PTFE involves liner macro molecular chains with very low surface energy that slip easily against each other. In terms of particle shape and size, MoS_2 mainly consists of flakes that may appear similar to graphite, with wide size distribution that can be further separated by filter sieves, and PTFE micro/nano particles can be formed into perfect spherical shapes via emulsion polymerisation processes with particle size distribution controlled over a narrow range. These differences in properties will fundamentally affect the behaviour of MoS_2 compared to the trialled and proven commercial processes for PTFE in composite electrodeposition. Some properties of MoS_2 particle will pose significant challenges to control deposit structure and composition, which would critically influence the tribological performance of the coating.

This study will review the state-of-the-art research on Ni-MoS_2 composite electrodeposition for self-lubricating surface treatment, and further explore the mechanism and process controls for improving its tribological performance as a potential alternative to Ni-PTFE self-lubricating coating.

1.5 Research aim and objectives

The present study is intended to investigate process control strategies to improve the tribological performances of Ni-MoS_2 composite coatings.

The according research objectives are:

- To review the state-of-the-art of composite electrodeposition and related work on Ni-MoS_2 coatings.
- To identify challenges for Ni-MoS_2 composite electrodeposition.
- To examine the effect of major operational parameters on Ni-MoS_2 composite electrodeposition by characterising coating composition, structure and tribological performances.
- To analyse feasibility of Ni-MoS_2 composite coatings as an alternative candidate by comparing with benchmark Ni-PTFE.
- To explore potential of innovative processes for improved tribological performance of Ni-MoS_2 coating.

1.6 Outline of the research

Chapter 2 reviews fundamental mechanisms and applications of composite electrodeposition. The subsections provide further information on nickel based composite materials for self-lubricating applications and current state of the art, especially for the more traditional Ni-PTFE composite deposits as well as for the more recent Ni-MoS_2 composite deposits.

Chapter 3 describes the methodologies for composite deposit preparation, microstructural and surface characterisation, as well as tribological wear tests.

Chapter 4 presents initial observation of Ni-MoS_2 composite coatings and discusses the mechanism of its deposition process. Comparison with Ni-PTFE composite deposition are presented in order to highlight the effect of particle type on composite electrodeposition process. Challenges for electrodeposition with MoS_2 particles are listed.

Chapter 5 presents studies on saccharin as a brightener additive in modifying the morphology and composition of Ni-MoS_2 composite coatings. When coordinated with other deposition parameters, the addition of saccharin at suitable amounts will further improve the coating property as well as tribological performances.

Chapter 6 studies process control of MoS_2 particle concentration during electrodeposition. Instead of pursuing the highest particle content in coatings with high bath loading concentrations, lower concentrations in bath are studied in detail for suitable coating structure and tribological performance.

Chapter 7 studies the effect of bath agitation on coating morphology and composition. At suitable bath particle concentrations, controlled agitation could improve both particle content and refine surface morphology. In addition to single layer composite coatings via fixed agitation rates, a gradient layer composite coating is developed via stepped agitation rate as an example of process control for versatile coating structures with enhanced tribological performance.

Chapter 8 elaborates particle dispersion of hydrophobic MoS_2 particles in the aqueous plating bath. The performance of magnetic stirring and high shear mixing are compared to showcase the superior performance of the latter in breaking down particle agglomeration and stabilising particle suspensions in the presence of suitable surfactant additives. Successful particle dispersion is found to be a key prerequisite in composite electrodeposition.

Finally, conclusions and future work are presented in Chapter 9 and 10, followed by list of references and additional information.

1.7 Research highlights

Original findings and novel contributions in this study include:

- Like-for-like comparison between Ni-MoS_2 and Ni-PTFE composite coatings produced from similar deposition conditions for illustrative insight on particle type influence over deposit property.
- Systematic process control strategies for improved and innovative coating structures, showcasing a gradient composite coating from stepped bath agitation for improved load bearing performance.
- Novel application of higher shear mixing for effective nanoparticle dispersion in composite electrodeposition, and comparative studies questioning the practicality of magnetic stirring for nanoparticle dispersion.
- Expanding the application of additive saccharin from nanocrystalline grain refinement in pure metal deposition to microstructural morphology control in composite electrodeposition.

Chapter 2 Literature review

2.1 Overview of surface finishing industry in the UK

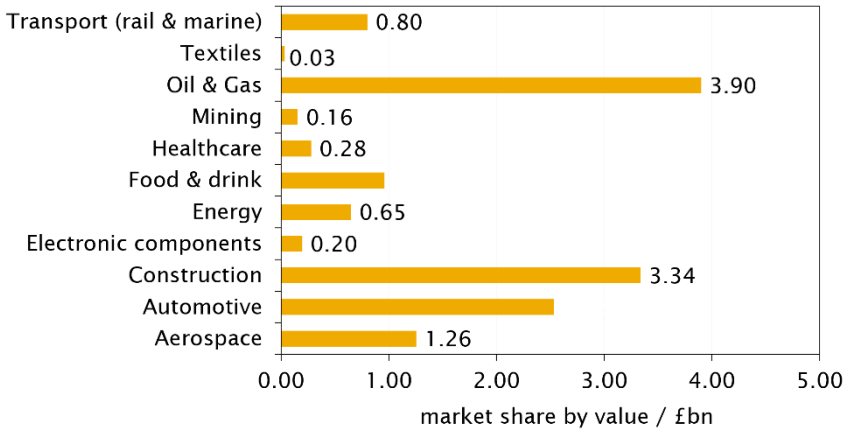

Figure 2.1 Industry sector market value for surface coating in 2015[36]

According to a research by the Institute of Materials Finishing (IMF)[36], the total sales from the manufacturing sector of UK is valued at £358bn in 2015, over 50% of which (£173bn) is estimated to have benefited from the surface coating industry, which generated £13.5bn (Figure 2.1) towards the country's economy. A wide range of manufacturing sectors require surface coating services for added value and performance of their products, which is dominated by oil & gas, construction, automobile and aerospace.

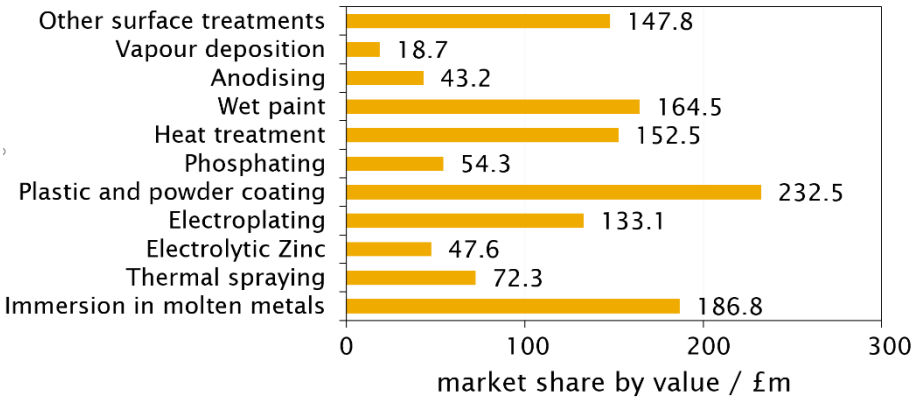

Figure 2.2 Surface treatment process market share by value in 2015[36]

While each industry may have its particular requirement for specific types of coatings, the surface finishing industry saw the use of over 40 different advanced engineering coatings, with a large percentage of coating processes involving electrochemical treatments, including but not limited to: anodising, electroplating and electrolytic Zinc (Figure 2.2). A growing industry in this field is composite electrodeposition, which could produce unique composite materials based on metals and metal alloys that could not be manufactured otherwise. The composite materials have been applied to the leading industrial sectors for corrosion protection, abrasive tooling, wear / friction control, electronics and electrical circuits, etc. The development of advanced engineering coating processes is expected to contribute more to the added value of UK's future manufacturing economy.

2.2 Electrodeposition for tribological applications

Electrodeposition or electroplating may be described as depositing metal coatings on conductive substrates by the action of an electric current. It is usually applied to enhance corrosion resistance, appearance, hardness, wear resistance and other physical or chemical properties of the substrate surfaces[37].

The reduction of soluble metal ions in most cases of electrochemical deposition is represented by

$$M^{z+}_{solution} + ze^- \rightarrow M_{lattice} \quad (2.1)$$

According to Faraday's Laws of electrolysis:

$$n = \frac{q}{zF} \quad (2.2)$$

n is the amount of material, q is the electrical charge passed, z is the stoichiometric electron number, and F is the Faraday constant.

From this, the thickness of the coating (x) can be derived from

$$x = \frac{M.I.t}{\rho.A.z.F} \quad (2.3)$$

M is the molar mass of the metal, I is the current, t is the time of electroplating, ρ is the density of the metal and A is the exposed area of the work-piece. The parameters for nickel in the above equations are all well known, which means that the average coating thickness of a pure nickel coating can be roughly estimated by calculation. This also means that the thickness of nickel coating can be easily

controlled given the current and time. Due to hydrogen evolution, current efficiency in electrodeposition can be less than 100%, which could be calculated by dividing the average coating thickness with the theoretical value of x from equation 2.3.

A wide election of metal and metal alloy deposits can be produced by electrodeposition. The advantages of electrodeposited coatings are:

i) The ease of metal coating formations at a relatively low temperature compared to the melting points of the metals deposited;

ii) The ease of coating thickness control within fractions of a micron;

iii) Fine structure and unique physical / chemical properties for specific applications;

iv) A rapid deposition rate compared to other techniques, especially vacuum deposition.

Empirical approach played a large part in the early development of the electroplating industry, but more scientific studies of the electrodeposition process are necessary due the increasing complexity for new bath chemistry and process control. From the industrial perspective, large-scale mechanized plants are often faced with stringent pollution controls which may affect the availability of some coating systems in certain areas. For example, the REACH regulation[38] has included chromium VI compounds for hexavalent chromium plating as carcinogenic (category 1A) and mutagenic (category 1B) substances that may expose those who work in the plating industry to serious health risks. Although chrome plating is highly effective for wear resistant, corrosion resistant and reflective surface finishing, such coatings within EU are effectively restricted unless special applications are accepted to gain authorization for continued. Search for chrome replacement is underway and although many coating systems have been studied[39], there has yet to be an alternative coating with all characteristics for chrome plating combined, namely high hardness, low-friction and anti-adhesive properties. Many chrome coatings are used in combination with nickel undercoats, which prompted research for chrome replacement coatings based on electroplated nickel.

2.3 Electrodeposition from a Watts nickel bath

During the electrolytic deposition of nickel, a nickel ion (Ni^{2+}) dissolved in the electrolyte obtains two electrons on cathode surface and is reduced to nickel metal, forming a deposit on the substrate. Nickel ions are replenished from anode dissolution which is usually made of nickel foil or sheet (Figure 2.3).

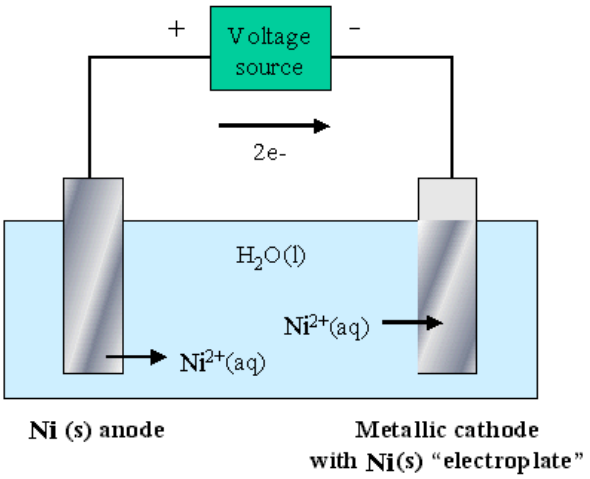

Figure 2.3 Schematic of a nickel electroplating cell

Introduction of Watts nickel bath in 1916 paved the way for rapid plating of ductile nickel at elevated bath temperatures with high anode and cathode efficiencies[40]. The Watts bath is especially suitable for laboratory studies due to its high throwing power from concentrated nickel ions dissolved in the solution, which allowed for the ability to achieve uniform coating thickness on substrates of irregular shapes in practical applications. Modern Watts type nickel plating bath is described in Table 2.1[37]:

Table 2.1 Typical Watts type bath composition and plating conditions

Chemical	Concentration in bath / g L^{-1}
Nickel sulphate heptahydrate, $NiSO_4 \cdot 7H_2O$	240 - 340
Nickel chloridehexahydrate, $NiCl_2 \cdot 6H_2O$	30 - 60
Boric acid, H_3BO_3	30 - 40
Temperature	45 - 65 °C
pH	1.5 – 4.5
Current density	2.5 – 10 A dm^{-2}

The major composition of the Watts bath is nickel sulphate [38-41], which is highly soluble in aqueous solutions and readily available commercially. As one of the least expensive nickel salts, nickel sulphate offers a stable anion that cannot be cathodically reduced or anodically oxidized. The cathode limiting current density depends on the nickel ion concentration of the bath. The large nickel sulphate concentration in the Watts bath is necessary to raise the cathode limiting current density and also to lower the resistivity, which improves distribution of the electrodeposite.

The addition of chloride ion is to improve the anode dissolution by reducing polarization[42]. Nickel chloride also helps increase bath conductivity and cathode efficiency, hence higher throwing power.

Boric acid serves as a weak acid buffer in controlling the pH of the Watts bath[43]. It is stable and non-volatile. Nickel deposits without the buffer tend to suffer from defects including cracking and pitting. Pure boric acid is readily available.

Concentrations of the Watts bath ingredients may be varied over certain ranges. The typical formula of the Watts bath is excellent for a cathode current density of 5 A dm^{-2} at a temperature of 50°C. Lower nickel salt concentrations may be used at a lower current density which could still offer excellent deposition. For current densities above 10 A dm^{-2}, it is usually necessary to increase chloride and sulphate ratio, bath agitation speed and temperature[44].

Other factors governing the properties of the nickel film are pH[45], temperature[46] and degree of agitation[47]. Throwing power, or metal distribution over the cathode, can be accurately studied with a Hull cell[48].

Bright nickel baths are mainly Watts type bath added with organic brighteners[49]. Extensive research has been carried out this field to eliminate the expensive process of polishing the dull nickel deposits[50,51]. Brighteners for nickel may fall into two major classes. Sulphonamides, sulphonamides, and aromatic sulphonic acids are designated class I nickel brighteners. Class I brighteners are usually used in high concentrations (1 – 10 g L^{-1}) without significant influence on the adhesion or limiting current density of the bath. They could also reduce the tensile stress in the nickel deposit, and with increasing concentrations induce compressive stress, thus preventing the formation of cracked, peeled plate due to its internal tensile stress[52,53]. Quantitative analysis of the stress in the plate can be carried out by measuring the extent of bending of a strip with nickel plated on one side, or with other configurations that are based on similar principles. Class II brighteners are usually used together with Class I brighteners to achieve a higher lustre[54–56]. The most effective class II brighteners are bath soluble, unsaturated organic compounds containing HC=O (formaldehyde), C=C (coumarin), C≡C, C=N (pyridine), C≡N (ethylene cyanohydrin) linkages. Class II brighteners are not used alone due to the excessive tensile stress and brittleness that could be induced in the plate. Bath pH and temperatures are found to affect the effectiveness of the brighteners, most of which function best at a

pH of about 3 – 5 and temperatures of about 50 - 65°C. Boric acid is the most widely used pH buffering agent for the application of brighteners. Brightener additives have been shown to affect the electrocrystallization of metal with preferential adsorption on the most active growing sites, thus inhibiting their growth which leads to a uniform surface texture. The use of class I and class II brighteners also provided a levelling effect for the nickel deposit which makes possible the filling in of scratches and micro-irregularities on the substrate surface, thus reducing the expensive cost of polishing or buffing procedures.

Wetting agents are used in nickel plating to prevent hydrogen bubbling on cathode surface that would cause pits in the deposit[57]. The function of the wetting agents is to reduce the surface tension between the liberated hydrogen, the electrolyte and cathode surface. Interfacial contact angle could be reduced to zero with the correct wetting agents and the hydrogen bubbles would disengage before they could grow in size to cause pitting by blocking the access to electrolyte on the plate surface. Anionic wetting agents such as sulphates of common primary alcohols in concentrations of 0.1 – 0.5 g L^{-1} have been used commercially in bright nickel-plating baths. The most common wetting agent of this class is sodium lauryl sulphate, which is found to have little adverse effect on the deposit[58].

2.4 Composite electrodeposition of suspended particles into a metal matrix

The practice of composite electrodeposition has evolved from unwanted plating defects due to insoluble bath impurities, to well controlled proprietary processes carried out in industrial scales today. It has been widely known since the beginning of plating practices that impurity particles left in the baths could be codeposited into the coating, affecting its finishing and property. The cause of impurity particles could be either contamination from the outside, corrosion of the plating equipment, breakdown of sacrificial anode materials or by-products from electrodeposition process. As a result, it is necessary to carry out bath maintenance including filtration to remove insoluble impurities so that the freshness of the bath could be maintained for consistent coating qualities[59]. However, as the demand for advanced applications pushed for performances beyond that of traditional metal deposits, attention is brought to inclusions deliberately chosen with special properties for tailored coating performances. Although alternative solutions may be available, the main drive behind composite electrodeposition is the relatively low cost of electrodeposition that could also be readily scaled up for commercial productions. Depending on the type of application, the function of the coating would likely be derived from the inclusions with the metal deposit acting as a binder, and the synergetic effect of deposit and inclusions would outperform a metal deposit without inclusions.

One of the earliest applications of composite electrodeposition is a copper/graphite coating for low friction application in automobile engines[60]. However, it is not until 1960s that composite electrodeposition underwent progressive development[61], receiving interests from automobile and aerospace industries. From 1970s to 1980s, more studies are carried out to produce coatings with marked improvements in mechanical strength, corrosion resistances and tribological performances[62–67]. The special properties of composite electrodeposits are continuously studied into 1990s, not only for the surface finishing industry, but also for developing novel materials including nanocrystalline microstructures for strengthened coatings[68,69], modified electrical conductance for electrical contacts[70,71], microporous hierarchical structures for electrocatalysis[72–74], special magnetisation properties for information storage devices[75], and ultra-hard abrasive composites for precision machining industry[76–79].

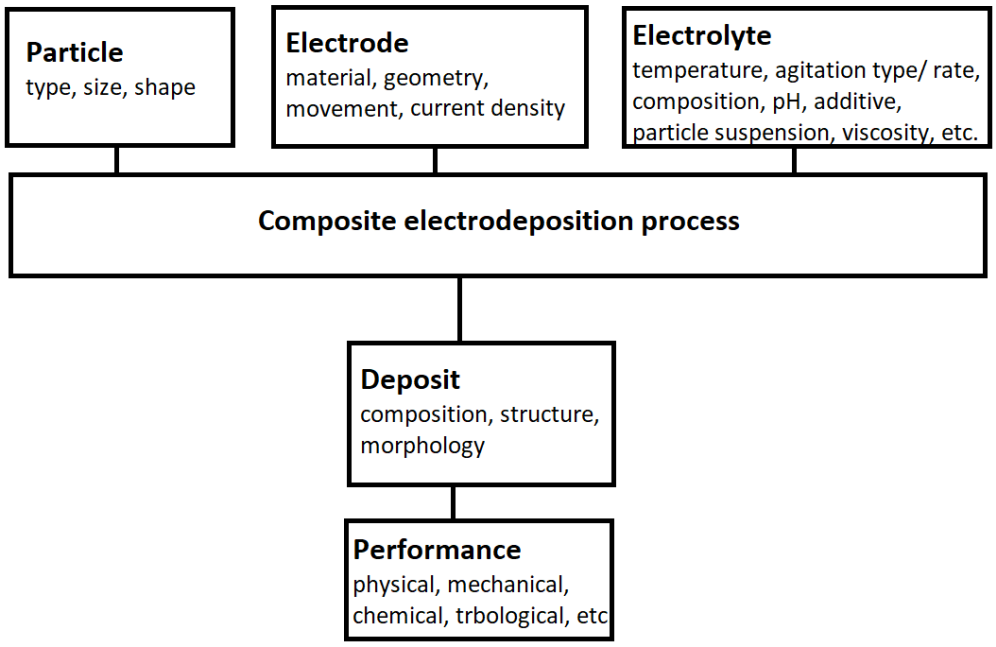

Figure 2.4 Influence of process parameters on deposit properties and performances

Chrome replacement coatings via composite electrodeposition has been pursued by industry since hexavalent Cr (VI) species received tighter restrictions due to legislative regulations and environmental concerns. Traditional function for tribology and corrosion protection is still the major focus of composite coating application, but new materials are also emerging for interests in novel properties. The number of publications on composite coating materials have increased exponentially, indicating that this field is receiving growing attention in spite of its roots originating from a more

traditional plating industry. A major reason behind the renewed interest in composite electrodeposition technique is that it offers facile and versatile ways to produce novel composite materials that could not be made otherwise. Development in new deposition methods as well as new materials opens up promising potentials of future applications. However, there still exists a gap between laboratory studies and industrial practices that need to be bridged. The meticulous process controls applied for consistent, optimised coating properties for large scale industrial production are less characterised or practiced by small scale laboratory studies. Many proprietary processes are not immediately available for non-commercial publications. The pursuit of novel composite coatings in both industry and laboratories may expand the boundaries of composite electrodeposition technology in both inclusion material and electrodeposition processes (Figure 2.4). More studies are addressing the future market demands, which is application driven and favours environmentally friendly manufacturing process, ease to apply and control deposition conditions, production economy, longer coating life with even higher performances.

2.4.1 Mechanism for the particle codeposition process

Many mathematical models have been proposed for the codeposition of particles with metals. Some important models on composite electrodeposition mechanism are summarised chronologically in table 2.4.1.

Guglielmi (1972)[80] first studied the codeposition of TiO_2 with Cu and SiC with Ni. Adsorption and electrophoresis are considered as the main mechanism for particle codeposition. The resulting model is able to explain the dependence of particle incorporation on current density and particle bath concentrations. Foster and Kariapper (1974) included the effect of hydrodynamics in their model, although quantitative studies to validate the model is limited due to the complex interrelationship between some of the factors[81]. Celis *et al.* modified the models based on two fundamental postulates: first, the particles are surrounded by an adsorbed layer of ionic species in the plating solution; second, incorporation of particles in the metal matrix requires the reduction of some of the adsorbed ionic species.[82]

It is interesting to note the diverse range of electrodeposition baths and particles used for model validation, showing the versatility of composite electrodeposition and the compatibility of some common governing principles for different processes. The effect of particle bath concentration, current density, and hydrodynamic conditions (agitation) received most attention for studies.

Particle concentration in the bath contributed to the effective particles present near the electrode surface during composite electrodeposition. Higher particle loading in bath will increase the chances

of particle collision with electrode for successful incorporation. The models describing particle concentration adopted classic adsorption isotherm theory to describe the non-linear dependence on particle concentration. This is assuming good particle suspension is maintained throughout electrodeposition and particles are evenly distributed over the electrode surface. Particle agglomeration may occur before or after achieving the saturation point, leading to non-uniform composite electrodeposition.

Current density is thought to affect the particle incorporation in following aeras: charged particle electrophoresis towards the electrode by the electric field, particle adsorption onto electrode surface with an interface electric field, and the rate of metal layer growth which incorporates adsorbed particles into the composite coating. Most studies applied fixed current density in their models, but there are emerging reports studying the effect of pulse current plating on composite electrodeposition which have received less analysis via modelling to explain the change in particle incorporation process.

Agitation not only affects the mass transport of metal ions which may affect the potential – current relationship for metal electrodeposition, it also helps to maintain a stable particle suspension in bath, distribute the particles evenly throughout the plating container and facilitate particle transport from bulk solution towards the electrode surface (and their removal). It is not mentioned in some early reports on mechanism but it received increasing attention in later reports and are also extensively controlled in industrial practices. Although composite electrodeposition can still be carried out with even zero agitation, provided the particle suspension in bath is extremely stable, such cases are rare and particles as a second phase tend to separate from bath suspension without suitable means of dispersion. It is important to note that particle dispersion before electroplating should be disguised from particle dispersion during electroplating, due to the fact that the former usually employs powerful turbulent high shear processes to break down particle agglomerates from a dry powder state and allow effective wetting to form stable suspension in the electrodeposition bath. Particle distribution in bath during electrodeposition is also vitally important, as the hydrodynamic conditions can either aid or inhibit particle incorporation with most studies employing laminar flow regimes via agitation for successful particle incorporation. Turbulent flows may reduce the concentration gradient layer thickness near cathode surface which is required for particle adsorption, it may also shorten particle dwell time on electrode surface and accelerate particle removal rate from surface, all of which would lead to a significant drop of particle incorporation rate when the agitation is increased beyond a suitable range.

In general, many studies adopted a process describing particle transfer from the bulk solution to cathode surface for incorporation, which is thought to proceed through five major stages[60] as illustrated in a widely cited review by Walsh *et al*. (Figure 2.5):

1. Particle surface charge formation via adsorbed ionic species (bath composition and particle type);

2. Movement of the particle by forced convection and electrophoretic migration towards the hydrodynamic boundary layer near cathode surface (bath agitation and particle surface charge);

3. Transport of the particle through the diffusion boundary layer (bath and particle concentration);

4. Adsorption of the particle through a potential gradient onto the cathode surface (particle surface charge and current density);

5. Physical incorporation of particles into the growing metal matrix via reduction of surrounding ionic species on particle surface (local bath flow regime, current density).

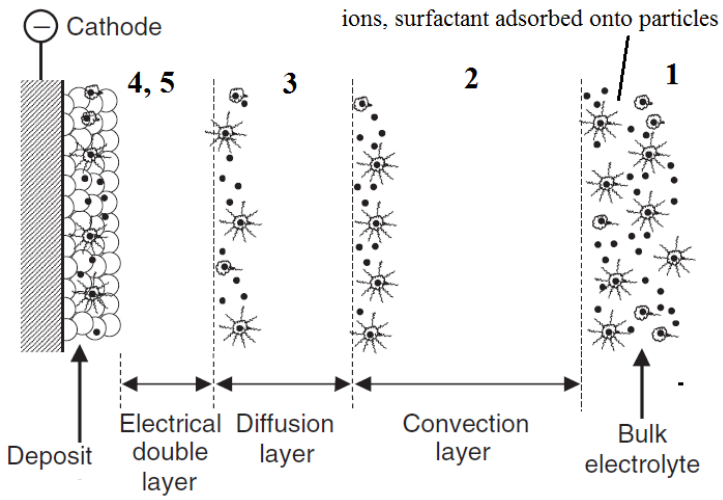

Figure 2.5 Schematic of a five-stage (1-5) process for particle transfer to cathode and incorporation into the metal matrix[83]

Compared with models for particle free electrodeposition which have more comprehensive and detailed mathematical approaches to describe the growth of the metal matrix, the composite electrodeposition is focused more on particle incorporation into the growing metal matrix and would introduce more approximations on factors affecting the particles by assuming more or less "ideal" conditions. For example, particle-electrolyte interactions are deliberately controlled by selecting and / or assuming "inert" particles, the definition of which are not always presented, but many would infer that the particle does not chemically degrade in the electrolyte, nor does it interfere with the electroplating process to form the metal matrix. Although widely adopted, the so-called inert particles would serve to reduce complexity of the scenarios by substantially simplifying the composite

electrodeposition process. All particles are considered a second phase in the plating bath system (the first being the electrolyte) and various degrees of solid-electrolyte interactions will ensue, followed by a deviation from standard electroplating processes in classic one phase systems. The major factors contributing to this are the adsorbed particles and species near the electrode surface presenting a very different picture from that of the pure metal electrodeposition. Surface tension, boundary layers, concentration gradient and electrolyte flow regime will all be altered in the presence of particles at high loading concentrations in the electrolyte.

Other process parameters for electrodeposition are also subjected to changing conditions in laboratory and industrial practices. For example, the form of agitation in bath will affect the hydrodynamic force on the particles, with rotating disc electrodes (RDEs) and rotating cylinder electrodes (RCEs) providing more uniform and quantitative convections than mechanical stirring in a beaker cell[83], with plane parallel electrodes, but these may not be suitable for large scale tank plating processes, which often employ propeller stirring, pumped circulation, aerating and flow eductors with or without flow baffles. Model validation may be limited to a narrow range of parameters for corresponding composite systems. Further improvements in the models, including the complex process parameters and interactive variables is a challenging task, while empirical laboratory trials remain essential in supporting such studies.

The early work on composite electrodeposition focused on popular metal/particle matrices (Ni/SiC, Ni/Al_2O_3, Co/SiC, Ni/PTFE)[80-82] for their practical applications and are followed closely by modelling work that are less sophisticated but successful in validating or rationalising experimental results. In this study, results will be compared with published models when MoS_2 particle behaviour during composite electrodeposition is considered. One major drawback of citing conventional models in this study lies in some very peculiar properties of MoS_2 particles, namely particle shape, hydrophobicity and conductivity. Flake like MoS_2 particles could lead to higher surface protrusions if positioned vertically onto the electrode surface. Hydrophobicity makes particle dispersion challenging without a suitable wetting aid to maintain a stable suspension, which can often be easily assumed but prove rather challenging in practice. Conductivity coupled with particle size and shape will alter electrodeposition on cathode surface under DC current and deviate from classic modelling assuming a uniform current distribution across the surface, especially when large particle inclusions are adsorbed. The challenges involving MoS_2 must be highlighted for these studies.

Table 2.4.1 Selected modelling studies on the mechanism of composite electrodeposition, adapted from Walsh et al[83].

Model	Proposed Mechanism	Solution (Particle)	Particle size, μm	Particle loading, g/L	Current density, A/dm^2	Agitation, rpm
N. Gugliemi (1972)	A two-step adsorption process for both ionic species adsorption onto particle surface and particle adsorption onto electrode. Considered particle concentration in bath and current density but did not include bath convection (mass transport)	Nickel sulphamate (TiO_2, SiC)	1 - 2	c.a. 3 - 30	2 - 10	N/a
J. P. Celis et al. (1987)	Assumes 5 stage process of particle codeposition: ionic cloud formation, convection, diffusion, adsorption and reduction. Mass transport is considered proportional for both ionic species and particles.	Acidic copper sulphate, Au cyanide (Al_2O_3)	0.05	20	2 - 10	400 - 600 (RDE)
J. Fransaer, et.al. (1992)	Proposed a trajectory model considering the effect of hydrodynamic forces acting on non-Brownian particles during codeposition on electrode.	Acidic copper sulphate (Polystyrene)	20	0.07 - 6.3	0.2 - 7.0	100 - 600 (RDE)
G. Maurin, et al. (1995)	Investigated the effect of hydrodynamic fluid flow on SiC incorporation into Watts nickel as a function of rotation rate, particle concentration, size and current density. A long chain polysaccharid surfactant is also found to increase SiC content.	Watts nickel (SiC)	0.1 - 10	10 - 100	1 - 20	200 - 1500 (RDE)
B. Hwang, et al. (1993)	Proposed a model describing silicon carbide codeposition rate with electrolytic cobalt determined by the reduction of H+ and Co^{2+} on particle. The effect of current density on primary reduction species is studied and validated with experiments.	Cobalt sulphate (SiC)	3	2 - 10	0.1 - 6.0	400 rpm (Magnetic stirrer)
P. Vereecken, et al. (2000)	Accounted for convective-diffusion involving the effect of gravitional force and hydrodynamic force on particle codeposition as a function of current density. Only valid for particle size no larger than the diffusion layer thickness.	Nickel sulphamate (Al_2O_3)	0.3	79	0.5 - 4.0	2500 - 2000 (RDE)
P. Bercot, et al. (2002)	Developed Guglielmi's model by introducing a corrective factor to describe the effect of adsorption and hydrodynamic forces on particle codeposition in relation with particle concentration and current density. Acknowledged the limit of magnetic stirring as an agitation method for foundamental studies.	Nickel sulphamate (PTFE)	<0.5	5 - 50	1 - 7	400 - 1000 (Magnetic stirrer)

2.4.2 Particle material for nickel composite electrodeposition

This study primarily concerns nickel for composite electrodeposition, which has been most widely studied due to the readily available nickel plating technology that can be easily converted for particle incorporation, which introduces new functionalities to the coating and build up on the corrosion resistance, wear resistance and mechanical durability imparted by nickel onto the treated parts. A wide range of particle materials have been selected for nickel composite deposits for different tribological or electrochemical functions. As mentioned in 2.4.1, most types of particles chosen for composite electroplating are regarded as "inert", which mainly involves physically incorporating particles into the growing nickel coating without inducing any chemical change to the particle surface or its surrounding electrolyte. The particle should also be relatively inert to the electric field applied in DC electrodeposition process, with most being non-conductive to ensure a uniform current density distribution for ease of coating thickness control, however exceptions have been made when non-uniform surface morphology is of less concern or even of benefit for specific applications, for example, using MoS_2, WS_2, Graphite particles in self-lubricating coatings with surface roughness for better oil retention, and conductive diamond particles for rough surface cutting edge in semiconductor wafer manufacturing process.

The functionality of many composite deposits arises from excellent tribological performances, including but not limited to wear resistance and lubrication. Composite deposits with hard ceramic particles such as diamond[84], *c*-BN[85], WC[86,87], SiC[88–95], Al_2O_3[96–100] and TiC[101–105] have been shown to exhibit improved wear resistance compared to pure metal deposits. For example, Ni-SiC composites have been reported with an increase of Vickers hardness to 700 Hv compared to 200 Hv of the original nickel deposit, as well as a reduction in the wear loss by four times in the composite deposit. The particle volume fraction is usually kept below 10 % to avoid brittle deposits[106]. The incorporation of hard particles into the metal matrix provided dispersion hardening or strengthening of the metal by blocking the movement of dislocations, resulting in increased resistance to deformation. Hard particles protruding out from the surface of the deposit may cause severe wear on the counterpart, hence extensive polishing and grinding may be required. Particle inclusions could also reduce the grain size of the metal matrix by increasing the presence of grain boundaries that reduces the dislocation motion. Composite deposits therefore saw increased yield strength compared to pure metal deposits.

The property and application of the deposits are influenced by the nature, size, shape, bath bath concentrations of the particles, and the choice of the nickel bath. For example, diamond powders in micrometre sizes have been codeposited with nickel for use in abrasive tools[107], while nickel deposits with diamond powders in nanometre sizes[108] could see improved lubrication, wear resistance and heat conductance for protective coatings on engines parts. Celis *et al.* studied the nickel composite deposits

containing micron and submicron SiC particles and concluded that the decrease in SiC particle size affected the wear of the composite in a positive way[106]. Large particles tend to be pulled out during wear and cause adverse abrasive wear. SiC particles of smaller sizes are also found to codeposit easier than large particles.

Surface morphology of the composite deposit is found to be influenced by particle type. A study on codeposition of copper with various particles[109] found that inclusion of inert particles, such as Al_2O_3, SiC have smooth deposit surface features, while codepostion of conductive MoS_2 particles and graphite particles significantly increased the surface roughness of the deposits (

Table 2.2). Similar work by others and in this report have found that semiconductive and conductive particles tend to induce surface nodular growth, which is caused by the adsorbed particle acting as a conductive high point attracting current density. This may give porous deposits with high surface areas that are desirable for catalyst systems, but are problematic for tribological applications which favour compact and smooth deposits.

Table 2.2 Effect of particle conductivity on surface roughness for codeposited copper composites (current density 6 A dm^{-2}, particle concentration 60 g L^{-1}, stirring speed 600 rpm in an acid copper sulphate bath)[109]

Particle type	Particle size / μm	Particle electrical resistivity[110,111] / Ω cm	Surface roughness / μm
Al_2O_3	0.3	$1x10^{17}$	4.42
SiC	2.3	$1x10^{8}$	7.27
MoS_2	6.1	$1x10^{4}$	26.6
Graphite	5.4	$1x10^{-7}$	72.7

Ni-SiC composites have also shown increased lubricant oil retaining abilities due to the micro roughness of the protruding SiC particles, which may lead to improved lubricated wear resistance than nickel. In addition, solid lubricant materials such as graphite[112,113], PTFE[114–118], MoS_2[119–121], WS_2[122,123] and *h*-BN[124–126] have been codeposited for composite deposits. The deposit hardness is decreased by the incorporation of such soft materials. The coating would slowly erode away during frictional contact and the incorporated lubricant material is released and smeared out over the surface. The weak

molecular bonding force in the solid lubricant materials allowed for the ease of shear and formation of tribofilms which would separate the counterparts and provide low coefficient of friction. Composite deposits containing microcapsules with lubricant oil have also been reported[127], which released the liquid lubricant instead of solid lubricant as the coating wear away. Friction coefficient of less than 0.1 is reported for self-lubricating composite deposits, compared to 0.6-0.8 for pure nickel.

The electrochemical functions of the composite deposits include corrosion resistance and catalysis. Composite deposits with SiO_2 particles[128] dispersed in bright or semi bright nickel baths may acquire a hazy and satin-like surface finish, which is desired for decorative purpose and for improved corrosion resistance with nickel-chromium plate for industrial and marine environments. Nickel composite deposits with particle dispersions could induce porosity in a thin chromium finish layer covering the surface, and the corrosion current density of nickel is reduced by forming numerous tiny chromium cathodes and nickel anodes. In contrast, smooth nickel plate covered with chromium finish suffered from severe corrosion pitting due to the relatively large chromium cathode area and a small nickel anode area. Single layer composite deposits of Ni and Al_2O_3[129], TiO_2[130], SiC[131,132], Cr_2O_3[133], and Si_3Ni_4[134] have shown improved corrosion resistance. The codeposition process is found to cause graining refining by changing the crystal growth of the nickel grains in the deposit. The presence of the inert particles may also provide passivation of the surface against the anodic current, reducing the corrosion rate of the deposit. Some other composites are also reported to have increased corrosion rate with higher particle contents. The corrosion resistance of the composite deposits is thought be mainly affected by the electrochemical activities of the particles, the change in microstructure of the metal deposit and the interaction on metal/particle interfaces.

Composite deposits could also be applied to electrodes with high surface area for catalytic processes. Electroactive materials in powder forms are codeposited into the metal matrix serving as the current collector. Ni-TiO_2[135], Ni-CeO_2[136] and Ni-$LaNiO_3$[137] composite deposits have been produced for hydrogen evolution catalysis and are found to be more catalytic than sintered or electrodeposited nickel. The improvement in catalytic performance is attributed to the synergic effect of incorporated particles with nickel (also a co-catalyst) as well as the increased surface areas in the electrodeposited composite material. Also mentioned in some studies are self-cleaning, water repelling surfaces produced by including hydrophobic particles into a microporous coating with hierarchical superficial structures.

The function of composite coatings could be further expanded by the use of novel inclusion materials. Nano silver particles codeposited in the chrome coating is reported to show antibacterial property for sanitary surface finishing. Innovative polymeric micelles with tailored hydrophilic / hydrophobic molecular structures could be readily stabilised in aqueous suspensions without the need of additional surfactant in composite deposition. The micelles could serve as molecule carriers for drug delivery

purposes, and their inclusion into a zinc deposit is also reported to enhance the corrosion resistance of the coating.

2.4.3 Effect of particle bath concentrations

Particle concentrations in bath and the final content in the deposit have been shown to follow a Langmuir isotherm adsorption phenomenon by Guglielmi[80], in which he proposed a two-step adsorption mechanism for the non-linear concentration dependence of particle content in Ni-TiO_2 composite coating from a sulfamate bath. The first step is physical in nature, in which the particles covered by ions and solvent molecules loosely adsorb onto the coating surface with limited interaction due to shielding, the second step is electrochemical in nature where the particles become stripped of the surrounding ions and molecules and strongly interact with the cathode to be incorporated into the growing metal matrix.

Particle content in deposits could be significantly increased by increasing particle concentrations in bath from low concentrations up to a saturation concentration, after which the particle content in deposit receives little or no increase despite further increasing its bath concentrations[19, 28, 80]. The saturation concentration depends on particle species, particle size and dispersion in bath, bath composition and agitation conditions. Particle bath concentrations could be controlled over a wide range to produce the varying particle content in functional deposits, from a few grams per litre in a very dilute bath to a few hundred grams per litre where a slurry of bath-particle mixture is formed. The optimum range of particle bath concentration must be carefully chosen for each specific application, with considerations also given to bath economy and ease of maintenance.

The operating range of particle concentration in bath varies by each particle/bath system but can be easily assessed by measuring the final particle content in coating against an increasing particle bath concentration from zero upwards. Once the coating achieves its maximum particle content, the particle bath concentration will also reach its upper limit. Moreover, the particle bath concentration range in a bath is not fixed, but also related to other operating conditions such as current density and agitation methods[176], which are set by the requirement for, e.g., plating speed and electroplating set-up in respective applications. When the other operating parameters are changed, the bath concentration may vary and can be reassessed by repeating the same method.

2.4.4 Effect of bath agitation

Before the initiation of electrodeposition, there is a major challenge to produce stable particle dispersions in baths, especially with the increase in use of nanoparticles which are more difficult to

disperse as compared to traditional micron sized particles. While mechanical agitation via magnetic stirrers is often applied in many academic studies due to its easy access, the effectiveness of such method is subjected to debate. Some literatures have quoted stirring for over 24 hrs in order to achieve desired dispersions[138], which is time-consuming and inconvenient. Particle dispersion in plating bath for industrial applications usually involves the use of industrial mixers[139] and or ultrasonication[140]. For delicate particles that are susceptible to damage by cavitation during sonicating, shear mixing is recommended as a non-destructive and scalable alternative[141]. Most effective micro/nano particle dispersions subject the particle/bath mixture to processes that generate highly localised intensive energy enough to breakdown the particle agglomeration from a microscopic scale. Intensive processes may be carried out just before the plating process to ensure fresh suspension stability and could even be incorporated into the plating process to ensure effective dispersion throughout.

During the electrodeposition process, agitation is required to provide particle suspension and effective mass transport for codesposition[60,83]. No agitation or weak agitations may cause particle agglomeration and sedimentation, resulting in inadequate deposit properties. In contrast, high speed agitation may cause violent turbulence in the electrolyte, and particle adsorption could be hindered by rapid particle removal due to hydrodynamic shear forces. Therefore, an optimum range of agitation is usually found for particle codeposition, usually provided by mechanical stirring, electrode rotation, air bubbling or flow pumping. The preferred method of agitation in laboratory studies may differ from industrial applications due to the design of electrode geometry and volume of the bath. Hence there is a need to characterise bath agitation during electrodeposition in the universal form of relative movement of electrolyte against cathode surface rather than reporting the operational parameters for each agitation method. Studies by Cobley *et al.*[126, 142,143] have also reported reviews and development on ultrasound assisted electrodeposition to achieve advanced composite deposits. In their work, ultrasonicators attached to the plating tank provided a combined ultrasound/mechanical agitation, which produced the most stable particle suspension for *h*-BN and WS_2 particles in a Watts nickel bath with smaller mean particle sizes compared to agitation by either method only[126]. Ni-WS_2 coatings produced under ultrasound/mechanical combined agitation show superior structural integrity compared to ones produced under mechanical agitation only, which suffered from excessive particle agglomeration. The ultrasonication could promote uniform particle dispersion and refine grain structure of the metal deposit, showing improved tribological properties[143]. Cobley's work is carried out in an additive-free bath, which reflected the benefit of ultrasonication in suspending hydrophobic materials in aqueous baths, although in their cases deposit of sludge WS_2 is still found for coating near the bath surface.

2.4.5 Effect of surfactant

Although stabilization of particle dispersion in additive-free suspensions can sometimes be achieved, more often surfactants are required for the aqueous nickel baths which may include cationic surfactant, anionic surfactant and non-ionic surfactants. One study on Ni-SiC composite deposition show that particle incorporation is improved by surfactant additions from 5 vol% to 54 vol%[144]. Another study found cetyltrimethylammonium bromide (CTAB) is effective in promoting SiC particle incorporation, but better particle suspensions are achieved with sodium dodecyl sulfate (SDS). Surfactant adsorption on particle surfaces promote the wettability of particles in the solution, and static or steric repulsions introduced by the surfactants help prevent particle agglomerations. Particles may acquire a surface charge in the electrolyte, and those containing positive surface charges are codeposited to a larger extent than those with neutral or negative surface charges during cathodic depositions. Electrophoresis migration towards cathode surface under the applied electric field is favoured by a positive surface charge, hence some common cationic surfactants are frequently used to modify the surface charge of particles for nickel composite deposits.

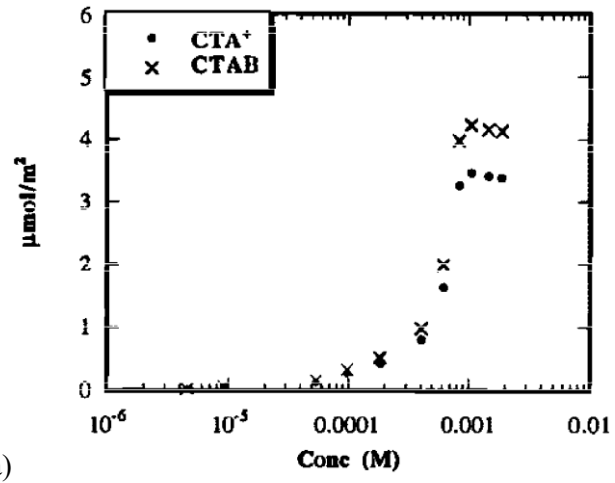

(a)

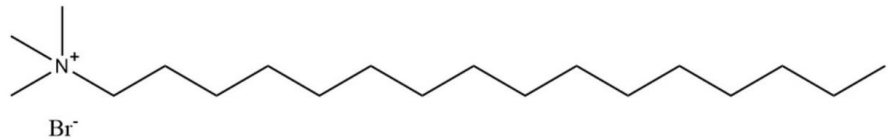

(b)

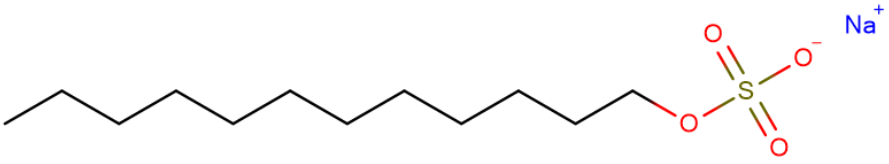

(c)

Figure 2.6 Adsorption isotherm of CTAB (crosses) and CTA^+ (circles) at the silica–aqueous interface[145] (b) CTAB molecule (c) SDS molecule

Atkin *et al.* studied surfactant adsorption at the solid-liquid interface and found that discrete surface aggregates are present in many surfactant-substrate systems instead of the simple monolayer or bilayer interpretation[145]. Adsorption is controlled by electrostatic and hydrophobic interactions between the surfactant and the substrate. For a given concentration of particles, the adsorption of surfactant onto particle surfaces first increases and then reaches a saturation point for increasing concentrations of the surfactant (Figure 2.6). Mechanisms are proposed to explain the adsorption isotherms.

For the codeposition of composite materials, the use of surfactants must be carefully monitored to control their influence on the nickel deposit, as some are known to alter the surface morphology and induce tensile stress in the deposit, which may lead to a defect finish. The choice of surfactant types is also very important, as various surfactant molecules may show different affinity to particles and hence different levels of particle dispersion capability. Studies on the use of CTAB and SDS on SiC and Al_2O_3 have shown that particle dispersion in bath is improved by increasing the surfactant concentrations in bath up to an optimum point, after which deposit degradation is observed due to excessive brittleness[146].

Surfactant concentrations in bath are usually kept at low levels to avoid poisoning of the deposit. The choice of surfactant types is also very important, as various surfactant molecules may show different affinity to particles and hence different levels of particle dispersion capability. For hydrophobic particles such as PTFE, MoS_2 and WS_2, a surfactant molecule with long hydrocarbon chain (Fig 2.3 b, c) is favoured due to its strong affinity with the particles, which will promote dispersion stability and require less surfactant concentration in bath. A cationic surfactant such as CTAB will also enhance particle adsorption via electrophoresis towards cathode during electrodeposition. Neutral or anionic surfactants have been less reported for such effects[171,172,187].

It is common practice for industry to develop proprietary surfactant formulations for optimised particle suspensions that could facilitate the ease of composite electrodeposition. The successful case of fluorocarbon surfactants developed by the chemical industry is particularly favoured for PTFE (Teflon) composite applications due to the ease in achieving stabilised bath suspension over traditional surfactants[147]. However, their strong chemical stability and affinity with bio-tissues led to long lasting water pollution affecting cattle and human life which is the centre of numerous lawsuits and significant industrial regulations[25]. The lesson being that the choice of surfactants should also bear in mind the iste disposal or treatment process and be as eco-friendly as possible when selecting surfactant candidates.

2.4.6 Effect of current density

In electrodeposition when a current is applied to drive the deposition of coating on the cathode surface, there exists an optimum current density range for suitable deposit qualities. This could be studied via plating in a hull-cell, which could offer both visual and metallographical comparison of coating quality by varying current densities on a single cathode panel placed at an angle to the anode. The principles in composite electrodeposition is likewise, regarding the influence of current density on particle content in the composite coating. For direct current (DC) electrodeposition of SiC particles, a maximum particle content in the coatings could be seen across a range of current densities studied[144]. This may vary depending on the bath composition, particle species, choice of surfactant as well as bath agitation.

Anodic deposition processes have been explored for novel composite coatings such as particle inclusions in Plasma Electrolytic Oxidation (PEO) deposits, contrary to traditional cathodic deposition. This type of coating is applicable to traditionally anodised workpieces such as aluminium magnesium and titanium alloy substrates[148–151]. A high current density is applied that could lead to plasma discharge in the electrolyte to for a thick and adherent ceramic layer over the substrate surface. Solid lubricant particle additions have been reported for PEO composite coatings to control dry sliding friction.

Other studies have also reported the effect of pulsed current (PC) rather than DC for controlled composite electrodeposition, some of these are covered in critical reviews[152,153]. By controlling cathodic / anodic current and current on / off time, the incorporated particle content could be increased, with additional benefit on refined metal deposit microstructure for enhanced deposit properties[154,155]. For industrial application, pulsed current electrodeposition is receiving growing attention with advancement in current control. However, current efficiency as well as coating deposition rate are still important factors to be considered for production economy and ease of process control. For example, pulse reverse current alternating between cathodic deposition and anodic dissolution are claimed to offer increased particle contents in the composite deposit. The introduced reverse current pulses would reduce current efficiency as well as deposition rate of the coating, making it slower and more costly than cathodically pulsed deposition or direct current deposition.

2.5 Solid lubricant materials and their tribological functions

Sloid lubricants have been in use for many decades to control friction and wear in a wide range of applications[26]. The most common solid lubricants include lamellar solids (e.g. MoS_2, WS_2, NbS_2, graphite, h-BN, boric acid), soft metals (e.g. Sn, Pb, Ag, In, Au, Ag, etc), organic polymers (e.g. PTFE, polyrthylene, polyimides, etc), diamond and diamond-like carbon films (DLC), oxides (e.g. MoO_3, V_2O_5, B_2O_3, etc), chlorides, fluorides or iodides (e.g. $CdCl_2$, CeF_3, PbI_2), borates (e.g. $Na_2B_4O_7$) and sulfates (e.g. Ag_2SO_4). Typical solid lubricant friction coefficients are listed in

Table 2.3.

Table 2.3 Typical solid lubricant and friction coefficient range[26]

Type	Examples and friction coefficients
Lamellar solids	MoS_2 (0.002-0.25), WS_2 (0.01-0.2), h-BN (0.15-0.7), graphite (0.07-0.5), boric acid (0.02-0.2)
Diamond and diamond like carbon (DLC)	Diamond (0.02-1), DLC (0.003-0.5)
Polymers	High density Polethylene (0.1-0.2) PTFE (0.04-0.15)
Soft metals	Ag (0.2-0.35), Pb (0.15-0.2), Au (0.2-0.3), In (0.15-0.25), Sn (0.2)
Oxides	B_2O_3 (0.15-0.6), Re_2O_7 (0.2) MoO_3 (0.2)

2.5.1 Operating environment of solid lubricant

Table 2.4 Common solid lubricants and environmental parameters for their application[161]

Type	Advantages	Disadvantages
Graphite	Low cost, mass produced, low friction, moisture tolerant.	Limited operating temperature ceiling at 300 K. Lower load carrying capacity compared to MoS_2.
MoS_2	Higher load carrying capacity than graphite and PTFE. Can operate in vacuum up to 1373 K.	Sensitive to moisture and oxidation in atmosphere.
PTFE	Chemically inert, moisture resistant, operate up to 523 K.	Low load carrying capacity. Limited to slow sliding applications, low thermal conductivity.
Soft metals	Low friction in both vacuum and atmosphere, Effective for rolling contact at temperatures up to 1273 K.	Ineffective against sliding contact.
Fluoride	Low frictions above 500 K up to 1600 K for extremely high temperature applications.	Ineffective at low temperatures below 500 K.

The wide range of friction coefficient of solid lubricants reported in

Table 2.3 results from the influence of the environment (Table 2.4). For example, the presence of humidity lowers the friction of certain solid lubricants such as graphite, h-BN, boric acid and DLC, due to the absorption of water molecules which further weakens the interlayer bonding between basal planes of the molecules. In inert atmosphere or in vacuum where there is a lack of water vapour, friction coefficient and wear rate of graphite are much higher than that in normal atmosphere. In

contrast, MoS_2 and WS_2 exhibit the lowest friction coefficient in vacuum. The presence of water may induce chemical degradation in these materials which leads to the formation of oxides and an increase in friction coefficient. Polymers such as PTFE are chemically inert, making them less susceptible to the influence of humidity and may provide excellent lubrication at extremely low temperatures. However, polymers may suffer severe degradation when exposed to high temperatures or radiations in space environment. On the other hand, oxides, fluorides and sulphates tend to soften at elevated temperatures, obtaining a favourable low shear property for solid lubrication.

2.5.2 Mechanisms of solid lubrication

The lubrication mechanism for solid lubricants depend on the molecular structure of the material[162]. For lamellar solids such as graphite and MoS_2, shear along the atomic plane could take place easily due to weak interlayer bonding by van der Waals force (Figure 2.7). For DLC coatings the main mechanism is thought to be interface slipping and smoothening. For soft metals and oxides, intrafilm flow and shear deformation are thought to be the low friction mechanism. For polymers such as PTFE, the low friction mechanism is related to the smooth molecular profiles and easy slip between macromolecules.

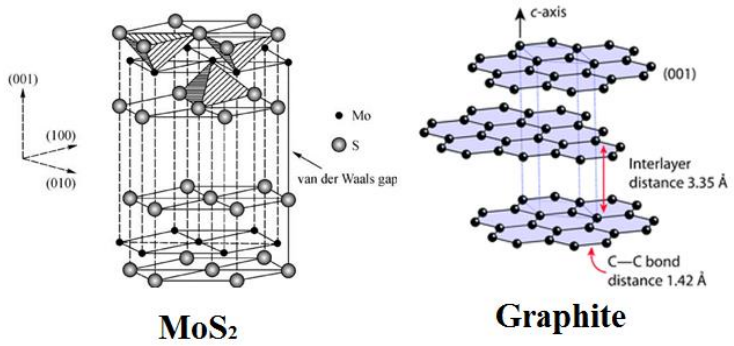

Figure 2.7 Lamellar molecular structure of MoS_2 and Graphite[162]

Solid lubricant can be easily transferred from the substrate to the wear counterpart, subsequent wear usually involves the shear between the transferred film and the lubricant film. A basic lubrication involves the shear of a very thin layer of solid lubricant under very high contact loads. The dynamic flow of the lubricant between the counterparts includes its build up before the contact area followed by its shear across the contact area and exit out of the contact area. The endurance life of the lubricant film could be improved by controlling the surface roughness of the substrate, which helps prevent

lateral flow of the lubricant away from the contact area and serves as a reservoir for controlled lubricant release.

2.5.3 Self-lubricating coatings with solid lubricant material

Over the past few decades, advance in thin film deposition technology has prompted the development of various self-lubricating films. Composites of graphite[112,113], MoS_2[170-179], PTFE[8-25] and h-BN[124,125] particles with nickel, copper, chromium and other metal coatings have been produced via electrolytic or electroless codeposition[22-30]. The metal deposits provided a tough matrix for excellent bonding with metal substrates and good thermal conductivity. The incorporated solid lubricant is slowly released onto the wear track and very low friction coefficient could be achieved, which also reduces wear damage on the metal matrix.

Advanced vacuum deposition techniques including physical vapour deposition (PVD) and chemical vapour deposition (CVD) have been used to produce thin films of solid lubricant materials (MoS_2, WS_2, DLC, etc.) with very dense morphology, strong bonding, preferred basal orientation, low residual stress and controlled stoichiometry[31-33]. In addition, doping or alloying of lubricant materials (e.g. MoS_2, WS_2, C) with other metallic ingredients (e.g. Ni, Au, Ag, Ti, Cr) have also been reported. By combining the solid lubricant with hard phases on a nanoscale, the doped coatings are far more durable and insensitive towards the environment than their monolithic analogues[34]. Multilayer, gradient and nano composite designs are also possible via such techniques for enhanced bonding, load bearing and multi-functional properties[35].

The drawbacks for vacuum deposition techniques are the complicated equipment set-ups, high vacuum and high temperature conditions in production, expensive cost, slow deposition rate, thin coating thickness and restriction on the substrate size due to limited vacuum chamber space. These have been partially resolved by recent advance in deposition techniques but may still persist due to the increasingly complex nature of the deposition processes.

2.6 Nickel based composite materials for solid lubrication

Self-lubricating composite materials based on nickel or nickel alloys and solid lubricant materials have been developed for various applications. Nickel based self-lubricating composite materials demonstrated thermal stability and excellent mechanical performances at high temperatures of up to 1000°C[156,157]. Therefore, they are of special interest for applications in advanced engine systems. Powder metallurgy and plasma spray techniques are used to produce bulk materials, which contained metal binders (Ni, Ni-Co, Ni-Cr, NiAl, Ni_3Al, etc.), solid lubricant (Ag, BaF_2, CaF_2, etc.) and

hardeners (Cr_2O_3, Cr_3C_2, WC, SiC, TiC, Cr, etc.)[158]. The choice of solid lubricant materials mainly involves soft metal and fluorides with thermal stability and low friction coefficient (0.2 – 0.4) at elevated temperatures. The use of MoS_2, WS_2, PTFE and graphite are limited for these applications due to their low oxidation temperatures or interaction with metal binder phase under the production conditions. In spite of its thermal stability, the use of h-BN in these materials is restricted by its poor wettability with molten metal binders during the sintering process. Oxide and carbide particles are used as hardeners for structural reinforcement and oxidation resistance.

Ni is also used as a dopant in co-sputtered Ni/MoS_2 composite films for aerospace applications where vacuum environment limits the use of liquid lubricants[159]. The range of friction coefficient for such composites is between 0.04 – 0.2, with the lower friction coefficients achieved at high load and high sliding speed. The presence of Ni dopant also decreased sensitivity of MoS_2 to humidity, making it more resistant to environmental contaminations during production and storage.

Electrodeposition is another convenient technique for the codeposition of solid lubricant materials (Graphite, MoS_2, WS_2, PTFE, h-BN, Microcapsules, etc.) and nickel based metallic matrixes (Ni, Ni-P, Ni-Co, Ni-W, etc.)[160]. Various techniques such as electrolytic deposition (DC, PC, brush plating) and electroless deposition are reported with extensive studies focusing on process parameters that control the solid lubricant content and microstructure of the composite deposits. Friction coefficient between 0.1 and 0.4 are reported, depending of the type of solid lubricant, its content in the deposit and testing conditions. Generally the friction coefficient is higher than vacuum deposited solid lubricants due the amorphous form of dispersed lubricant particles. However, electrodeposition is considered as a versatile and convenient method for producing nickel based self-lubricating composites under conditions close to the ambient environment. With the combination of hardener particles (Al_2O_3, SiC, etc.) and proper heat treatment the durability of such coatings could see significant improvement. Applications include anti-friction and anti-seizure coatings for bearing, gear and engine component in automobile and aerospace industry, non-stick mold release coatings in manufacturing industry.

2.6.1 Ni-PTFE composite deposits by electro-codeposition

PTFE is a non-conductive polymer material with low wettability, chemical inertness and low fiction coefficient. It has been widely used for anti-fouling, anti-stick and solid lubrication applications in industry. PTFE particles dispersed in a metal matrix could see significant improvement in terms of adhesion with substrate, wear resistance and heat conductivity compared to pure PTFE coatings.

A challenge for PTFE codeposition with metals is its high repellence against water, which limits its compatibility with aqueous electrolyte baths. Surfactants have been used for surface modifications of PTFE particles. Wang *et al.* [163] reported the use of N-[3-(perfluorooctanesulfonamide)propyl]-N,N, N-trimethylammonium iodide (Figure 2.8) as a surfactant for codepositing PTFE in a Watts nickel bath. The fluorocarbon chain on the hydrophobic end of the surfactant molecule facilitated its adsorption onto PTFE particle surface, while the ammonium cation on the hydrophilic end of the surfactant molecule is known to show good wettability with water.

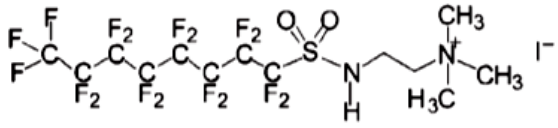

Figure 2.8 N-[3-(perfluorooctanesulfonamide)propyl]-N,N,N-trimethylammonium iodide molecular structure[163]

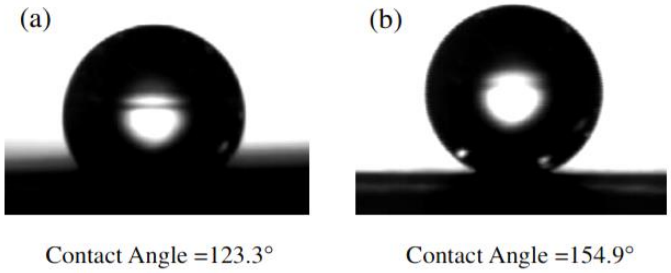

Figure 2.9 Contact angle images of Ni-PTFE composite deposits: (a) 28.0 vol%, (b) 47.4 vol%[163]

PTFE particles with a narrow particle size distribution between 0.2 – 0.4 μm is finely dispersed in bath at 2.5 – 37.5 g L^{-1}. Maximum PTFE content of 30 vol% and 47 vol% are achieved separately for current density of 5 A dm^{-2} and 10 A dm^{-2} with 25 g L^{-1} PTFE in bath, which are among the highest reported in literature. The surface smoothness of Ni-PTFE composite deposits is improved by the use of surfactant, which led to grain refinement by blocking preferential deposition sites during electrodeposition. Contact angle of water droplet on surface is reported to be 123.3° – 154.9° for PTFE 28.0 – 47.4 vol% in deposit (Figure 2.9). The use of surfactant is found to greatly facilitate PTFE dispersion in bath and its subsequent incorporation into the deposit. Ni-PTFE composite deposits with high PTFE content show hydrophobicity or even superhydrophobicity, which is due to the low wettability of PTFE particles.

Straffelini *et al.*[164] reported a friction coefficient of 0.07 for electroless Ni-P-PTFE composite deposits with PTFE 15 – 20 g L^{-1} in bath. The friction coefficient of pure electroless Ni–P deposit is reported to be 0.7 – 0.9 elsewhere. Solid lubrication effect in atmosphere for PTFE is found to be superior to MoS_2 in electroless Ni-P composite deposits for similar particle concentration in the plating bath, although the author did not specify the incorporated particle content in each deposit.

Huang and Wu et al. studied the friction and wear of electroless Ni-P-PTFE and Ni-P-PTFE/SiC composite deposits165,166. The addition of PTFE is found to decrease the hardness of Ni-P matrix from 453 Hv to 340 Hv, while the addition of SiC (3.5 μm) is found to give a higher hardness of 530 Hv (

Table 2.5). Ni-PTFE-SiC is observed to have a moderated hardness of 453, which is due to a combination of PTFE softening effect and SiC reinforcement. All composite deposits saw increased hardness after heat treatment at 400 °C, with Ni-P-PTFE gaining a slight increase by 23%, and Ni-P-SiC gaining the largest increase by 157%.

Table 2.5 Effect of particle types on microhardness of electroless Ni-P composite deposits

Main properties of EN and EN-composites

	Microhardness (HV50)	
	As-plated	Heat-treated
EN	453	956
EN–PTFE	340	421
EN–SiC	530	1365
EN–PTFE–SiC	450	701

Composite deposits containing PTFE saw a significant reduction of friction coefficient by over 70 % from Ni-P electroless deposits. Ni-P-PTFE and Ni-P-PTFE-SiC composite deposits both show friction coefficient of around 0.2, with higher wear resistance and longer endurance life found for Ni-P-PTFE-SiC composite deposits. The presence of SiC particles provided dispersion hardening in the hybrid composite deposit, which increased the load bearing capacity and reduced the wear rate under high load (Figure 2.10).

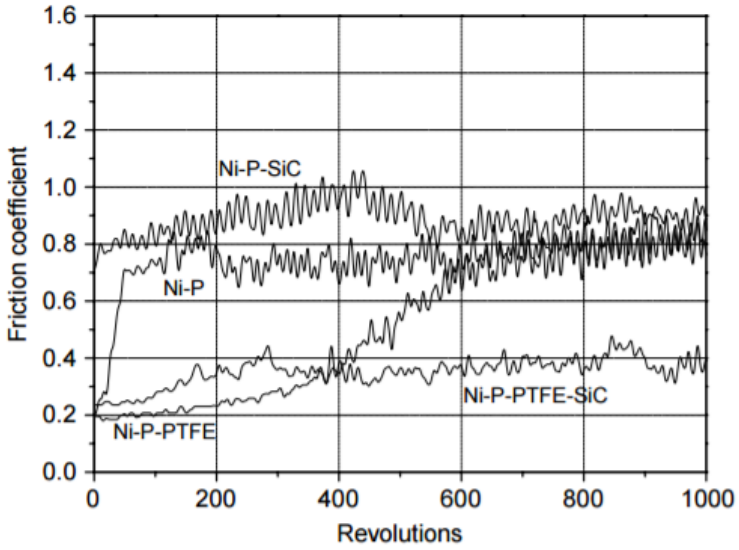

Figure 2.10 Effect of particle types on friction coefficient of electroless Ni-P composite deposits

Cheng reported the synthesis of Ni-P-PTFE-Al2O3 nano-composite deposits by electroless deposition167. The addition of nano-Al2O3 particles (50 nm) is found to increase the wear resistance by up to 40% and reduce the friction coefficient by up to 30% compared to Ni-P-PTFE composite deposits. However, when Al2O3/PTFE bath concentration ratio exceeded 1:3, the friction coefficient of the hybrid deposits is increased with higher wear loss during the wear test (

Table 2.6). Tang et al.168 also observed a similar trend for Ni-PTFE-Al2O3 nano-composite deposits by electrolytic codeposition in anhydrous ethanol with MgCl2•7H2O as the dielectric media. Both reports have shown that the strengthening effect of Al2O3 particles could be achieved for an optimum Al2O3/PTFE ratio, beyond which the aniti-friction property is reduced by excess amount of Al2O3 particles, and a negative effect on the overall wear resistance of the deposit will be induced.

Table 2.6 Effect of Al_2O_3/PTFE bath concentration ratio on friction and wear behaviour of composite deposits

Sample No	Additive content of nano-Al_2O_3/(g/L)	Additive content of PTFE emulsion/(mL/L)	Wear loss/(mg)	Friction coefficient
1	1	15	19.7	0.24
2	2	12	14.6	0.19
3	3	10	12.0	0.17
4	4	8	16.5	0.22
5	5	5	18.3	0.27

Moreover, the improvement in tribological performance is more significant by using nano sized Al_2O_3 particles compared with Ni-P-PTFE-SiC composite deposits using micro sized SiC particles[165] (4 μm) mentioned before. Particle of smaller sizes could be uniformly distributed in the metal matrix with more particle-grain boundary interfaces which promotes the blockage of dislocation movement. An increase in the particle size not only prevented the incorporation of additional particles, but also increased the inter-particle distance and induced high abrasive wear on the wear track. The resulting increase in friction and wear may thus limit the effectiveness of deposit reinforcement for particle of large sizes.

Zhao *et al.*[169] reported a graded electroless Ni–P–PTFE composite deposit by using multiple baths with different ratios of cationic surfactant ($C_{20}H_{20}F_{23}N_2O_4I$, FC-4) to PTFE particles. Single layer deposits with PTFE content over 30 vol% is found to have poor adhesion and heat conductivity for anti-fouling applications. The graded electroless Ni–P–PTFE composite deposit is found to exhibit excellent anti fouling ability when coated on a cylindrical stainless-steel heater rod, and no $CaSO_4$ scale is found after 1400 min flow boiling test.

In summary, it could be concluded that PTFE has great potential for anti-fouling and low friction applications. Although the water repellence of PTFE posed a challenge for studies on PTFE-metal composite deposits via electrodeposition, it could be resolved by adopting appropriate type and surfactant/PTFE ratio to enable effective particle dispersion in aqueous baths. Incorporated PTFE particles led to smooth surface features and decreased hardness of the metal deposit. Hybrid composite deposits with hard particles such as micro or nano sized SiC and Al_2O_3 may improve deposit wear resistance by dispersion strengthening, although important parameters such as particle size and hard/soft particle ratio must be carefully studied to achieve a positive synergetic effect. Multilayer or gradient layer structures could also be explored with tailored PTFE distribution in deposit for desired surface features and tribological performance.

2.6.2 Ni-MoS_2 self-lubricating coatings by electrodeposition

Ghouse *et al.* (1980)[170] carried out some early studies on codeposition of Ni-MoS_2 composite deposits. Conventional electro-codeposition (CECD) and sediment codeposition (SCD) techniques are used for sample fabrications. Particle contents for deposits obtained via SCD under same conditions increased by almost 50 % compared to CECD deposits. The SCD deposits also show more uniform morphology with less porosity. The optimum MoS_2 content in deposit for lowest coefficient of friction is found to be abound 12 vol%. In comparison, this research finds that of 8 – 10 wt% MoS_2 in the nickel composite coating produced the best wear and friction reduction performance, which agrees with the finding that a detectable amount of MoS_2 in the coating is a prerequisite for successful self-lubrication. Increasing the load of a rotating disc counterpart (30 mm in diameter, thickness 5 mm)

from 1.5 N to 6.0 N (contact pressure 2.1 kPa to 8.5 kPa) could decrease the friction coefficient from 0.4 to 0.2. Under higher contact pressure, the MoS_2 intermolecular planes are more easily sheared hence the enhanced anti-friction performance measured in tribological tests. MoS_2 is found to be a superior solid lubricant compared to graphite, and the addition of lubricant oil further loared the friction coefficient.

Chang *et al.*[171] studied the electrolytic codeposition of Ni-MoS_2 composite in a Watts nickel bath ($NiSO_4$•$7H_2O$, 310 g L^{-1}; $NiCl_2$•$6H_2O$, 50 g L^{-1}; and H_3BO_3, 40 g L^{-1}). The effect of process parameters such as MoS_2 bath concentrations, current density, bath temperature, pH and agitation rate are studied by a fractional factorial design of screening experiments (Table 2.7). The MoS_2 particles are blended with a wetting agent (sodium lauryl sulfate, SLS, 0.4 g / g MoS_2) to obtain uniform dispersion. The weight percentage of MoS_2 in the deposits is found to be influenced by all factors mentioned. At lower current densities (1 - 2 A dm^{-2}) the codeposition of MoS_2 could be described by Guglielmi's kinetic model but not at high current densities, suggesting a different mechanism. The nickel deposition efficiency is also found to be loared by the presence of MoS_2. The current research found out that accelerated nickel dendrite growth is found in the vicinity of adsorbed MoS_2 particles, which could contribute to the change in composite codeposition mechanism because of MoS_2 particle's electrical conductivity. It has also been thought that the presence of MoS_2 could lower the H^+ reduction potential in the acidic plating bath and lead to more hydrogen evolution which lowers the deposition efficiency.

Chang's study is limited by the small number of samples for each factor (no more than 3) and no conclusive results are discussed. Other important factors such as surface morphology and friction behaviour of the deposit are also not mentioned. No tribological tests are performed in Chang's report.

Table 2.7 Process parameters studied in the electrolytic codeposition of Ni-MoS_2 composite by Chang[171]

Factor	Level 1	Level 2	Level 3	Unit
A: current density	100	200	400	A/m^2
B: rotation rate	500	1000	1500	r.p.m.
C: particle concentration	10	25	50	kg/m^3
D: pH	0.5	2.0	4.0	
F: temperature	298	313	328	K

Cardinal *et al.*[121] studied nanostructured Ni–W–MoS_2 composite deposits prepared by reverse pulse current plating. Wetting agent SLS at 0.1 g L^{-1} is used. MoS_2 particle bath concentrations is varied

from 0 – 2 g L^{-1}. The hardness of Ni-W-MoS_2 composite decreased from 650 Hv to 33 Hv when MoS_2 bath concentrations increased from 0 to 2 g L^{-1}. The matrix softening effect is accompanied by the formation of a porous, sponge-like deposit structure especially at MoS_2 concentration of over 1 g L^{-1}, which is considered to introduce a great error for the hardness measurement by author. This has been previously shown in copper-MoS_2 deposits and is attributed to the conductive nature of MoS_2 particles which accelerated nodular growth of metal deposits on the adsorbed particle surfaces. Friction tests are carried on a pin-on-disc tribometer (stainless steel ball of 6 mm diameter, load 6 N, contact pressure 0.51 GPa), and the incorporation of MoS_2 decreased the friction coefficient by 50 % from 0.27 (Ni-W) to 0.14 (Ni-W-MoS_2). However, low wear resistance and poor coating adhesion are found for deposits with high MoS_2 concentrations (1 and 2 g L^{-1}) as a result of their porous, inhomogeneous surface morphology (Figure 2.11). The results are found to agree with the current research in that the presence of MoS_2 particles at over 1 g L^{-1} in bath (wetted with a surfactant) could significantly alter the structure of electrodeposited nickel coatings, namely increased porosity, and dendritic nickel growth. In comparison, non-conductive particles such as PTFE led to a compact and porosity free cross section of the composite coating. It is a common issue for electrically conductive particles such as MoS_2 to affect the electroplating process and care should be taken to mitigate this effect, especially for tribological applications.

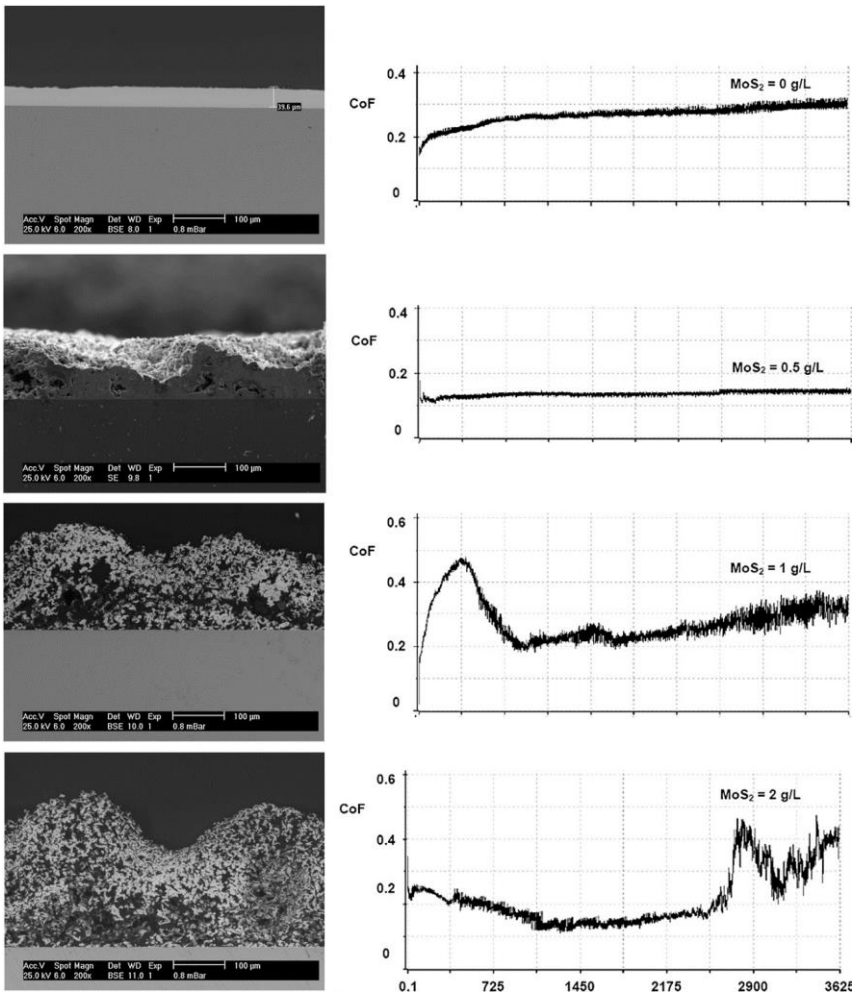

Figure 2.11 Effect of MoS_2 bath concentrations on porosity and friction of Ni-W-MoS_2 deposits[121]

Shi et al.119 reported a Ni-Co-MoS2 composite deposit with 1 g L-1 of nano sized MoS2 in the plating bath and a proper amount of SLS as wetting agent. The composite deposit is tested on a tribometer with a ball-on-disc configuration (SAE52100 steel ball, Ø 3 mm). It is found to have much smaller friction coefficient and lower wear rate than the Ni-Co coating. The friction coefficient further decreased from 0.4 – 0.5 for pure Ni-Co to 0.15 – 0.22 for Ni-Co-nano MoS2, when the load is increased from 1.0 N to 4.0 N (contact pressure 0.44 – 0.7 GPa). Higher wear rate is found for high loads. Wear track analysis revealed severe adhesion, scuffing, plastic deformation and large wear debris for samples tested at high loads (4 N), while smooth wear track with slight deformation and scuffing is found for samples tested at low load (1 N). The author concluded that the prepared Ni-Co-MoS2 coating is suitable for mild load tribological applications. The use of nano particles may reduce average particle size and lower the porosity in coating structure as reported by previous studies. The cross section of the composite coating is compact and porosity-free in the report. However, MoS2 content level in the composite coating could not be found in Shi's report. Wang172 studied process

parameters for MoS2 codeposition in a Watts nickel bath (NiSO4•7H2O, 330 g L-1; NiCl2•6H2O, 45 g L-1; and H3BO3, 40 g L-1) in addition with various types of surfactants added to 0.1 g g-1 MoS2 (

Table 2.8).

Table 2.8 Surfactant types and their effect on Ni-MoS_2 codeposition studied by Wang[172]

Surfactant	Commercial name	Codeposition adhesion to the substrate after wear test
Anionic	Stepanol (Ammonium Lauryl Sulfate)	Weak
	960SF (NH_4 P.O.E. Nonyl Phenyl Ether Sulfate)	Weak
	290MH_2 (Sodium Dialkyl Sulfosuccinate)	Weak
Cationic	960SN (Na P.O.E. Nonyl Phenyl Ether Sulfate)	Weak
	BAS (Benzyl Ammonium Salts)	Strong
Noionic	Ammonyx	Weak
	Ninol	Weak
Amphoteric	R2 (Lauryl Betain)	Weak
	L7 (Alkyl Tripolyoxyethylene Ammonium Hydroxide)	Weak
Operation condition: pH = 4, 4 A dm^{-2}, T = 45 °C, MoS_2 = 10 g L^{-1}, rpm = 1,500		

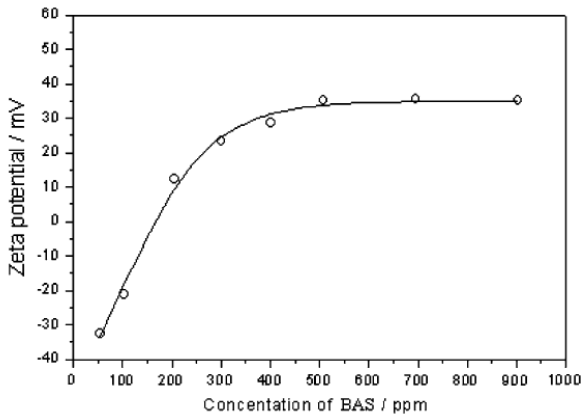

Figure 2.12 Zeta potential of MoS_2 diagram after BAS surfactant addition[172]

Cationic surfactant Benzyl Ammonium Salts (BAS) is found to increase the zeta potential of MoS_2 particles in bath which led to enhanced particle dispersion and incorporation into the composite deposit (Figure 2.12). BAS addition in bath is also found to affect the smoothness, uniformity and homogeneity of Ni-MoS_2 composite deposits in a positive way. The author proposed that BAS adsorption on conductive MoS_2 particles provided surface coverage and insulation which reduced the preferred nickel deposition on MoS_2 surfaces, hence less porosity and stronger adhesion for Ni-MoS_2

deposit could be obtained. Although the mechanism of surfactant action is not yet fully understood, the report pointed out the importance of surfactant addition to help control and modify the codeposition process for improved tribological performance. In the current research, another cationic surfactant similar to BAS, CTAB, is selected for MoS_2 codeposition and found to be effective in achieving high particle loading in coating at low particle concentrations in bath to avoid early particle agglomeration, which may render the bath ineffective.

Huang *et al.*[173] reported a Ni-MoS_2/Al_2O_3 composite deposit via electrolytic codeposition from a Watts nickel bath ($NiSO_4$•$7H_2O$, 330 g L^{-1}; $NiCl_2$•$6H_2O$, 10 g L^{-1}; and H_3BO_3, 40 g L^{-1}) with cetyltrimethylammonium bromide (CTAB, 50 mg L^{-1}) as a surfactant. $Al(NO_3)_3 \cdot 9H_2O$ is added to a suspension of MoS_2 particles in water followed by filtering and heat treating the MoS_2 particles to obtain a Al_2O_3 outer shell (Figure 2.13).

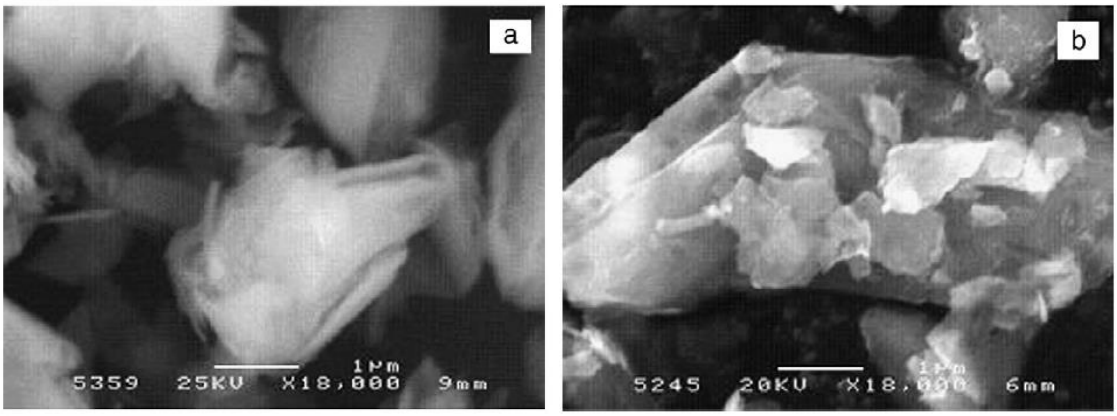

Figure 2.13 SEM images of (a) pristine MoS_2 powder; (b) 5 wt.% Al_2O_3 coated MoS_2 powders[173].

Deposits with the MoS_2/Al_2O_3 core-shell structured particles show higher hardness and much less porosity compared to Ni-MoS_2 composite deposits with similar particle content (vol%). The Al_2O_3 outer shell provided structural reinforcement and electrical insulation for MoS_2 particles, which resulted in enhanced uniformity and tribological performance of the hybrid composite deposits. It is also stated in the paper that wear resistance of Ni-Moly/Al_2O_3 deposit is improved over Ni-MoS_2 deposit with higher particle concentrations in bath. A drawback for this design is the lack of control for particle size distribution after the hydrothermal treatment. MoS_2/Al_2O_3 core-shell structured particles seemed to be three times larger in size than pure MoS_2 particles, which is probably due to agglomeration during the hydrothermal reaction. Compared to Ni-MoS_2 coating, Ni- MoS_2/Al_2O_3 coating show slightly higher friction coefficient (10 – 15%) but lower wear (by 20%), which is attributed to the higher hardness of the latter. Particle content level in the coating is 5 -11 vol%. The

tribological test is carried out against a ceramic ball with contact pressure at around 0.5 GPa. This report supported findings in the current research that MoS_2 particles are conductive in plating bath and its presence is a main cause for the dendritic nickel growth. Insulating MoS_2 particles is a novel pathway to mitigate this effect. However, the core/shell structure may shield MoS_2 from effective contact with the counterpart for solid lubrication and increase friction. The author also did not mention whether the particle loading in the coating versus particle concentration in bath is changed after the MoS_2 particles are coated with Al_2O_3, nor is it discussed whether there is an optimum means of adjusting the MoS_2/Al_2O_3 ratio in the modified particles for optimum tribological performance.

Wu and Ma *et al.*[174,175]developed an automatic brush plating system for codepositions of Ni-MoS_2 and Ni-Graphite and Ni-MoS_2/Graphite composite deposits. The nickel sulphamate bath contained 254 g/l $NiSO_4 \cdot 7H_2O$, 105 g/l $NH_3 \cdot H_2O$, 56 g/l $(NH_4)_3C_6H_3O_7$, 23 g/l CH_3COONH_4 and 0.1 g/l $(COONH_4)_2 \cdot H_2O$. The particles are suspended in the electrolyte bath which is pumped to flow through anode and cathode. The brush plating is carried out at room temperature with high current densities (20 – 40 A dm^{-2}) for 30 minutes. SEM images show that the surface morphology of the deposits is smooth and compact, which is attributed to the brush abrasion movement across the cathode surface, removing loose and porous content during the deposition process. Friction coefficient of the deposits is between 0.05 and 0.1 at 0.68 GPa contact pressure and a sliding speed of 1.25 m/s. The Ni-MoS_2/Graphite composite deposit also show improved resistance against humid environment during storage. The automatic brush plating system eliminated the dependence of human factors in traditional manual brush plating techniques and offered good quality control of the deposits by introducing precise anode movement, contact load control between anode and cathode, thermal management and short step changing time.

2.6.3 Effect of tribology test parameter on Ni-MoS_2 friction coefficient

There is a range of tribological tests reported for self-lubricating coatings and it is obvious that the test parameters could affect the outcome of friction and wear. Load, mode of contact, relative moving speed and dry/wet conditions are the main differences when different literatures are compared.

As self-lubricating material are designed for little or even non-lubricated scenarios, they are usually tested without lubricant oil (dry) to directly observe the friction and wear reduction brought by the solid lubricant contained in the coating[119,120]. Lubricated tribology tests have been less commonly reported and adds complexity to the tests due to the amount and type of oil used.

When operating at dry conditions the solid lubricant and the self-lubricating coatings have limited heat dissipation due to the lack of liquid lubricant that could act as coolant. High sliding speed leads to higher temperature on the contact area which could cause oxidation of the solid lubricant and

accelerate wear rate. Low sliding speeds are preferrable for samples of small size which could only provide a limited testing area that may undergo repeated friction and wear compared to large samples on a rotating disc[170, 171].

Load and contact mode determine the contact pressure on the coating. Some solid lubricant materials such as PTFE work best under low load bearing conditions as these are soft materials that may give way under high load and lead to high wear of the material. Sulphide materials such as MoS_2 and WS_2 work better under moderate to high load as sufficient contact pressure could shear the molecular planes effectively and "activate" the solid lubrication property [26,161,162].

MoS_2 may work best when embedded into a metal of reasonable hardness such as nickel, as the metal matrix will provide a firm base for the solid lubricant to be sheared upon. Flat pin-on-disc contact provided very low contact pressures (< 10 kPa) in literature due to larger contact areas, which saw friction coefficient of 0.2 – 0.4 for Ni-MoS_2 coatings[121]. Pin-on-disc contact using stainless steel or ceramic balls generated higher contact pressures ranging from 0.4 – 0.7 GPa in literature, with friction coefficients reported to be 0.1 – 0.2 in most cases[170 - 174]. This agreed with the previous summary for solid lubricants that MoS_2 works better under high load bearing conditions.

However, higher wear has also been reported for high load testing conditions, especially for coatings with low friction coefficient and high MoS_2 contents[121], which is probably due to the weakening of the coating by the solid lubricant and the resulting accelerated deterioration of the metal matrix layer. The imbedded solid lubricant particles usually decrease the load bearing property of metal matrix coatings due to lower overall hardness and more structural defects around the soft particles.

The contact mode should best simulate the operating condition for parts coated with self-lubricating coating in real world scenarios. Since most of these parts are not directly operating in highly loaded point contacts, but rather in sliding contact mode more commonly found in connectors, piston rings, valves and injection nozzles, it is important to consider a more suitable set up for testing Ni-MoS_2 coatings which can cover moderate contact pressures that are sufficient enough to activate the solid lubricant property of MoS_2 but avoid over stressing the base coating with contact pressures higher than the intended applications. A roller-on-plate set up is adopted in this work to provide a line contact mode with tuneable contact pressures that ranged from 0.1 – 0.3 GPa, to maximize the self-lubricating property of the coating without over stressing the metal matrix.

2.6.4 Summary for Ni-MoS_2 composite coating via electrodeposition

In summary, the electrolytic codeposition of MoS_2 with nickel deposits proved effective in producing self-lubricating coatings for reduced friction and wear. A major challenge is the conductivity of MoS_2 particles that led to porous, nodular growth of nickel matrix with adverse effect on its tribological performance. Such effect is more pronounced by increasing current densities and MoS_2 particle concentrations in bath. Another challenge is the softening of the deposit with increasing MoS_2 content, which limited the coatings to low load applications. A number of strategies have been used for improving Ni-MoS_2 composite deposits, including optimising process parameters during electrodeposition, addition of surfactants, and surface treatment of MoS_2 particles to alter the electrical and mechanical properties. A few more observations are presented here for future studies to consider in this field:

1. A wide range of MoS_2 bath concentrations (0 – 50 g L^{-1}) are reported with varying particle content (0 – 30 vol %) incorporated into the composite deposits. Low friction and good wear resistance are found for 5 – 12 vol% MoS_2 content in deposit. Higher MoS_2 contents could lead to soft, brittle deposits with poor adhesion and low wear resistance.

2. Various process parameters could affect the codeposition process, including pH, agitation rate, current density, particle bath concentrations, temperature, etc. Careful studies should be carried out to ensure that appropriate processing parameters are identified and adopted for producing the composite deposits.

3. Different particle dispersion techniques are reported, such as magnetic stirring, ultrasound agitation, ball milling, etc. Depending on the effectiveness of such techniques and the stability of the particle suspension, particle concentrations in bath could be as low as 0.5 g L^{-1} to 2 g L^{-1} for successful self-lubricating composite deposits. High particle concentrations in bath could increase the cost of productions, which may be uneconomic to scale up.

4. The effect of surfactants on MoS_2 particle dispersion and codeposition requires more systematic and quantitative studies. Random choice of surfactant types and concentrations are found in various literatures which show a lack of understanding for their working mechanisms. Other bath additives such as levellers and brighteners should also be considered to inhibit the preferential nodular growth of metal deposits over the conductive MoS_2 particles. Coating characterisations such as micro hardness measurement could be made more accurate on compact and smooth deposits, which would also offer superior tribological performances compared to porous and inhomogeneous coatings.

5. Different methods are reported for friction and wear tests of the composite deposits. There is a lack of consistency in reporting the testing conditions, including important parameters such as contact configuration, contact pressure, temperature and air humidity, which could affect the friction behaviour of Ni-MoS_2 composite deposits. More detailed analysis on the wear track would be essential to understand the wear mechanism and measure accurate wear loss, in addition to the general analysis of friction coefficient curves.

Chapter 3 Experimental Methodologies

3.1 Overview and approach

This study combined electrodeposition, coating structure/composition characterisation with tribological tests in order to draw connections between the process control during electrodeposition on the self-lubricating effect of Ni-MoS_2 composite electrodeposits.

As discussed earlier, Ni-MoS_2 coatings may face challenges in particle dispersion which leads to particle agglomeration with detrimental effect on coating property. Hence a screening on initial plating parameters that are commonly quoted in literature reviewed above such as current density, wetting surfactant, plating time and particle conductivity is carried out to establish the base parameters of the electroplating process that could keep MoS_2 agglomeration effect to the minimum and produce reasonable coating structures. The study then focused on particle dispersion method, particle bath concentration, bath agitation speed and a brightener additive as in-depth process control regarding their effects on coating structure, composition and tribological performance.

The study also included a parallel comparison of Ni-MoS_2 and Ni-PTFE coatings to justify the level of self-lubricating ability and explore the potential of the former as an alternative candidate for the latter in tribological applications.

3.2 Modified Watts nickel bath for composite electrodeposition

Table 3.1 Composition of the modified Watts nickel electrolyte

Component	Concentration / g dm^{-3}
Nickel (II) sulfate hexahydrate, $NiSO_4 \cdot 6H_2O$ (Sigma Aldrich)	250
Nickel (II) chloride hexahydrate, $NiCl_2 \cdot 6H_2O$ (Sigma Aldrich)	45
Boric acid, H_3BO_3 (Sigma Aldrich)	40
Molybdenum Disulphide, MoS_2 (1-2 μm) (Shanghai ST-NANO Science & Technology Co., Ltd)	0 - 40
Polytetrafluoroethylene PTFE (300 nm) (Sigma Aldrich)	1 - 7
Cetyltrimethylammonium Bromide (CTAB) (Sigma Aldrich)	0 – 2 (50 mg per g of MoS_2)
Saccharin (Sigma Aldrich)	0 - 10

Table 3.2 Operational conditions used for electrodeposition

Property	Value
Electrolyte pH	3-4
Temperature	50 ºC
Cathode current density	1 - 8 A dm^{-2}
Electrodeposition time	0 - 60 min
Rotation speed of magnetic stirrer follower	100 - 1000 rev min^{-1}

Particle dispersions are first carried out by mixing weighed out particles with 20 mL bath in a glass vial, then the mixture is diluted to 80 mL with Watts nickel electrolyte in a 100 mL cylindrical beaker. The bath composition and plating conditions are summarised in tables 3.1 and 3.2.

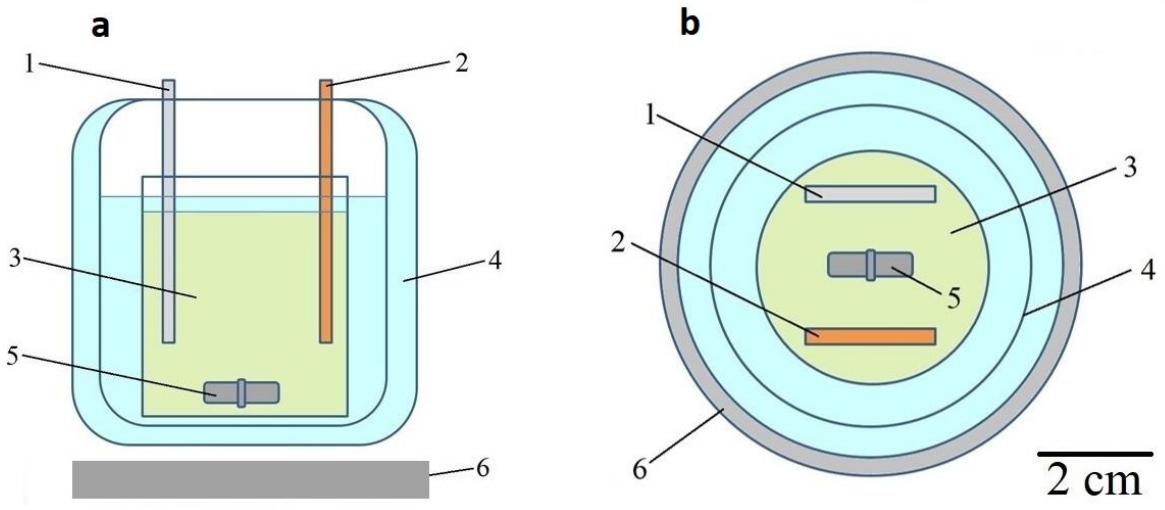

Figure 3.1 (a) cross-section and (b) top plan view of the electrodeposition set-up: 1) cathode, 2) anode, 3) Watts bath, 4) Water bath, 5) magnetic stir bar, 6) magnetic stirrer.

Electrodeposition is carried out using a mild steel plate cathode (AISI 1020, 80 mm × 20 mm × 3 mm) and a nickel plate anode (80 mm × 20 mm × 1 mm). The electrodes are sealed with waterproof tape, leaving an exposed surface area of 30 mm × 20 mm each for plating in a parallel-plate cell configuration as shown in Figure 3.1. Power is provided by a 24V DC power station with 1 – 10 A range.

3.3 Substrate preparation

Figure 3.2 (a) Precision saw, (b) Lapping machine, (c) Polishing plate

A mild steel plate (AISI 1020, 1000 mm x 2000 mm x 3 mm) is first cut by guillotine into plates of 80 mm x 200 mm x 3 mm, followed by cutting via a precision saw (Mecatome T210, Figure 3.2 a) into plates of 80 mm x 20 mm x 3 mm. The use of precision saw is to avoid build-up of deflection and torsion in final plates so that substrate flatness can be retained for the ease of sample analysis. Nickel plates (80 mm x 200 mm x 1 mm) are directly cut by guillotine into plates of 80 mm x 20 mm x 1 mm for use as anodes.

The protection paint on the as-received plate is removed by lapping (Kemet 15, Figure 3.2 b) with a 25 µm diamond suspension paste, which further ensured substrate flatness. The exposed mild steel surface is polished on a polishing plate (Struers LaboPol-21, Figure 3.2 c) with Silicon Carbide (SiC) polishing paper of 800, 1200 and 4000 grade, up to a mirror finish by visual inspection. After each stage of polishing, the steel plates are sonicated in ethanol and air dried to remove residue SiC abrasive particles, grease and moisture.

Immediately before electrodeposition, each substrate is first degreased, then activated in hydrochloric acid (HCl, 2 M) for 60 s, followed by rinsing with deionised water. The substrate is covered in water-proof tape leaving only a 30 mm x 20 mm area as cathode surface. A nickel anode plate is wrapped in

the same manner, leaving another area of 30 mm x 20 mm as the anode surface to ensure a uniform distribution of current density during electrodeposition.

3.4 Vickers hardness test

The hardness of coating samples is measured by a Vickers hardness indenter (Matsuzawa, Figure 3.3), which is equipped with a square-pyramidal shaped diamond head. The opposite faces of the diamond intersect at an angle (θ) of 136°. Upon indentation, the indenter would leave geometrically symmetrical and similar impressions, irrespective of size, with four well-defined points for accurate measurement of the indent diameters.

Figure 3.3 Vickers hardness indenter (Matsuzawa)

The Vickers hardness (HV) number can be calculated from the load applied to the diamond (F) divided by the surface area (A) of the resulting indentation [135]:

$$A = \frac{d^2}{2\sin\frac{\theta}{2}} \tag{5}$$

$$HV = \frac{F}{A} = \frac{2F\sin\frac{\theta}{2}}{d^2} \tag{6}$$

Five or more measurements are carried out for each sample and the mean value calculated is taken as the result. Each indentation is carried out under a load of 500 g for the duration of 15 s. The indent diameters are recorded and converted to HV hardness numbers according to a handbook for the indenter. To ensure that the indentations are not influenced by the substrate, the coating thickness is

checked to be greater than the indentation depth (h), which is calculated from the indent diameter (d) by the following equation:

$$h = \frac{d}{2\sqrt{2}\tan\frac{\theta}{2}} \tag{7}$$

For this work, the micro-indentation depth is controlled between 5 – 10 microns with indent diameters of 20 – 30 microns for coating thickness of 30 – 40 microns, to avoid the indentation reaching into the substrate. Nano-indentation is less used for coatings in this research as the small tip may be affected by the particle inclusions on a localised area and may not reflect the overall effect of particle inclusion on coating hardness. Its use will be specified in this study when coating morphology no longer allows effective measurement using micro-indentation.

3.5 SEM and EDS analysis

A scanning electron microscope scans the surface of a sample with a focused beam of electrons generated from an electron gun. Interactions of the electron beam with the sample at various depths produces different signals which could be picked up by detectors to extract sample information. Three of the most commonly used signals mentioned in this research are secondary electrons (SE), back-scattered electrons (BE) and photons of characteristic X-rays[136].

SEs are excited electrons emitted from sample surface atoms due to collisions with the SEM electron probe beam, hence they can provide high-resolution scanning-electron imaging (SEI) of detailed sample surface morphology.

BEs are SEM probe beam electrons reflected or back-scattered due to the elastic scattering interaction with sample atoms. BEs are used to detect chemical composition contrasts in samples as heavy elements backscatter more strongly than light elements. Back-scatter Imaging (BEI) is particularly useful to detect particle inclusions in composite deposits where the phase contrasts can be clearly indicated, whereas in SEI these may be difficult or impossible to tell apart.

X-ray photons are generated when high energy electrons in sample atoms move to fill inner shell vacancies left by the bombardment of the SEM probe beam. The X-ray signals are indicative of elemental compositions as well as their abundance in the sample.

A Scanning Electron Microscope (SEM, JEOL – JSM6500F, Figure 3.4) is used to investigate the surface morphology (SEI, 15 kV). BEI is used to investigate cross-sections of coating and substrates.

The compositions of the samples are measured by Energy-Dispersive X-ray Spectroscopy (EDS, Oxford X-Max SDD) in conjunction with SEM.

Figure 3.4 Scanning Electron Microscope (SEM, JEOL – JSM6500F)

Sample surfaces are required to be conductive in order to generate sufficient interactions with electron probe beams for SEM signals. Non-conductive samples may cause faults to SEI due to charging effect when scanned by the electron probe beam. This problem is sometimes resolved by covering the surface with ultra-thin conducting materials such as via gold-sputtering.

Figure 3.5 Plate degasser, Edwards PD3

All samples in this research are conductive in nature, so that no pre-treatment on conductivity is required for SEM analysis. Samples are degassed for 5 minutes in a plate degasser (Edwards, PD 3, Figure 3.5) before analysis.

3.6 Surface profiles by optical microscopy

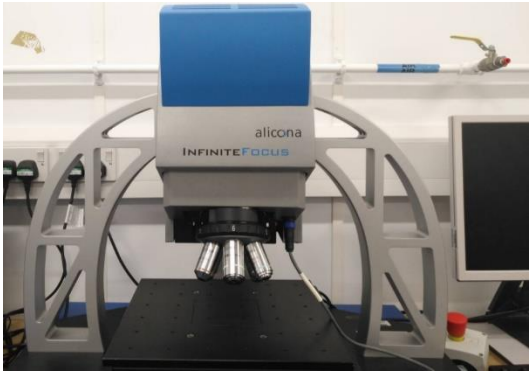

Figure 3.6 Optical microscopy for surface profiles (Surface 3D profile)

Surface profiles (morphology, roughness etc.) of the deposits is analysed by optical microscopy (Surface 3D profile, Figure 3.6). Sample images are taken with object lens magnifications of 5 and 20 times. 3D modelling of the surface morphology is created by a mathematical algorithm which combines multiple images taken from different levels of focus. Surface roughness is calculated from the 3D models which recreated the exact shape of the scanned surface area on a selected base plane.

3.7 Friction and Wear Test

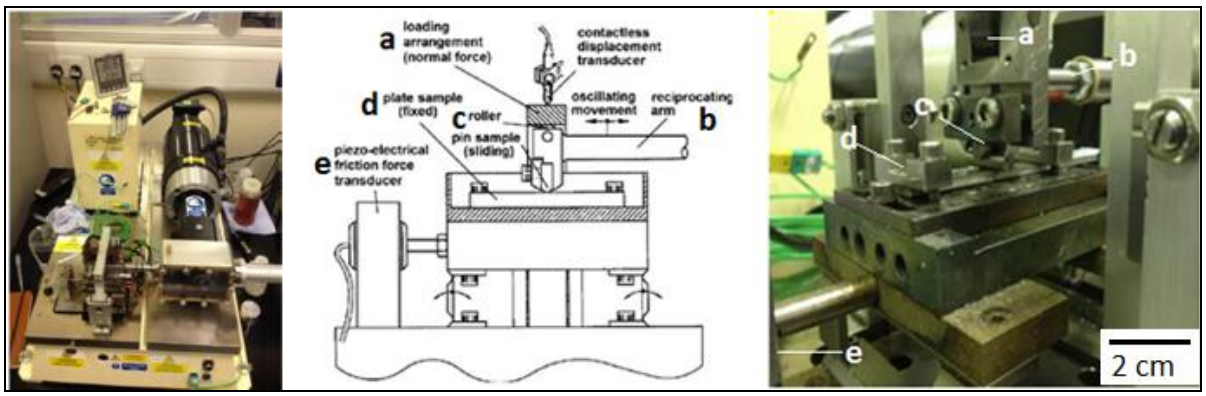

Figure 3.7 TE – 77 Tribometer and schematic of the testing platform

Wear tests are conducted on samples of tribological interest in this project. The wear behaviour and friction coefficient of the samples are observed using a TE-77 Tribometer (Phoenix Tribology Limited, Figure 3.7).

The testing conditions are chosen to simulate a piston ring on cylinder liner contact with the self-lubricating coating acting as the cylinder liner surface and a stainless-steel roller as the piston ring. Although not a perfect replication for the real-world scenario, the contact mode is a closer simulation using line contact instead of point contact quoted in most literature for pin-on-disc rigs. The load and contact pressure are chosen for sufficient activation of MoS_2 solid lubrication under moderate load without stressing out the nickel matrix which has been partially weakened by the high MoS_2 contents of the coating, since up to 0.1 GPa is the order of contact pressure in a harsh ring-on-liner contact found in engines[193]. Due to the test conditions being dry, temperature is kept to room temperature and sliding speed kept to low rates to allow friction heat to dissipate and the full benefit of friction and wear reduction by MoS_2 to be observed.

The tests are carried out at a controlled room temperature of 24 °C – 26 °C and humidity of 36 - 40.0% for consistency of MoS_2 solid lubrication. The counter body is an AISI-52100 stainless steel roller pin with a diameter of 6mm and a length of 10.00 mm, which is hardened to 60 HRC to simulate the hardness of piston ring material of alloy cast iron. Load range is 10 – 100 N, for mean contact pressures of 0.1 – 0.3 GPa. Each sample test is carried out with a separate pin to prevent cross contamination for the measurement of wear loss. The pins and holder are cleaned prior to the wear test with propan-2-ol followed by air drying to remove dirt or grease.

The wear tests are set to run for a fixed duration of 900 seconds, with a stroke length of 10 mm and at a frequency of 1 Hz. The contact load acting on the sample throughout the experiment could be fixed

at specified values or programmed to step up to a certain value at specified intervals. No external lubrication is applied to the samples. The friction force is determined by a piezoelectric transducer and automatically transferred onto a data sheet. The coating integrity could be monitored by comparing the number of friction coefficient with that of the substrate or pure Nickel. It is also observed that the pins are mainly fixed in the holder for all samples during wear tests up until the complete removal of the coating, thus guaranteeing that the friction observed is of a sliding motion and not of a rolling motion.

Chapter 4 The effect of MoS_2 particles on electrodeposition of Ni-MoS_2 composite coating

Nickel-Molybdenum Disulphide (Ni-MoS_2) coatings exhibit low friction coefficient due to the self-lubricating effect of MoS_2 particles. The study on Ni-MoS_2 coatings in this chapter covers some initial observations of electrodeposition with MoS_2 particle suspensions in the bath. Surface and structural characterisations are analysed in order to understand the influence of particles on deposit growth.

The electrodeposition deposition of Ni-MoS_2 coatings generally followed the descriptions given in Chapter 3, with specific conditions described in corresponding sections.

4.1 Ni-MoS_2 composite growth as a function of electrodeposition time

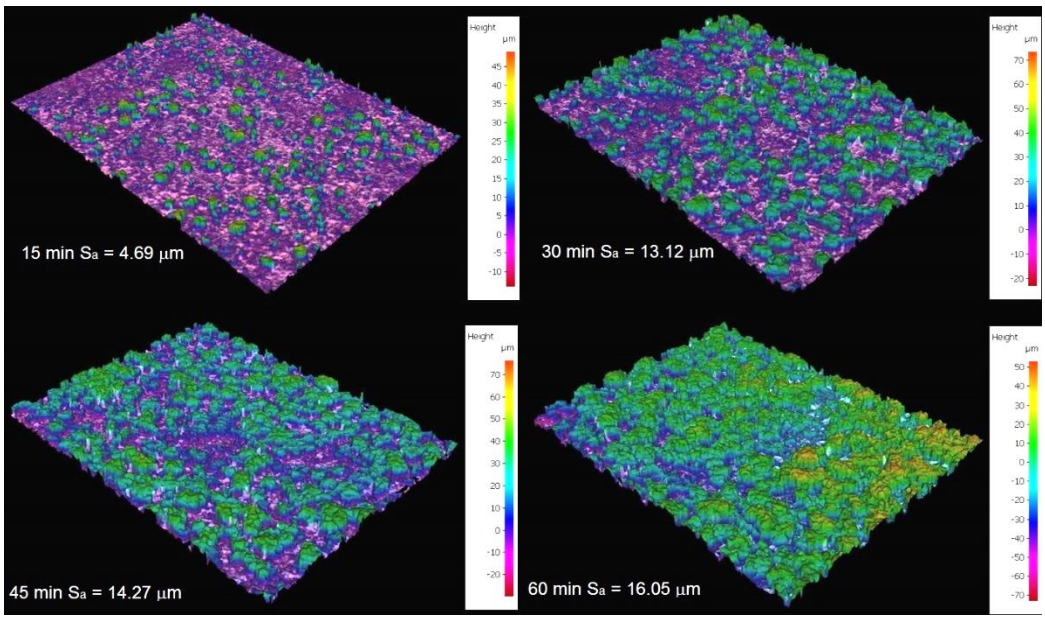

Figure 4.1 Surface 3D morphology of Ni-MoS_2 composite coating after different duration of electrodeposition

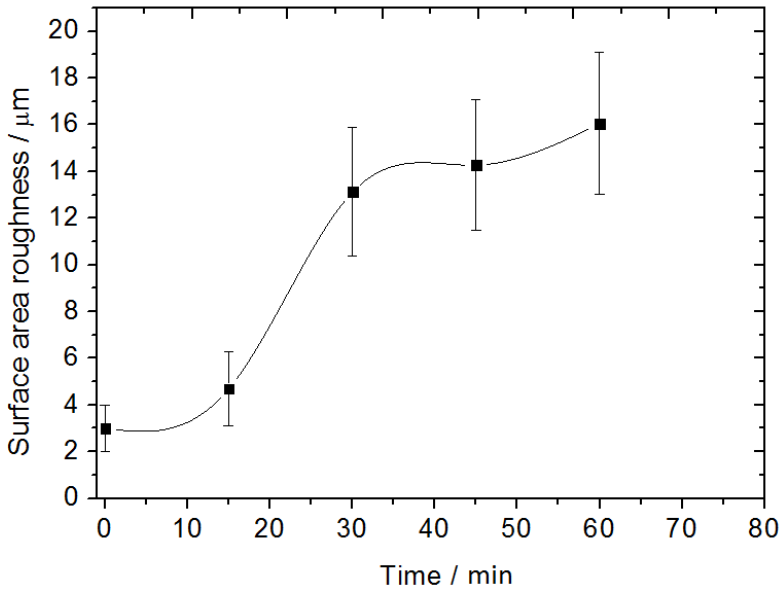

Figure 4.2 Surface roughness measurement of Ni-MoS_2 coating as a function of deposition time

The surface roughness of a Ni-MoS_2 composite coating is monitored during electrodeposition from a Watts bath solution containing MoS_2 1 gL^{-1}, CTAB 0.1 g L^{-1} and Saccharine 5 g L^{-1}. Current density is 5 A dm^{-2} and stirring is at 400 rpm (Figure 4.1). It show that the surface is gradually covered by protrusions and roughness features that indicated uneven growth of the composite coating. Surface roughness measurements (Figure 4.2) indicated the rapid onset of roughness features from the early stage of the electrodeposition process, which is first measured at 15 min into electrodeposition. This is followed by a fast increase of surface roughness between 15 min to 30 min, during which the size and density of surface roughness features both increased steadily. The surface roughness increase slowed down after 30 min of electrodeposition, when the roughness features became densely packed over the entire coating surface and seemed to reach saturation.

4.2 Effect of current density on Ni-MoS_2 composite coating

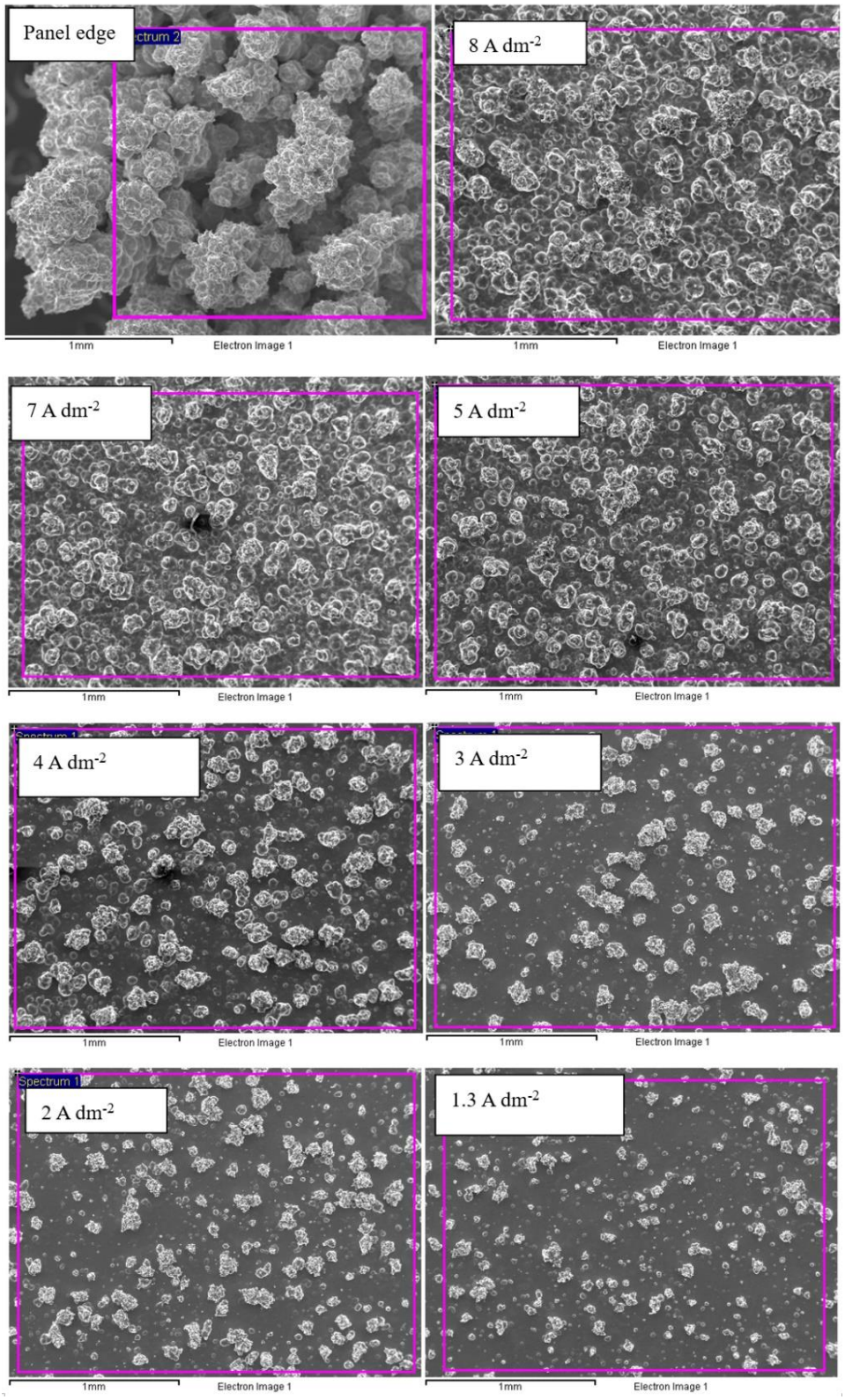

Figure 4.3 SEM images of hull cell panel for Ni-MoS_2 electrodeposition at reference distances for varying current densities

A modified Watts nickel bath (MoS_2 1 gL^{-1}, CTAB 0.1 g L^{-1}) is used for Ni-MoS_2 composite electrodeposition in a standard Hull cell, which allowed studies of changing current densities from 8 A dm^{-2} to 1 A dm^{-2} by placing the cathode at an angle to the anode. Magnetic stirring is kept at 400 rpm to prevent particle sedimentation during the electrodeposition process. Surface roughness features are very pronounced for current densities higher than 7 A / dm^2, which could be seen from SEM images taken at reference points for corresponding current densities (Figure 4.3). The size, height and density of the roughness features are gradually reduced with decreasing current density in the hull cell. For current densities below 3 A/dm^2, the coatings show low surface coverage with random and scarcely dispersed particle inclusions.

The results from this study indicated that current distribution is disrupted by the presence of MoS_2 particles during electrodeposition. Another study examining the effect of current density on Ni-MoS_2 composition electrodeposition[176] reported the best coating results at 5 A/dm^2. This study found that coatings deposited between 4 – 5 A/dm^2 show good surface coverage over the substrate. Their slightly increased surface roughness is within acceptable levels.

4.3 Effect of wetting additive on Ni-MoS_2 composite coating

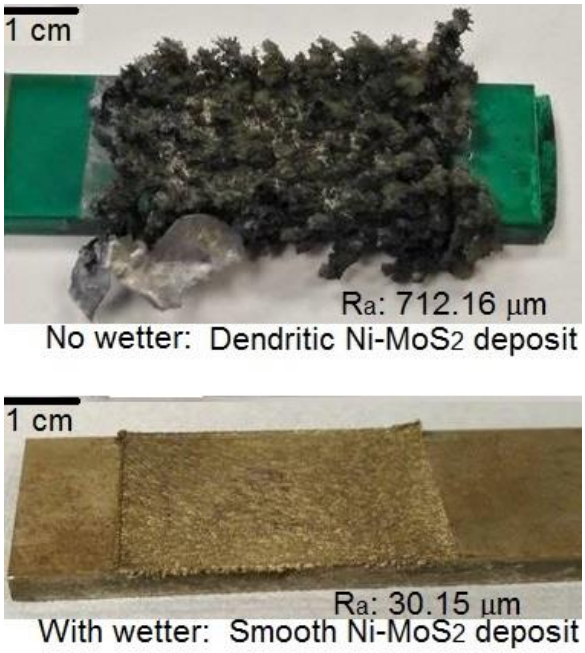

Figure 4.4 Comparison of Ni-MoS_2 coatings from baths with / without wetting additive

The presence of wetting additive is very important for Ni-MoS_2 composite electrodeposition, as shown by this example of a composite coating from a bath without wetter surfactant CTAB (MoS_2 1 gL^{-1}) compared with a bath (MoS_2 1 gL^{-1}, CTAB 0.1 g L^{-1}) with surfactant addition (Figure 4.4). Current density is 5 A dm^{-2} and stirring is at 400 rpm. Large particle agglomeration is formed without CTAB addition, and the resulting coating is extensively covered by large protruding roughness features rich in MoS_2 contents. It also show that the surface roughness features in Ni-MoS_2 composite coatings are directly related to a build-up of MoS_2 rich structures during electrodeposition. Without the wetting additive, the large particle agglomeration of MoS_2 particles led to an increase in size of the roughness features by an order of magnitude. MoS_2 particles are immiscible to water and require surfactant addition and particle dispersion procedures to stabilise particle suspension in the bath.

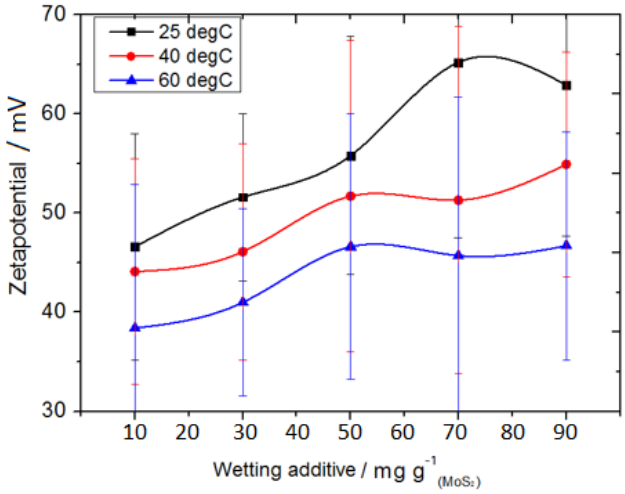

Figure 4.5 Effect of CTAB addition on particle surface zetapotential in bath

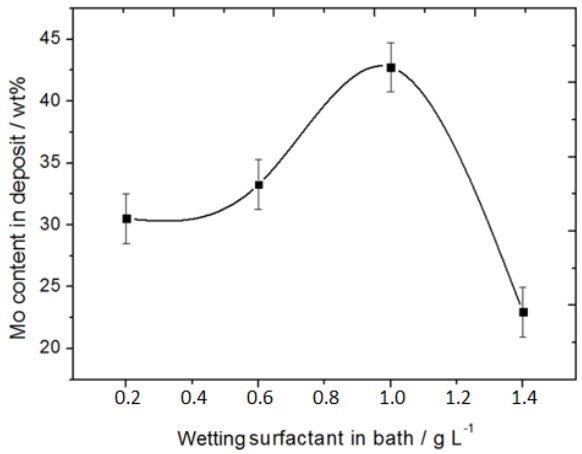

Figure 4.6 Effect of wetting additive on MoS_2 particle codeposition (MoS_2 particle concentration in bath: 2 g L^{-1})

Zetapotential measurement could reflect the surface charge of dispersed particles in bath which could indicate particle suspension stability. In the presence of CTAB addition, positive zetapotential values are measured for MoS_2 particle suspensions (Figure 4.5), which show that particle suspension is stabilised in the presence of the cationic surfactant. Surfactant adsorption onto MoS_2 particles is reduced at higher bath temperatures. Above 50 mg CTAB per g of MoS_2 in bath, there is no significant increase in particle zetapotential by further increasing the surfactant level, suggesting a saturation of adsorbed CTAB on particle surfaces. A maximum codeposited particle content in composite coatings is also observed at this threshold surfactant level (Figure 4.6). Higher surfactant levels could lead to poisoning of the bath and should be avoided in order to maintain good coating quality. A study by Wang on MoS_2 particles found similar adsorption behaviour for another cationic surfactant[172]. It is suggested that surfactant adsorption could partially insulate MoS_2 particles and promote uniform coating deposition. Therefore, CTAB addition is deemed beneficial for a suitable level below adsorption saturation onto MoS_2 particles in electrodeposition.

4.4 Particle conductivity and Ni-MoS_2 composite coating growth

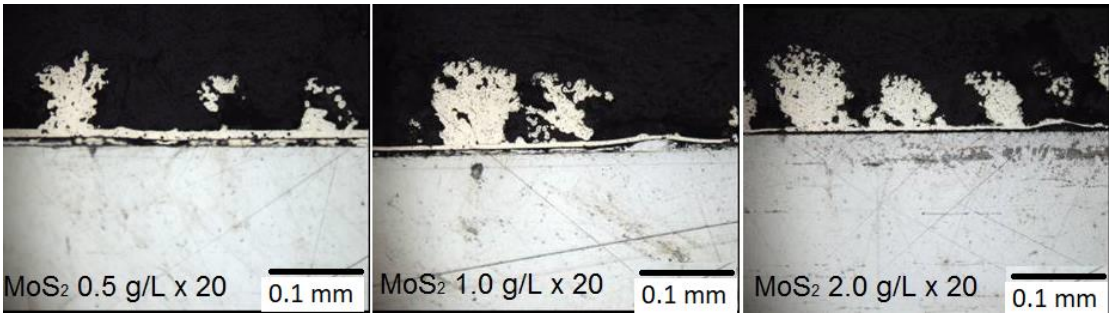

Figure 4.7 Ni-MoS_2 coating cross sections with changing MoS_2 bath concentrations

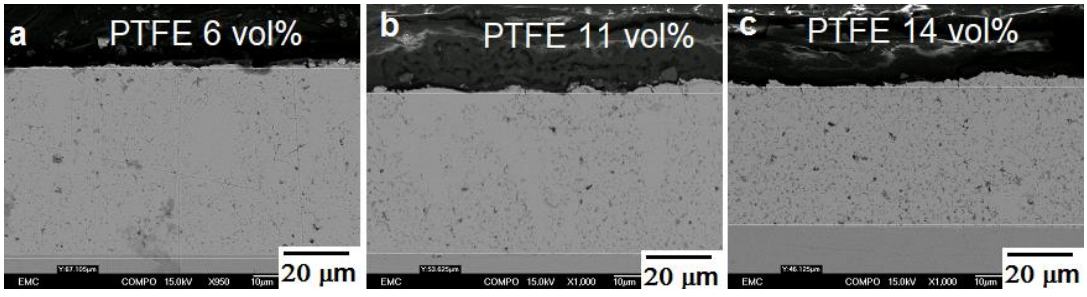

Figure 4.8 Ni-PTFE coating cross sections with varying PTFE contents

The theoretical thickness of nickel electrodeposition could be calculated from Faraday's law (eq. 2.3). Assuming a current efficiency of 95.5%, a coating thickness of around 60 microns is expected for current density at 5 A dm^{-2} over a deposition period of 60 min[177]. The theoretical calculation assumed uniform coating growth with a smooth and compact coating structure. However, the cross-section view of a Ni-MoS_2 coating (MoS_2 0.5 – 2 g L^{-1}, CTAB 0.025 – 0.100 g L^{-1}, current density 5 A dm^{-2} with stirring at 400 rpm) observed under an optical microscope show nodular protrusions with dendritic morphologies extending for over 100 μm in thickness (Figure 4.7). The porous coating could be divided into two layers: first, a thin layer of smooth coating covering the surface of the substrate; second, large Ni nodules containing MoS_2 inclusions covering the first smooth layer of coating. The compact layer thickness of N-MoS_2 coatings is reduced by increasing MoS_2 particle addition in the plating bath, suggesting that the uniform coating growth is disrupted by increasing particle addition into the plating bath.

In contrast, good agreements with Faraday's law of electrolysis could be seen from another Ni-PTFE composite deposit (PTFE 2-7 gL^{-1}, CTAB 0.025 – 0.100 g L^{-1}, current density 5 A dm^{-2} with stirring at 200 rpm) showing coating thickness within 60 microns without excessive porosity or surface roughness features (Figure 4.8).

Early mapping studies of Ni-MoS_2 surface morphology show that the nodular structures are formed from an early stage and underwent an accelerated growth in terms of their size and numbers throughout the electrodeposition process. The thin layer of compact deposit beneath the nodules is gradually depleted of current distribution and its growth rate is reduced to minimum after being overtaken by nodular growth.

The key to this unique growth behaviour difference for MoS_2 codeposition lies in preferential current distribution, which is thought to be related to the conductivity of MoS_2 particles[109]. The room temperature electrical resistivity of nickel, MoS_2 and PTFE are quoted as 6.99×10^{-8} Ω·m (Ni[178]), 9 – 400 Ω·m (MoS_2[179]), and 1×10^{23} – 1×10^{25} Ω·m (PTFE[180]). Electrical property characterisation of materials used in this study is carried out to confirm literature data. A MoS_2 pallet (30 mm diameter, 1.0 mm thickness) is produced via thermal pressing sample particles used in the current research, and its electrical resistivity measured by an automatic four-point probe meter (4D, model 280) is around 200 Ω·m, which is in agreement with reported values. The wide range of MoS_2 powder resistivity is due to difference in its crystallinity, defects and impurities, with the value reported for the amorphous pellet landing in the higher range. Attempts to obtain resistivity measurements of PTFE particles are rather challenging due to excellent insulation of the pellet sample.

Modelling of current density distribution over adsorbed particles as influenced by particle conductivity is discussed by Celis *et al.* in a review on composite electrodeposition mechanisms[181]. It

predicted higher current distribution over conductive particles on cathode surface than surrounding metal matrix, and the opposite for nonconductive particles.

The observations in this study supported literature predictions on metal deposit growth behaviour influenced by inclusion particle conductivity. Conductive MoS_2 particles adsorbed onto the cathode surface could attract preferential current distribution, which resulted in accelerated nickel deposition on particle surface than surrounding metal matrix. The simultaneous onset of numerous MoS_2 particle inclusions on Ni-MoS_2 deposits is able to build up a current distribution largely biased towards the top inclusion protrusions instead of the metal matrix underneath. In comparison, when PTFE particles are gradually incorporated into the growth of surrounding metal matrix during electrodeposition, the current distribution over nonconductive particles are significantly lower than surrounding metal matrix. Therefore, the deposition of nickel over the metal matrix is constant and uniform.

Chapter 5 Process control of saccharin as a brightener

5.1 Effect of saccharin on coating composition and structure

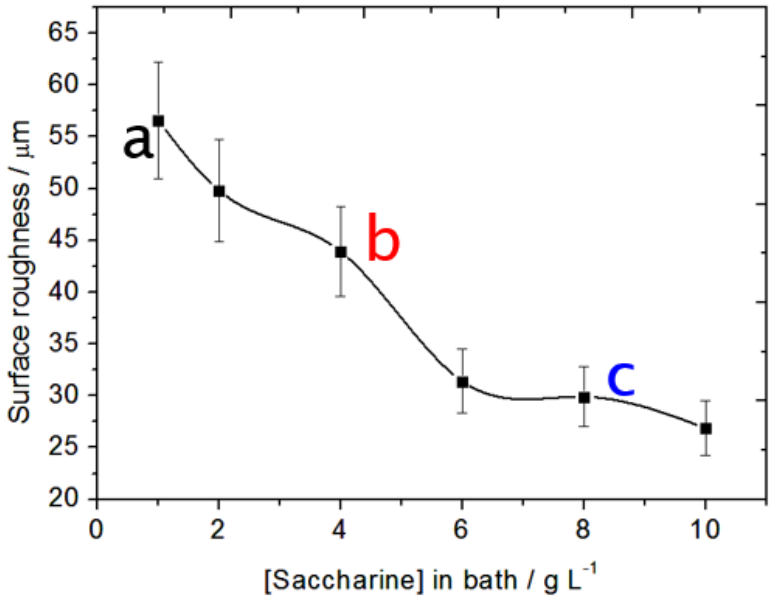

Figure 5.1 Effect of saccharin on Ni-MoS_2 composite coating surface roughness

Sodium saccharin (saccharin) is a common brightener additive for nickel deposition[46,51,56,59,192]. Saccharin promotes smooth coating finishing by blocking current density at adsorption sites. It also acts as a stress reliever by refining grain sizes of the composite coating. Because of its dual functionalities and the tolerance of high concentrations of saccharin in a Watts nickel bath without causing deleterious effect to nickel deposition, saccharin is chosen as a brightener additive for Ni-MoS_2 composite deposition. The intended effect is to smoothen the surface roughness features of Ni-MoS_2 composite deposits and additionally, to reduce coating stress for higher ductility and better adhesion with the substrate.

The surface roughness of Ni-MoS_2 composite deposits from baths containing various amounts of saccharin is measured by optical microscopy (Figure 5.1). When saccharin is increased from 1 g L^{-1} to 10 g L^{-1} in bath (MoS_2 2 g L^{-1}, CTAB 0.1 g L^{-1}, stirring 400 rpm, current density 5 A dm^{-2}, plating time 60 min), the resulting surface roughness of Ni-MoS_2 composite deposits is reduced by almost 50%, for Ra 55 µm to Ra 27 µm.

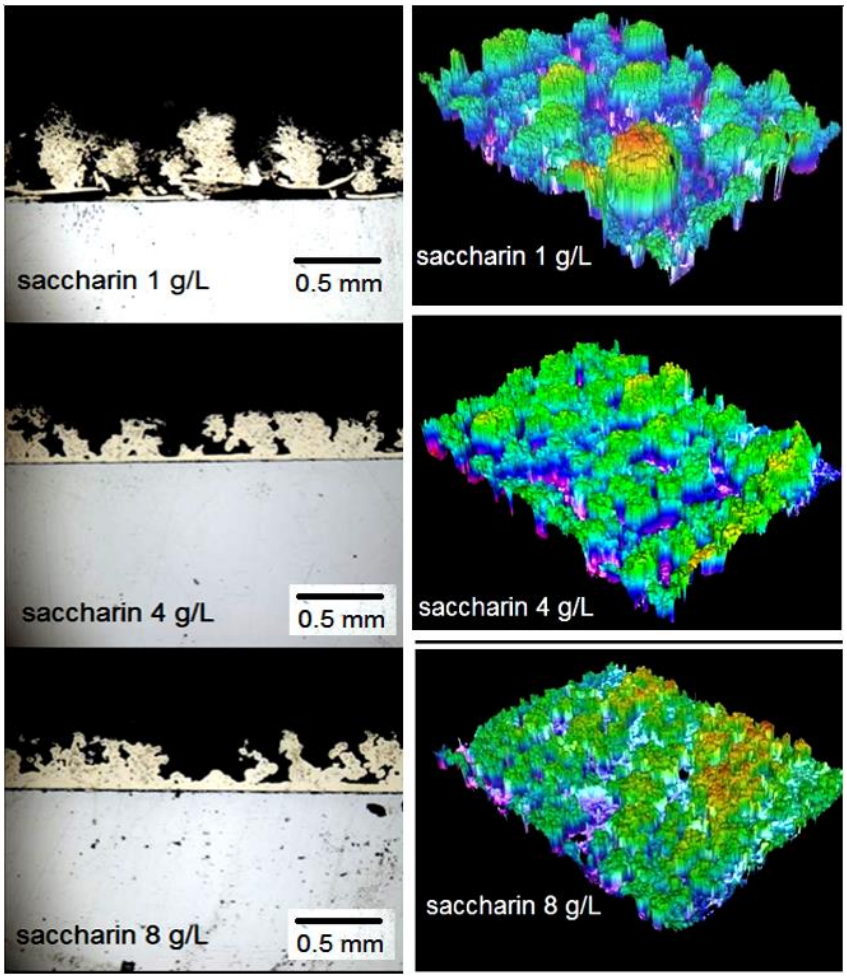

Figure 5.2 Cross section and 3D morphology of Ni-MoS_2 composite coatings with different saccharin concentrations in bath

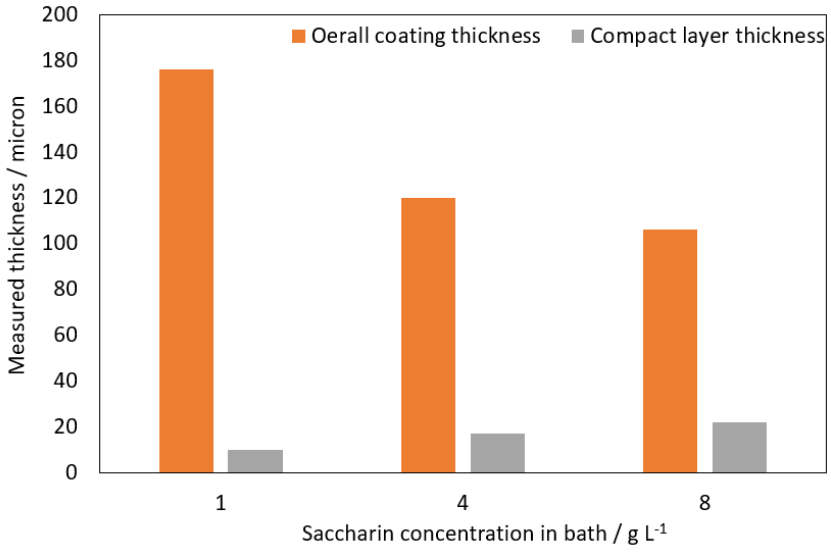

Figure 5.3 Effect of saccharin bath concentration on compact coating structure

The cross sections of Ni-MoS_2 coatings (Figure 5.2) from baths containing higher saccharin concentrations at 4 g L^{-1} and 8 g L^{-1} show higher structural integrity. Even though surface roughness features are still present, they are smaller in size and formed a continuous coating over the substrate. The compact film thickness measured by image analysis software (Figure 5.3) is also shown to increase at higher saccharin concentrations, while being adherent to the substrate.

Compared to that, a porous and fragile coating is formed from a bath containing less saccharin at 1 g L^{-1}, which show a thinner compact layer and higher porosity throughout the coating thickness. It subsequently suffered delamination and extensive fracturing during metallography preparation.

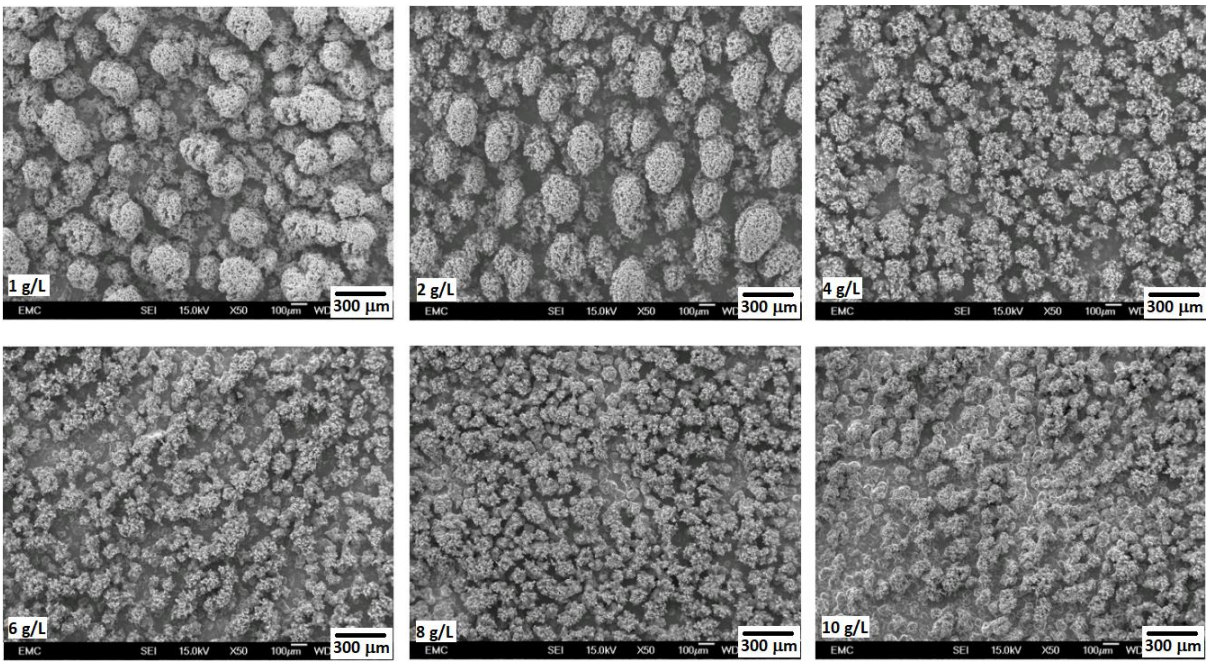

Figure 5.4 SEM surface characterisation of Ni-MoS_2 coatings with changing saccharin concentrations in bath

SEM observation show a more uniform coating surface containing smaller nudules covering the whole observation area with higher saccharin concentrations in bath, compared with large but isolated nodules loosely distributed on coatings with less saccharin in bath (Figure 5.4). This clearly shows that surface coverage of Ni-MoS_2 composite coating can be improved by saccharin, which reduced the growth rate of nodular and dendritic structures for a more uniform and smoothened surface.

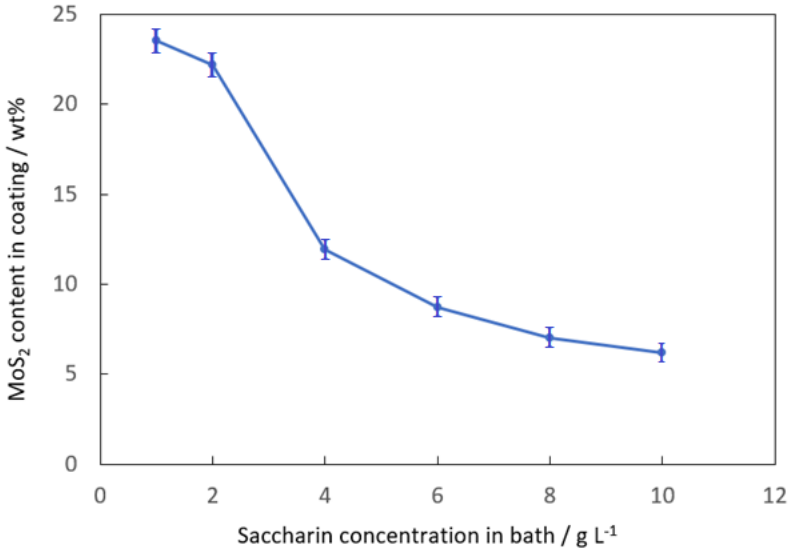

Figure 5.5 Effect of saccharin bath concentration on particle content in Ni-MoS_2 coating

However, it is important to note that adding saccharin to the bath also reduced MoS_2 content in the coating. MoS_2 content on coating surface is measured by EDX and show a decrease from 23.5 wt% to 6.2 wt% for saccharin in bath from 1 g L^{-1} to 10 g L^{-1} (Figure 5.5). The brightening effect of saccharin by blocking surface active deposition sites and its anionic charge for a more negative particle zetapotential could affect particle adsorption and electrophoretic migration towards the coating surface during electrodeposition. A smoothened coating surface also indicated that there could be more nickel coverage over pores and unevenness for a better envelopment and support of adsorbed MoS_2 particles in the composite deposit, which could yield less MoS_2 wt% reading from EDS scan.

5.2 Effect of saccharin on coating tribological performance

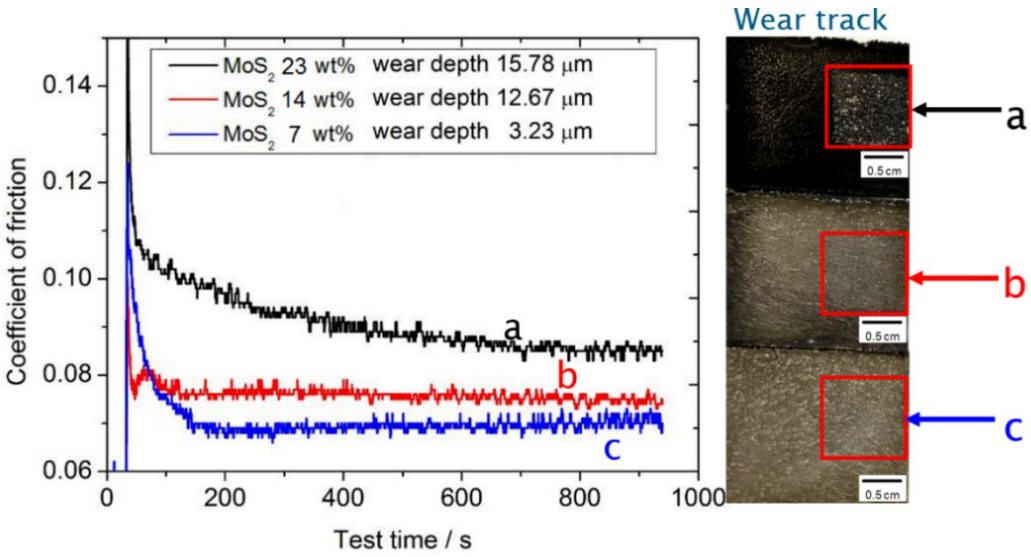

Figure 5.6 Coefficient of friction of Ni-MoS_2 composite coatings with saccharin concentration in bath at (a) 1 g L^{-1}, (b) 4 g L^{-1} and (c) 8 g L^{-1}.

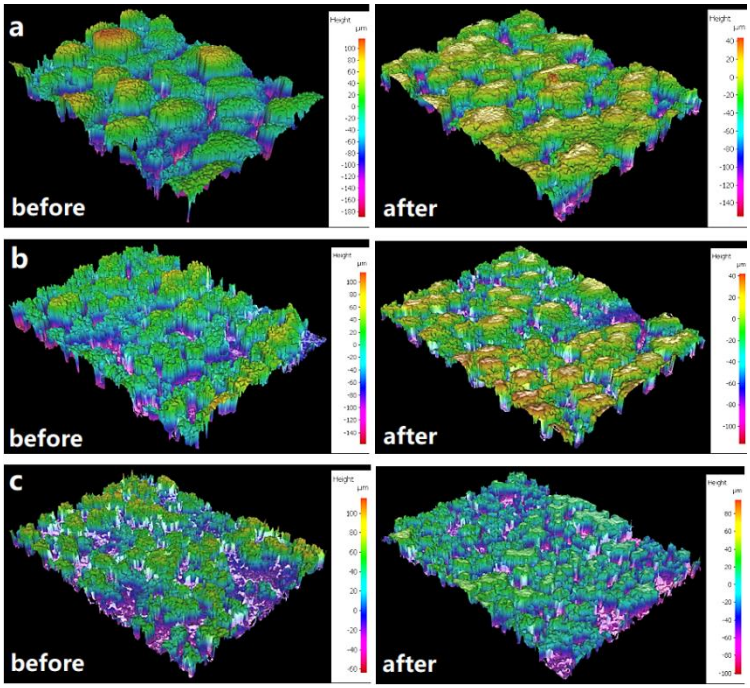

Figure 5.7 Before and after wear: Surface 3D morphology of Ni-MoS_2 composite coatings with saccharin concentration in bath at (a) 1 g L^{-1}, (b) 4 g L^{-1} and (c) 8 g L^{-1}.

Tribology tests on selected samples are carried out on a TE-77 tribometer: AISI-52100 bearing steel roller (diameter 6 mm, length 10 mm), load 20 N (roller, Hertzian contact pressure 0.16 GPa); sliding frequency 1 Hz; stroke length 10 mm. Coefficient of friction for selected samples are plotted against test time (Figure 5.6). In spite of its high MoS_2 contents on coating surface, sample a (saccharin 1 gL^{-1} in bath) shows a friction coefficient of 0.9 and wear depth of 15.78 microns across the wear track after 900s of wear test. In comparison, sample C (saccharin 8 g L^{-1} in bath) show a lower coefficient of 0.07 with an 80% reduction in wear even though it contained 70% less MoS_2 contents on coating surface.

Optical scans of surfaces before / after wear (Figure 5.7) show that for surfaces with large roughness features, the wear is localised on protruding nodules that underwent extensive wear. Smooth surfaces with smaller but more uniform surface coverage show small polishing wear evenly distributed across the examined area. For coatings of higher surface roughness containing higher MoS_2 contents, there should have been sufficient supply of solid lubricant particles for lubrication film formation during wear. However, the fragile and porous surface structures are more likely to give way during wear tests when they become stressed under localised wear conditions, therefore the coating structure could not provide a firm support for the lubrication film to achieve its maximum friction reduction performance. More energy is lost as a result of high rate of material removal, which contributed to higher friction coefficient measured by the tribometer.

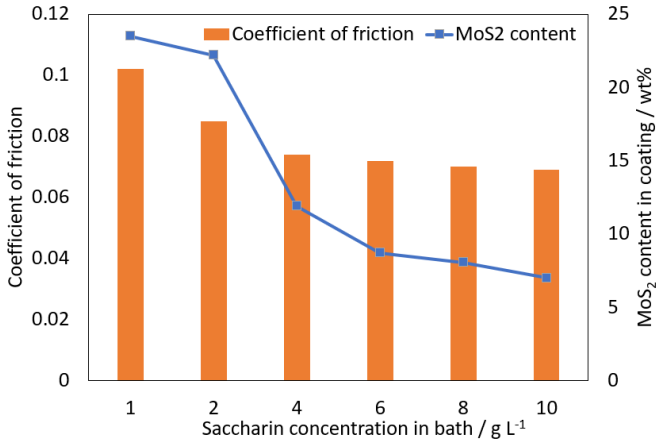

Figure 5.8 Effect of saccharin addition on coating composition and coefficient of friction for Ni-MoS_2 coatings with 2 g L^{-1} particle in bath

The wear test show that reducing coating surface roughness by additional saccharin in a plating bath containing MoS_2 2 g L^{-1} could make a positive impact on the tribological performance of Ni-MoS_2 composite coatings (Figure 5.8).

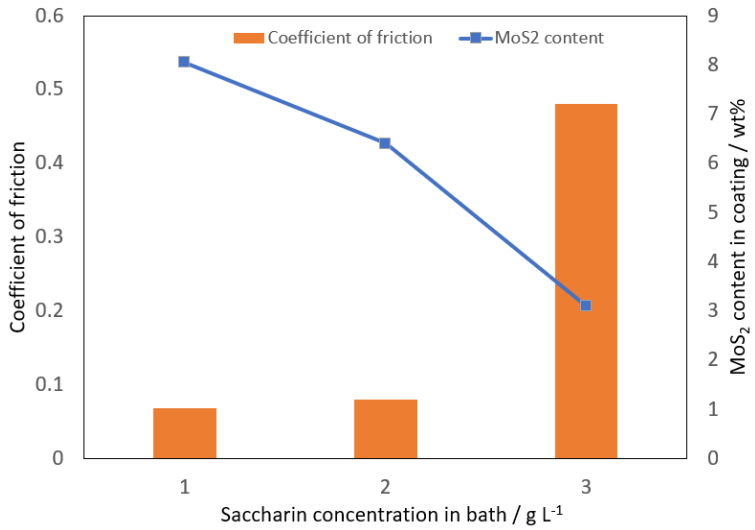

Figure 5.9 Effect of saccharin addition on coating composition and coefficient of friction for Ni-MoS_2 coatings with 1 g L^{-1} particle in bath

In comparison, Ni-MoS_2 composite coating from another bath with MoS_2 1 g L^{-1} without the brightener additive show good self-lubricity. However, upon addition of saccharin by up to 3 g L^{-1}, higher friction is observed in wear tests (Figure 5.9). The loss of self-lubricity is due to loared MoS_2 content in the coatings, which when reduced to beneath a certain level, would leave insufficient solid lubricant particles for effective tribological response.

5.3 Summary and comments

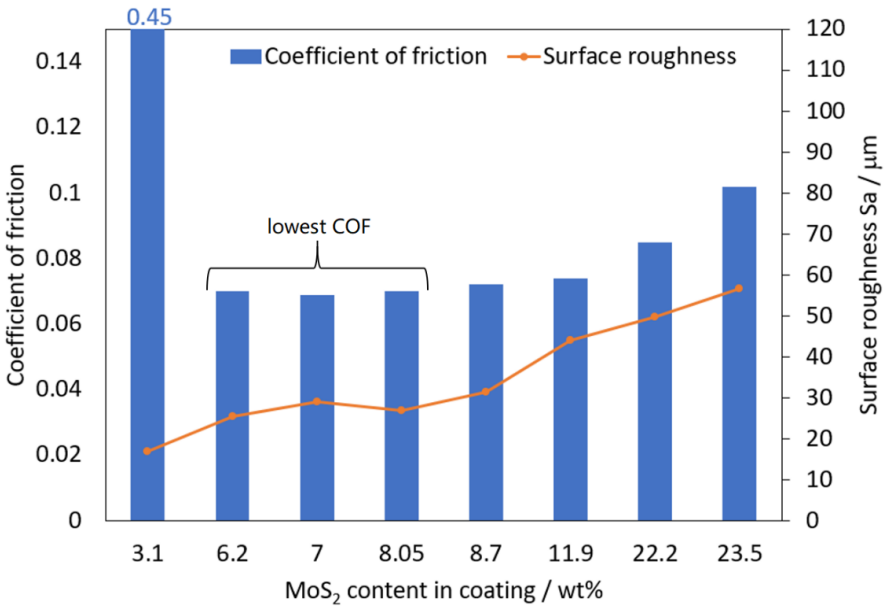

Figure 5.10 Effect of particle content and surface roughness on friction of Ni-MoS_2 coatings

From the above results, it could be seen that the addition of saccharin influenced both surface roughness and MoS_2 content of the coating. For tribological application of Ni-MoS_2 composite deposits, the addition of saccharin should be considered with other process parameters and aim to achieve a minimum surface roughness while maintaining a suitable level of solid lubricant particle in the coating for desirable tribological performances. Ni-MoS_2 coating containing MoS_2 6 - 8 wt% with controlled surface structure show the most enhanced self-lubrication effect in dry wear tests (Figure 5.10). The coatings are produced from a bath containing MoS_2 2 g L^{-1}, agitation rate 400 rpm and saccharin 6 – 10 g L^{-1}. Further increasing MoS_2 content in the coating could result in deteriorating tribological performances because of higher surface roughness and loss of coating structural integrity.

Saccharin addition is only beneficial for Ni-PTFE coatings in relieving stress and improving coating adherence. However, there is little effect of saccharin addition on Ni-PTFE coating surface morphology and composition. Another study even reported that saccharin is not recommended for superhydrophobic Ni-PTFE nanocomposite coatings via electrodeposition[115]. Therefore, no attempts are made on studying the effect of saccharin addition to baths for Ni-PTFE electrodeposition in this study.

Chapter 6 Process control of MoS_2 bath concentration

6.1 Effect of MoS_2 bath concentration on Ni-MoS_2 coating composition

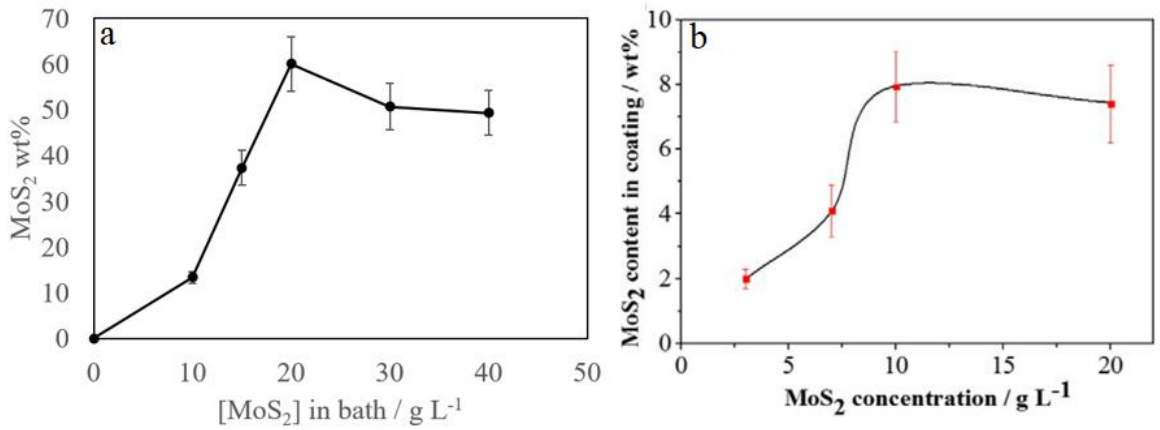

Figure 6.1 Effect of MoS_2 bath concentrations on MoS_2 content in composite deposits: (a) present results; (b) previous work by Yang *et al.*[186].

MoS_2 bath concentrations of 10 g L^{-1} – 40 g L^{-1} are used for initial studies (CTAB 0.5 g L^{-1} – 2 g L^{-1}, stirring 400 rpm, current density 5 A dm^{-2}, plating time 60 min). The MoS_2 content in the coating increased up to 60 wt% with the bath concentrations in bath from 10 – 20 g L^{-1}, after which there is a slight decrease down to 50% but the value remained stable despite further increasing MoS_2 bath concentrations (Figure 6.1 a). The saturation of particle inclusion in the coating has been observed in previous research by Yang *et al.* (Figure 6.1, b), and in other composite electrodeposition studies involving SiC particles[106]. Factors that influence the saturation point may include the bath composition, current density, particle sizes / species, and mechanical agitation of the system. MoS_2 content in coating from the modified Watts nickel bath is higher compared to those from nickel phosphorous bath. This show that MoS_2 particle codeposition could take place more readily under conditions used in this study. Before the saturation point, the increasing particle bath concentrations in bath could be accommodated by unoccupied active adsorption sites on the surface of the growing Ni matrix, while particle suspension and transport are assisted by ionic species via electrophoretic migrations. Above the saturation bath concentration, the dominant effect in bath is particle agglomeration which leads to poor wettability of particles as well as blocking of some active adsorption sites, hence a slight decrease of particle incorporation into the coating.

However, coatings with MoS_2 bath concentrations above 10 g L^{-1} are porous and fragile, consisting mainly of loosely adhered MoS_2 particles which can be removed from a slight contact. At the saturation point, Ni wt% in the composite deposit is only 10.74%, while MoS_2 wt% is 79.08%, which explained the dominant MoS_2 features. To meet the challenge of high wear resistance, lower MoS_2 bath concentrations (< 5 g L^{-1}) are studied in order to achieve a more compact coating with sufficient Ni composition.

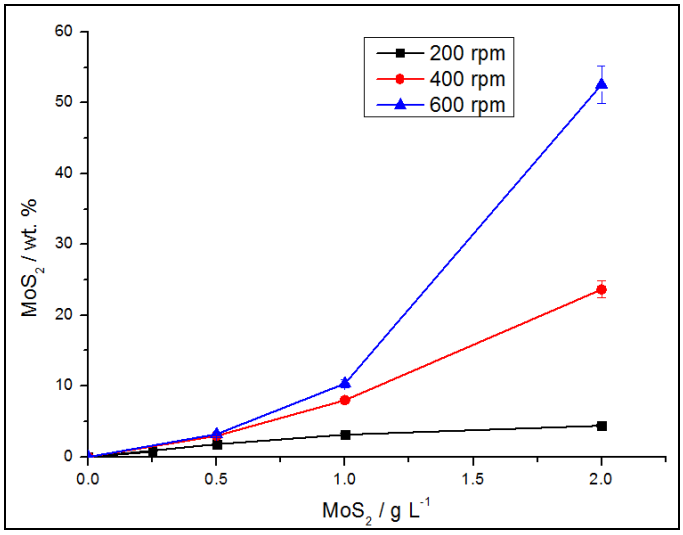

Figure 6.2 Effect of bath concentrations on MoS_2 content in the deposit

Samples are produced with MoS_2 bath concentrations at 0.50 g L^{-1}, 1.00 g L^{-1}, and 2.00 g L^{-1} separately (CTAB 0.025 g L^{-1} – 0.100 g L^{-1}, stirring 200 - 600 rpm, current density 5 A dm^{-2}, plating time 60 min). EDX scans indicated that MoS_2 content in coating increased with higher MoS_2 bath concentrations in the plating bath (Figure 6.2). The highest MoS_2 wt.% is obtained for MoS_2 2.00 g L^{-1} with agitation speed at 600 rpm.

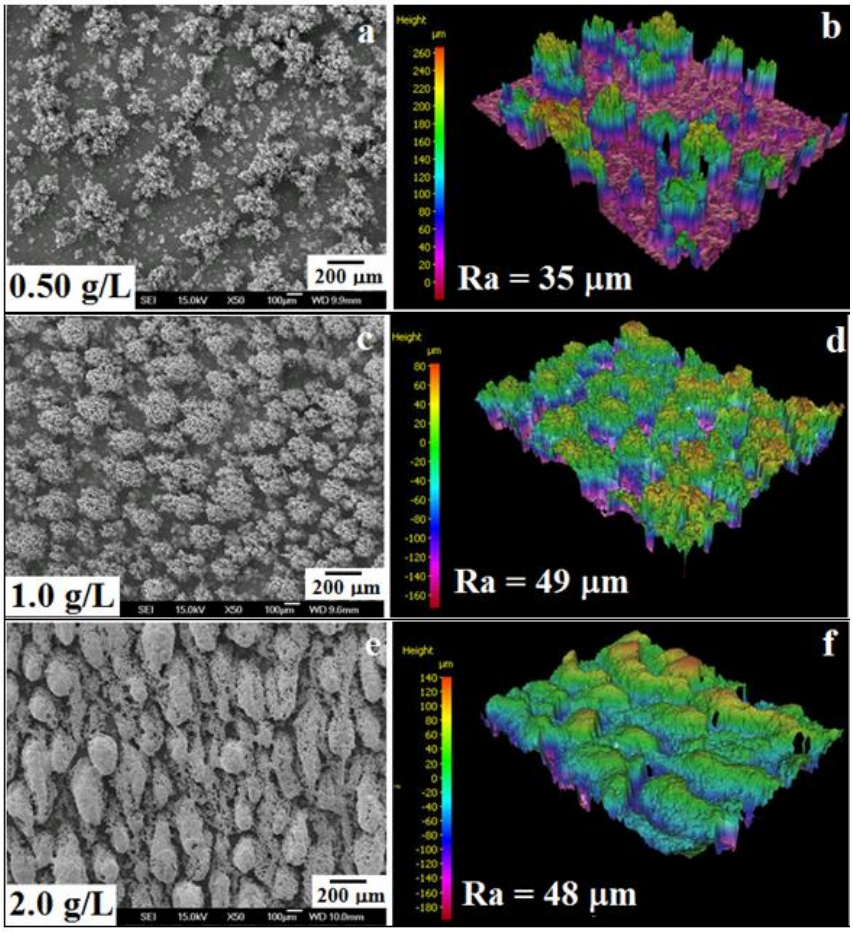

Figure 6.3 (a, c, e) SEM scan and (b, d, f) surface profiles of Ni-MoS_2 deposits with MoS_2 bath concentrations indicated for bath agitation speed at 600 rpm.

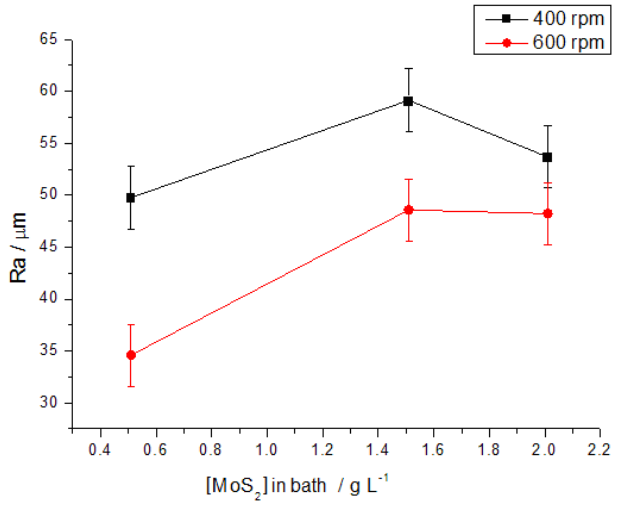

Figure 6.4 Influence of MoS_2 bath concentrations on average roughness (Ra) of Ni-MoS_2 deposits

Surface of Ni-MoS_2 coatings are covered with nodules which are shown in SEM and optical microscope scans (Figure 6.3). The number and size of the nodules increased with increasing MoS_2 bath concentrations, indicating a correlation between MoS_2 particles and the formation of the nodules.

A sharp increase in surface average roughness (Ra) is shown from MoS_2 0.50 g L^{-1} to 1.00 g L^{-1}, followed by a slight decrease to MoS_2 2.00 g L^{-1} (Figure 6.4). The first increase in Ra can be attributed to the increase in nodules numbers as indicated by SEM and optical microscope scans. The decrease in Ra is due to more surface coverage with less spacing between nodules.

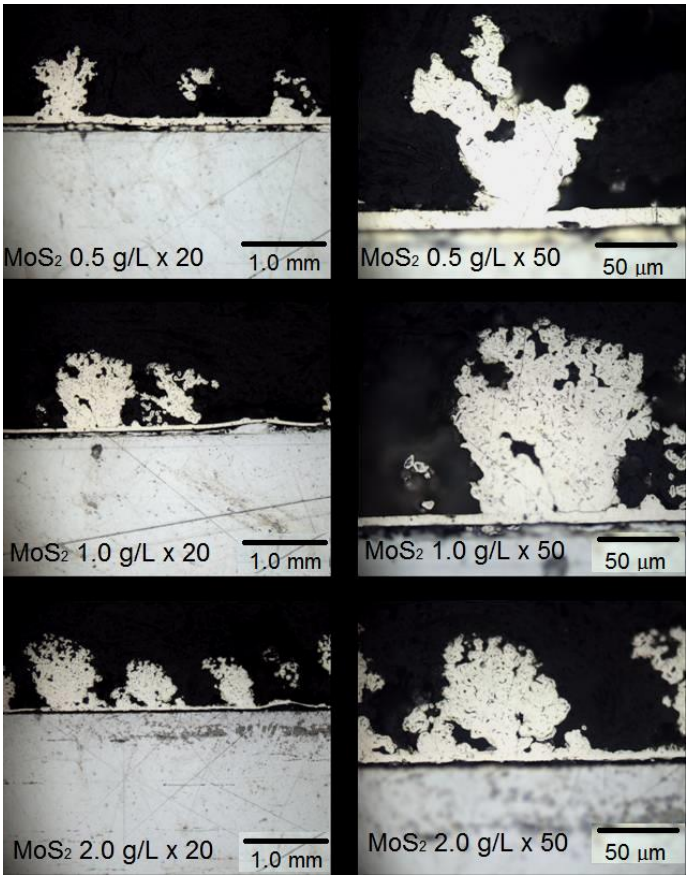

Figure 6.5 Ni-MoS_2 coating cross sections with various MoS_2 concentrations in bath

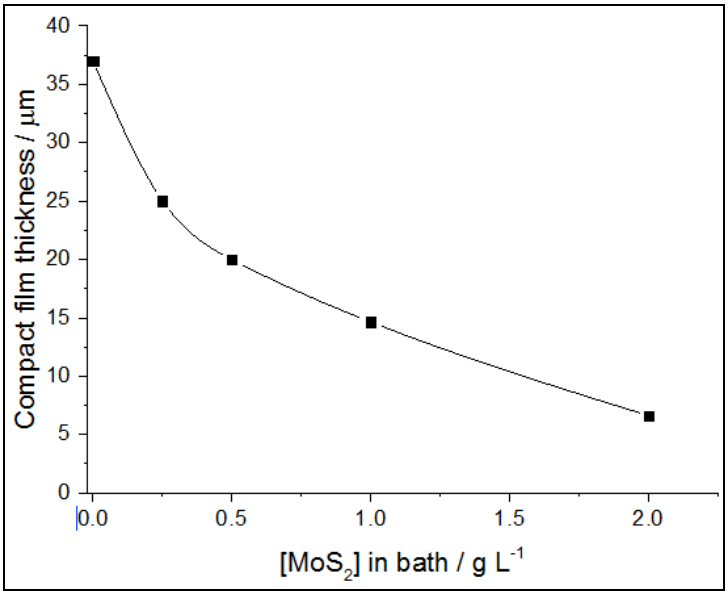

Figure 6.6 Compact film thickness for Ni-MoS_2 deposits

Cross sectional analysis show that the surface roughness features extended throughout the thickness of the coating, with only a thin layer of compact film over the substrate (Figure 6.5). The compact layer thickness of Ni-MoS_2 coatings is reduced by increasing MoS_2 particle addition in the plating bath (Figure 6.6), which is related to the increase of particle inclusion rate. It could be further inferred that the onset of nodular growth mechanism could also the promoted by higher MoS_2 concentrations in bath which led to the earlier termination of compact film growth.

A similar trend of surface roughness change is observed in report by Yang *et al.* [186] for Ni-P/MoS_2 composite deposits with MoS_2 bath concentrations of 1 – 20 g L^{-1}. At higher bath concentrations, the author attributed the decrease in roughness to the formation of dense and compact surface clusters rather than individual nodular structures with large spacing in between, leading to uniform and flat nodules surfaces.

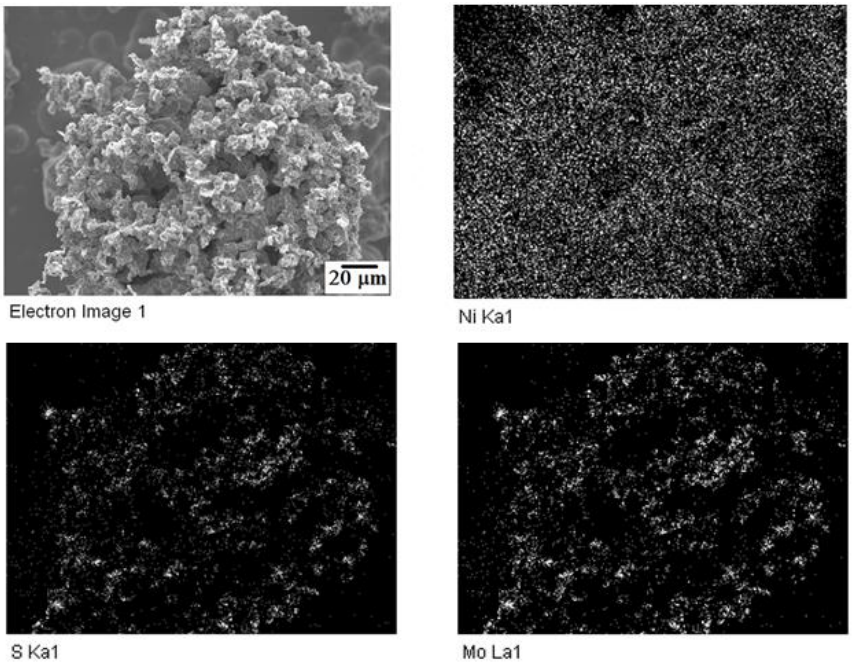

Figure 6.7 EDX mapping of a nodular structure on Ni-MoS_2 deposits

The elemental distributions of Ni, Mo and S are analysed by EDX mapping on a nodule surface (Figure 6.7). The majority of the nodules surface consisted of Ni, while Mo and S are located at concentrated areas where MoS_2 particle adsorptions took place. The adsorbed MoS_2 particles on Ni matrix during electrodeposition are thought to protrude to increase surface roughness and induce increased current densities at protrusion sites, which led to nodular growth for Ni-MoS_2 coating.

6.2 Friction and wear of Ni-MoS_2 coatings

Friction and wear behaviour of Ni-MoS_2 coatings are studied using a reciprocating TE-77 tribometer (Phoenix Tribology Ltd., UK). The atmosphere is controlled for humidity at 30 – 40 % and temperature at 20 – 25 °C. Two types of counterparts are used: AISI-52100 bearing steel roller (diameter 6 mm, length 10 mm), and AISI-52100 bearing steel ball (diameter 6 mm). Other testing conditions are as follows: load 20 N (roller, Hertzian contact pressure 0.16 GPa); load 5 N (ball, Hertzian contact pressure 1.13 GPa); sliding frequency 1 Hz; stroke length 10 mm. Coefficient of friction (friction coefficient) is calculated from the friction force recorded by a pizoelectric transducer.

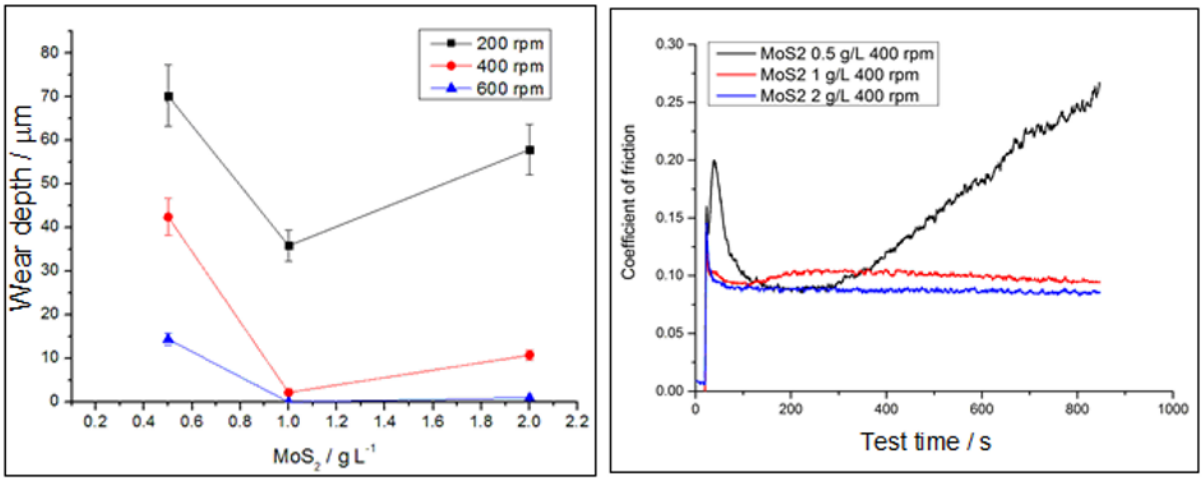

Figure 6.8 Effect of MoS_2 bath concentrations on wear and friction coefficient of Ni-MoS_2 deposit, Load 20 N, frequency 1 Hz

Dry wear tests are carried on the samples and the results are used to compare solid lubrication effect as well as wear resistance (Figure 6.8).

Ni-MoS_2 composite deposits with MoS_2 bath concentrations at or below 0.5 g L^{-1} are found to display early onset of coating failures with rapid increase in friction coefficient after 200s into the test. Samples with higher bath concentrations exhibited low and stable friction coefficient readings at around 0.1 throughout the test duration.

An initial run-in step can be observed in all Ni-MoS_2 deposits where a steep rise of friction coefficient at star-up is followed by its rapid decrease to reach stabilization. A common theory to explain this phenomenon is the difference between static and kinetic friction, in which the former is usually quoted with a higher value. It could be applied to samples that saw the run-in step completed within the first 5 s of the test. But some run-in peaks of friction coefficient are seen to extend over 30 s into the test when the reciprocating motion of the roller has already reached the designated frequency. A trend noticed for samples with lower MoS_2 compositions is that the peak friction coefficient during run-in step is higher and broader than those with more MoS_2 compositions. High friction coefficient is interpreted as an indication of potential high shear force and even high wear rate, while low friction coefficient could be used to indicate effective solid lubricant tribo-film formations.

Upon the onset of the run-in step, the initial contact between the roller and Ni-MoS_2 deposit consisted partially of direct metal-metal contact (Ni against steel) and MoS_2 compositions are confined to adsorption sites where the particles have been incorporated into the nickel matrix. The inter-metallic contacts required a high shear force to move the roller across Ni areas over the virgin Ni-MoS_2 deposit for the load and speed specified, hence the high friction force recorded. As the run-in step

proceeded, more MoS_2 particles are released from freshly worn wear tracks in addition to those already present on the surface, followed by shearing under the roller into a thin tribo-film which provided boundary lubrication for the counterparts.

As the dry wear test proceeded after the run-in step, the amount of MoS_2 available in the deposit determined the rate and also the thickness of the solid lubricant tribo-film formation, which is a dynamic process in competition against the wear rate of the deposit. If the tribo-film formation is not sufficient to cover the wear track, metal-metal contact would persist and the steady state of low friction coefficient could not be maintained for the duration of the test.

Moreover, the nickel debris from deposits with low MoS_2 content could be more abrasive due to the larger inherent sizes and greater numbers of nickel nodules in presence, hence the increase in friction coefficient for certain samples is observed that indicated increasingly higher shear force during the test. On the other hand, high MoS_2 compositions are able to reduce the number and size of nickel nodules on deposit surface that are prone to debris formation during the wear process.

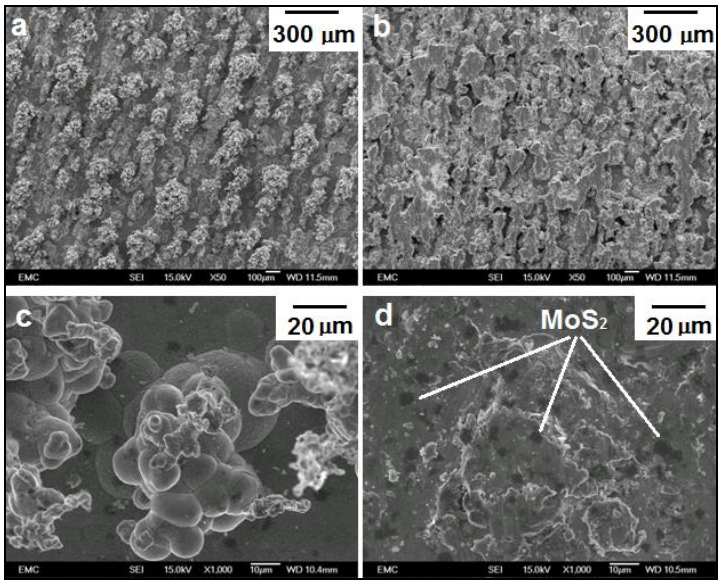

Figure 6.9 SEM images of Ni-MoS_2 coating before (a,c) and after (b,d) wear ([MoS_2] 0.5 g L^{-1}, bath agitation speed at 200 rpm)

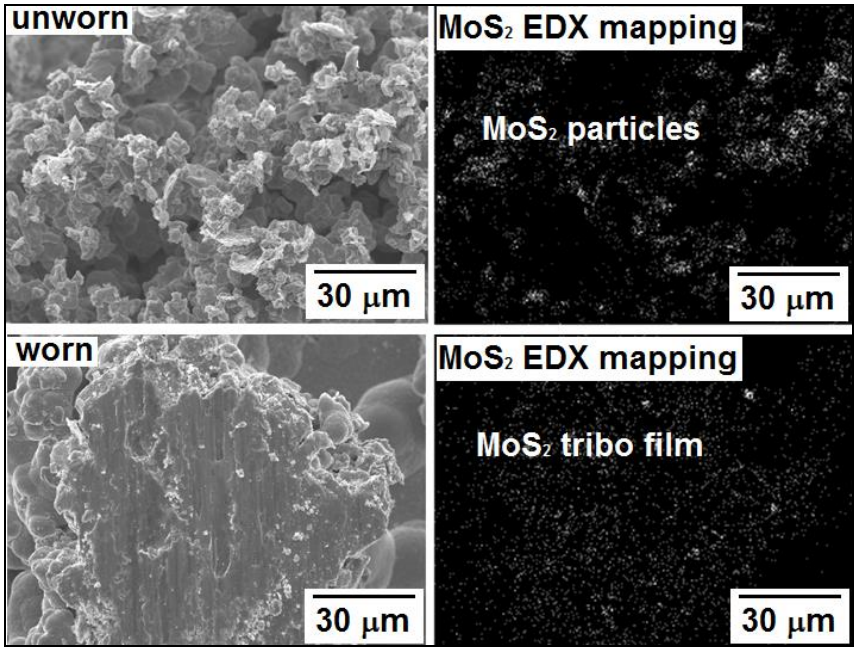

Figure 6.10 EDS mapping of Ni-MoS_2 deposit before and after wear

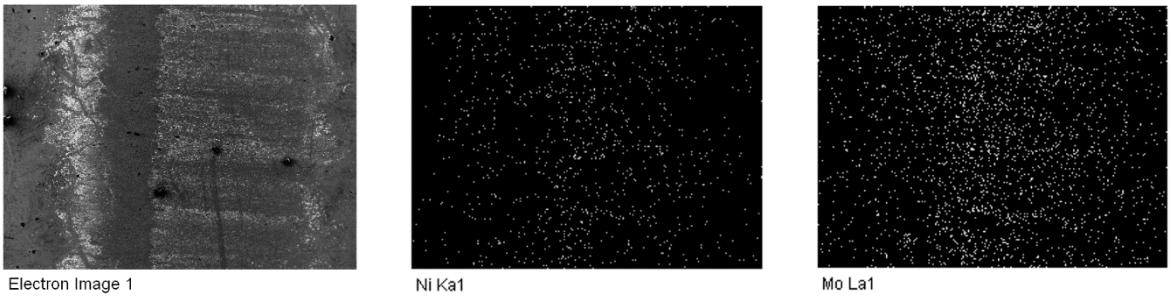

Figure 6.11 EDS elemental mapping on sample roller counterpart after wear test

The wear mechanism of Ni-MoS_2 coatings are examined by SEM and optical microscope. It could be seen that some original rouhness features due to nodular growth have been partially removed on sample wear tracks (Figure 6.9). The low friction coefficient values are attributed to the presence of MoS_2 particles which can be seen as black spots on SEM image at high magnifications (Figure 6.9, c, d). The MoS_2 particles are smeared into tribo films over the wear track and provided lubrication for the deposit (Figure 6.10). The dominant wear mechanism is found to be abrasive wear where material removal ocurred during contact of the soft Ni-MoS_2 composite with the hard bearing steel roller. Material transfer from wear track to the roller is noticed for all samples (Figure 6.11).

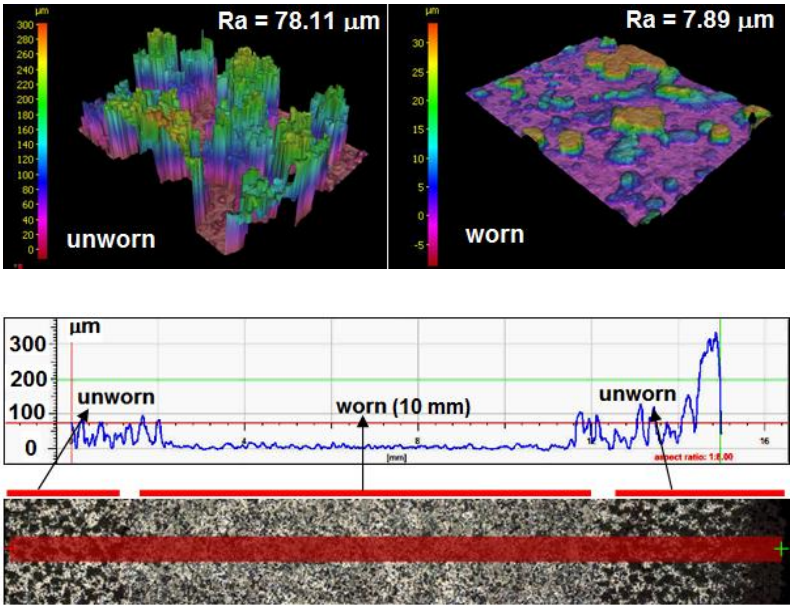

Figure 6.12 Wear track corss section profile of Ni-MoS_2 deposits ([MoS_2] 0.5 g L^{-1}, bath agitaion 200 rpm).

Table 6.1 Effect of bath concentrations on wear depth of Ni-MoS_2 coatings by cross section profile

[MoS_2] / g L^{-1}	Agitation / Rpm	Wear track cross section profile (Load 20 N, 10 mm roller, Hertzian contact pressure *c.a.* 0.16 GPa, test time 900s, stroke length 10 mm, 1 Hz)
0.5	400	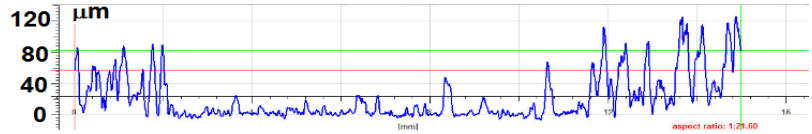
1.0	400	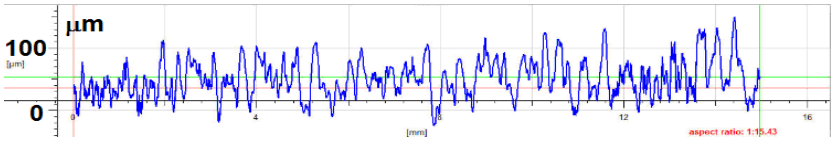
2.0	400	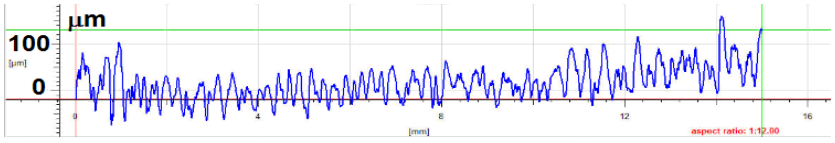

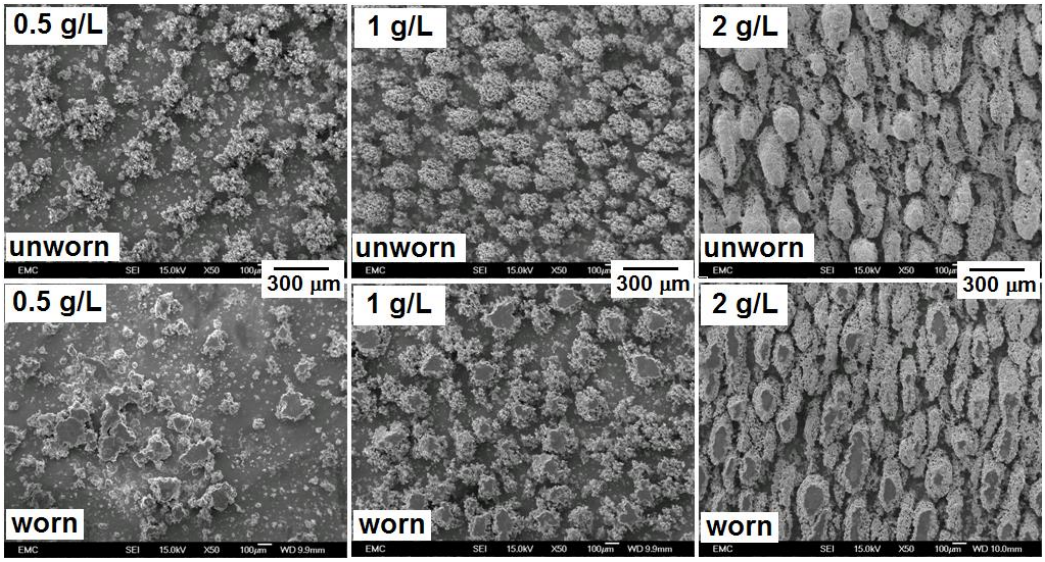

Figure 6.13 SEM scans of Ni-MoS_2 deposits before/after wear (agitation apeed 400 rpm)

Surface roughness measurements on worn and unworn parts of a Ni-MoS_2 coating show change of coating morphology before and after the wear test. The coating profile across the wear track (perpendicular to roller travel direction) is scanned for wear depth analysis, as shown by an example in Figure 6.12.

The effect of MoS_2 bath concentration on coating wear resistance could be analysed by comparing

wear track analysis (

Table 6.1). For MoS_2 bath concentrations at 1 g L^{-1} and 2 g L^{-1}, coating wear depth is signifiantly less than that of 0.5 g L^{-1}. On one hand, the increase in MoS_2 bath concentration is found to increase MoS_2 content in the composite deposits, providing more solid lubricant materials for effective tribo film formation over the wear track. On the other hand, the increase in MoS_2 bath concentration also led to a improved surface coverage due to a more densely packed nodular structure , which are able to offer larger contact areas to evenly distribute the load across the wear track, hence delaying the catastrophic abrasive wear in localised wear conditions (Figure 6.13).

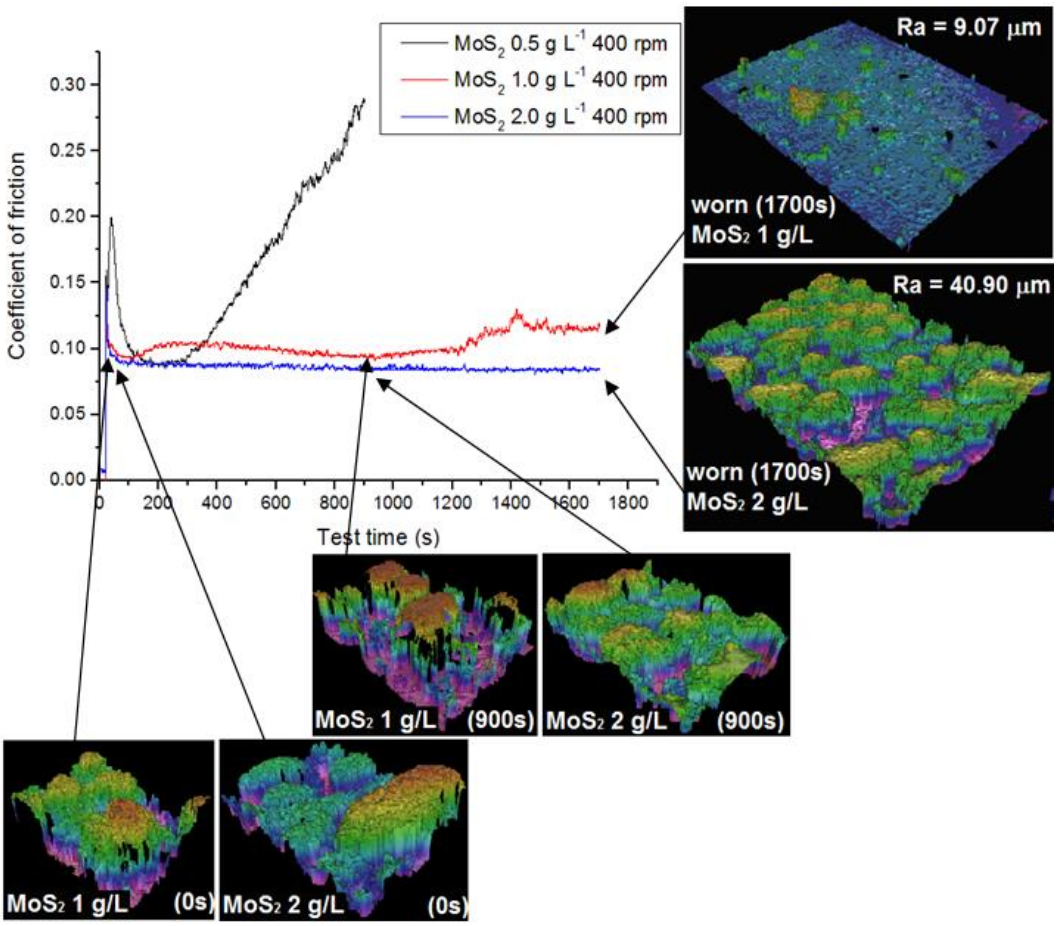

Figure 6.14 Friction coefficient of Ni-MoS_2 deposits with extended test times and corresponding surface profiles

AISI-52100 bearing steel roller (diameter 6 mm, length 10 mm), load 20 N (roller, Hertzian contact pressure 0.16 GPa); sliding frequency 1 Hz; stroke length 10 mm.

The test time of certain samples are extended from 900s to 1700s, where wear resistance of Ni-MoS_2 deposits with higher MoS_2 bath concentrations can be compared (Figure 6.14).

Ni-MoS_2 deposit with MoS_2 at 1 g L^{-1} (400 rpm) is found to exihibit failure onset from after 1200s into the test (reaching complete nodule removal). Surface nodular structures are seen to have been completely removed and the compact layer of nickel is exposed to the wear track. The changing from abrasive wear to adhesive wear is considered to be the mechanism behind friction coefficient increase and fragmentation could be seen on the wear track.

Ni-MoS_2 with MoS_2 at 2 g L^{-1} (400 rpm) is found to remain functional in terms of dry lubrication after 1700s of testing, with sufficient remaining nodular strucures which demonstrated resilience against wear.

6.3 Effect of PTFE bath concentration on Ni – PTFE composite coating

Ni-PTFE deposits are produced in lab using the same set up for Ni-MoS_2 composite deposition in order to provide a benchmark for comparison studies (PTFE 300 nm nanoparticle 1 – 7 g L^{-1}, CTAB 0.05 g L^{-1} – 0.35 g L^{-1}, stirring 200 rpm, current density 5 A dm^{-2}, saccharin 8 g L^{-1}, plating time 60 min).

PTFE content in nickel deposit increased up to a maximum of 30 wt% at PTFE 5 g L^{-1} in bath, followed by an onset of saturation in bath which needed to be confirmed by studies involving higher concentrations. The saturation effect is also observed previously in Ni-MoS_2 deposits although the saturation concentration of PTFE is lower than that of MoS_2. This may be due to many factors, especially the electrodeposition conditions as well as the surface chemistry of the species involved, which may include but are not limited to: bath convection conditions, particle wetting state, particle surface charge, particle size and affinity with surfactants, etc. One particular aspect in the case of PTFE is that it is often regarded as a highly hydrophobic material, and although its dispersion in aqueous solution is achieved via the addition of wetting agents during high shear mixing, the particle is still susceptible to poor wetting states which might lead to particle agglomeration and precipitation, hence the early onset of saturation effect.

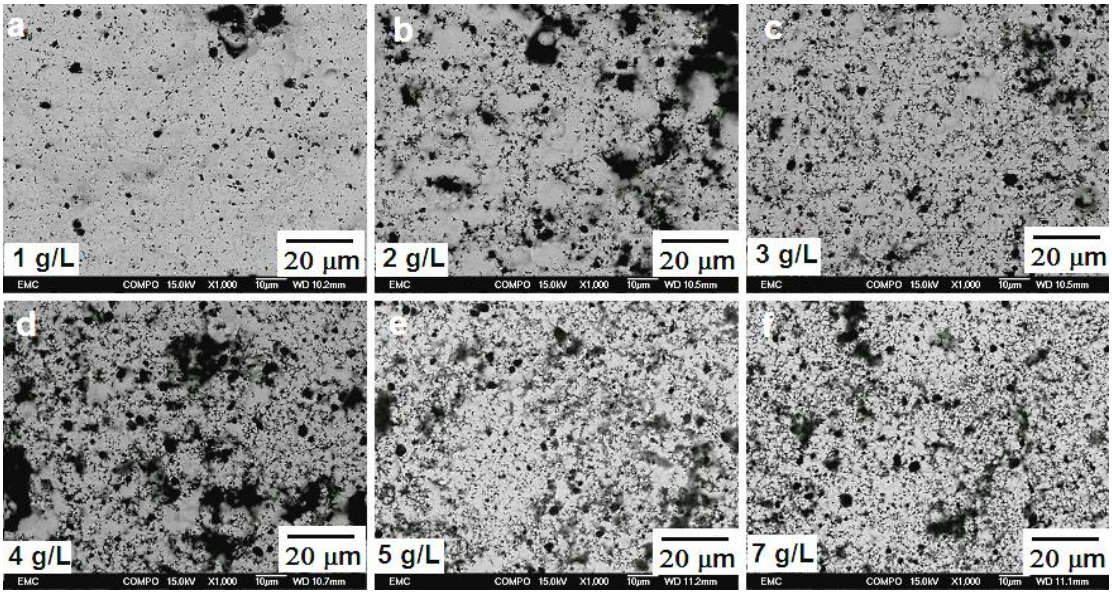

Figure 6.15 Back scattered image of Ni-PTFE deposits with specified PTFE bath concentrations

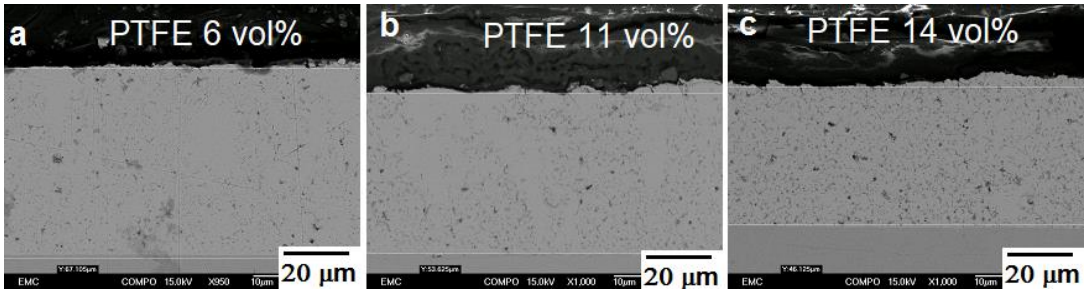

Figure 6.16 Ni-PTFE deposit cross sections with PTFE 2 g L^{-1} (a), 4 g L^{-1} (b) and 7 g L^{-1} (c)

Observation of Ni-PTFE deposits are mainly carried out with back scattered imaging due to the clear contrast between PTFE (dark area) and nickel (bright area). It could be seen from surface (Figure 6.15) and cross section (Figure 6.16) of the deposits that the amount of PTFE content in the deposit is also affected by bath concentrations. The lack of porous nodular structures as seen previously in Ni-MoS_2 coatings indicated a uniform nickel matrix growth which could be due to the low conductivity of PTFE that did not interfere much with current distribution during electroplating. The deposition rate of Ni-PTFE deposits is around 60 µm / hr at current density of 5 A / dm^{-2}, which is in good agreement with nickel deposition according Faraday's law.

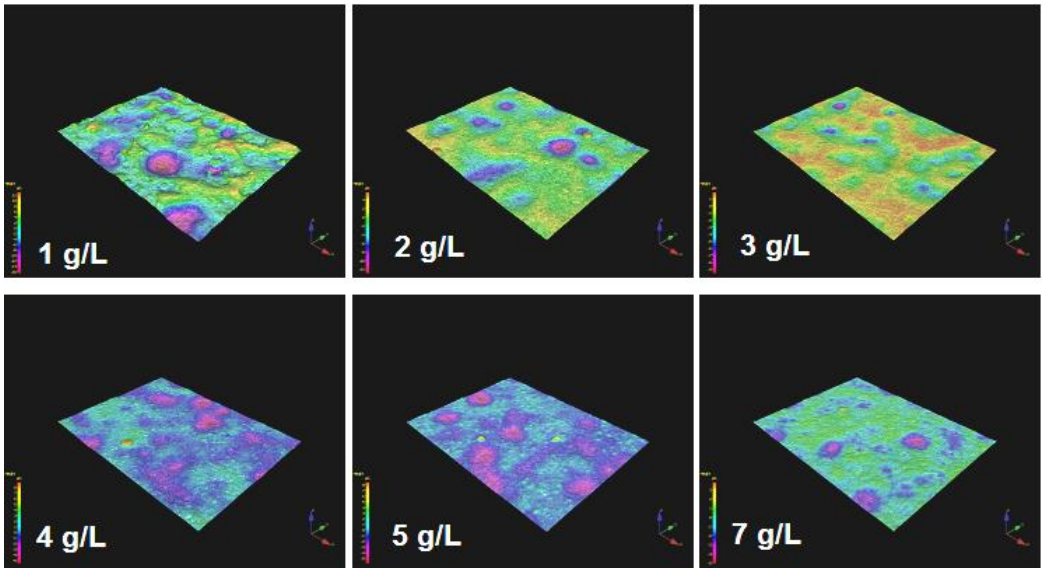

Figure 6.17 Surface 3D reconstruction via optical microscope scan of Ni-PTFE deposits

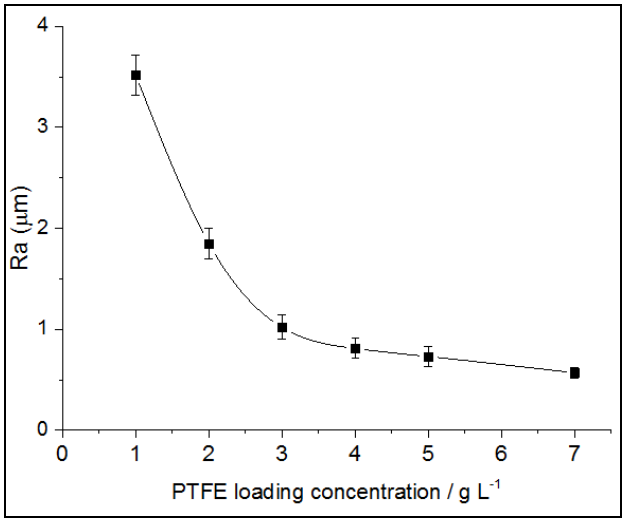

Figure 6.18 Effect of PTFE bath concentrations on surface roughness

Surface morphology analysis is also carried out with optical microscopy. The Ni-PTFE deposit surfaces are of a uniform feature with a dull light grey colour (Figure 6.17). The roughness values are below 3 microns and decreased with increasing PTFE bath concentrations (Figure 6.18). The inhibiting effect of PTFE against rough surface formation is related to the insulating nature of PTFE, which diverted current distribution away from adsorbed particle sites to surrounding metal matrix during electrodeposition.

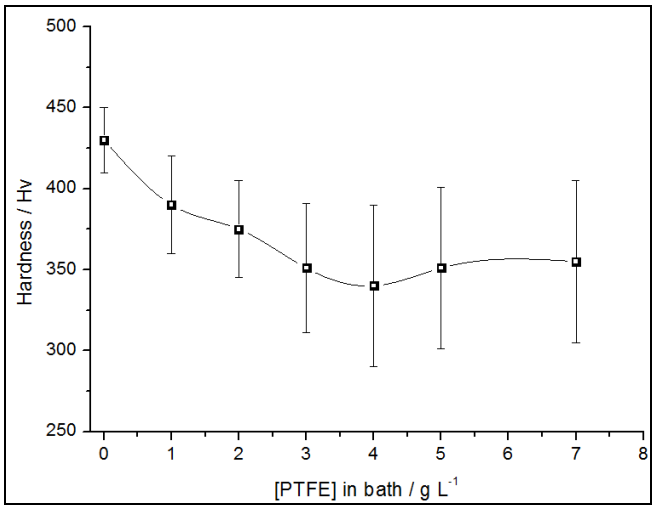

Figure 6.19 Effect of PTFE bath concentrations on hardness of Ni-PTFE deposits

Hardness measurement is carried out with a Vickers hardness indenter, which is made possible for Ni-PTFE composite coatings due to low surface porosity and a consistent coating structure. The load weight is 500 g for 15s. Each sample value is an average of 5 readings. Compared with pure Ni deposit with hardness of around 430 Hv, Ni-PTFE samples saw a gradual drop in hardness by up to 30% with increasing PTFE bath concentrations (Figure 6.19). This is due to the softening effect of more PTFE contents included into the matrix.

6.4 Friction and wear of Ni-PTFE coating

Friction and wear behaviour of Ni-PTFE coatings are studied using a reciprocating TE-77 tribometer (Phoenix Tribology Ltd., UK). The atmosphere is controlled for humidity at 30 – 40 % and temperature at 20 – 25 °C. AISI-52100 bearing steel roller (diameter 6 mm, length 10 mm), load 20 N (roller, Hertzian contact pressure 0.16 GPa); sliding frequency 1 Hz; stroke length 10 mm. Coefficient of friction (friction coefficient) is calculated from the friction force recorded by a pizoelectric transducer.

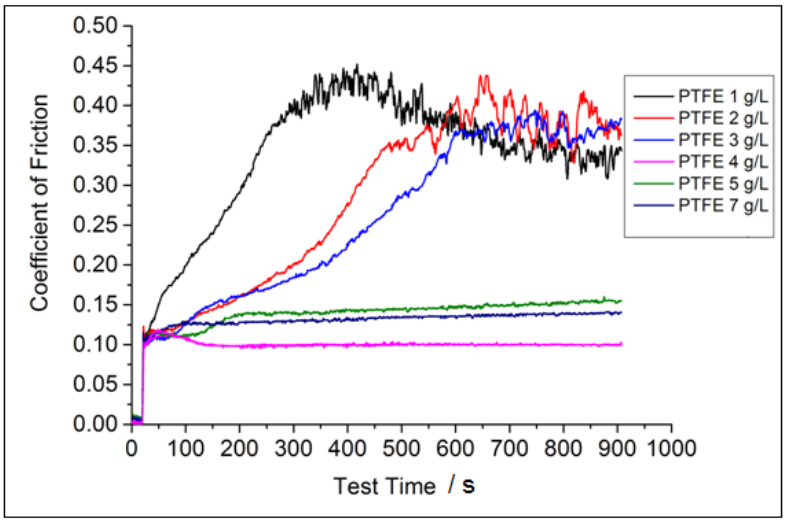

Figure 6.20 Effect of PTFE bath concentrations on coefficient of friction (20 N load, 1 Hz)

Friction and wear tests of Ni-PTFE deposits are carried out in the same way as described for Ni-MoS_2 deposits, where bearing steel roller counterparts are used.

Friction coefficient for Ni-PTFE deposits varied according to PTFE content in the coating (Figure 6.20). From PTFE 1 g L^{-1} to 3 g L^{-1}, the coatings saw a steady increase of friction coefficient from 0.1 up to 0.4 after which they are considered to have been completely damaged. The slope of friction

coefficient increase is reduced as more PTFE content became available in the deposit. For PTFE 4 g L^{-1}, the friction coefficient remained stable at around 0.1 throughout the wear test.

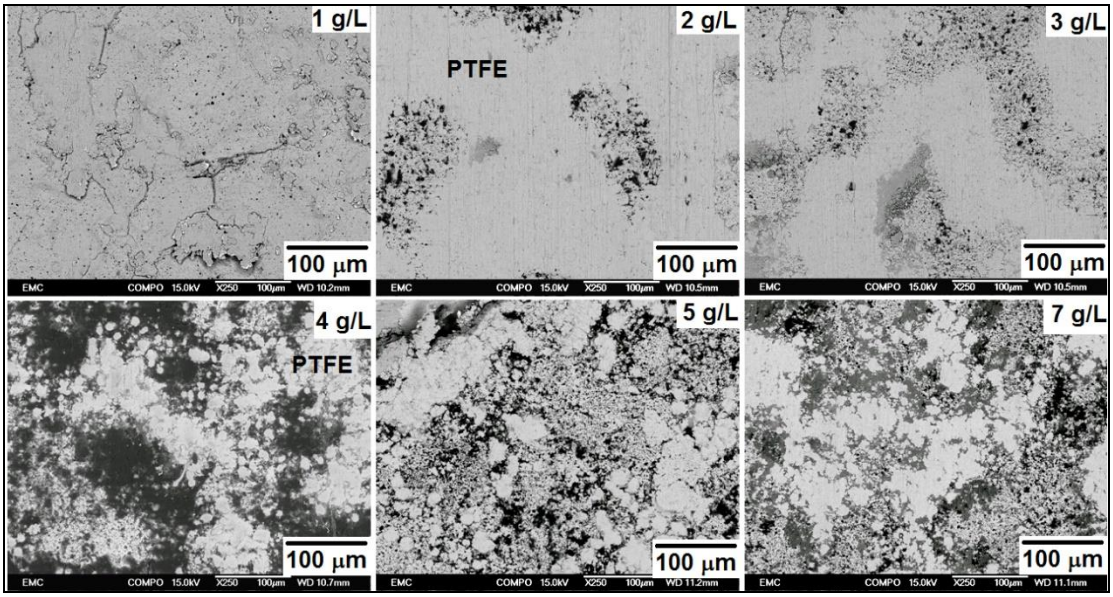

Figure 6.21 BSE image of Ni-PTFE composite wear track with specified PTFE bath concentrations

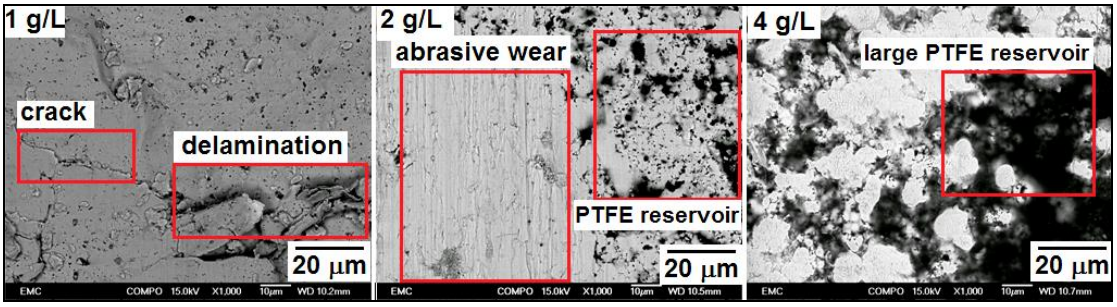

Figure 6.22 BSE image for magnified view of Ni-PTFE deposit wear track details

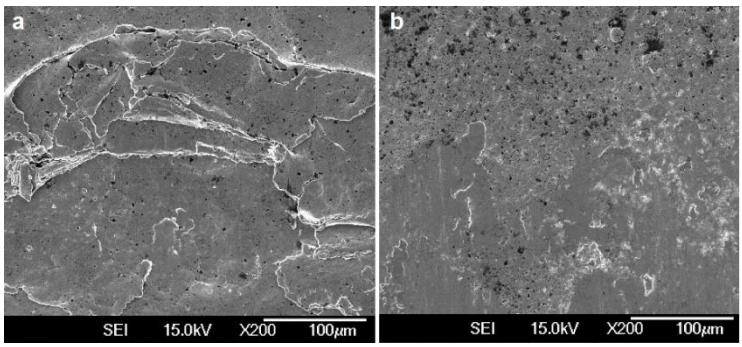

Figure 6.23 SEM on wear of Ni-PTFE: (a) [PTFE] 1 g L^{-1} in bath and (b) [PTFE] 2 g L^{-1} in bath

Surface examination of wear tracks by SEM (Figure 6.21) indicated abrasive wear is the most common mechanism, which could be explained by the fact that the hardness of Ni-PTFE deposit (430 Hv) is only half of that of the roller counterpart (900 - 1000 Hv). PTFE inclusions are exposed on the wear track and are thought to act as reservoirs which released PTFE particles for solid lubrication.

Very little PTFE presence could be detected on deposits with low PTFE bath concentrations, especially for PTFE 1 g L^{-1}, where plastic deformation, wear debris delaminating and surface cracking could be found (Figure 6.22). These are thought to indicate the presence of high shear stress and fracturing of the deposit during the wear test. By increasing PTFE from 1 g L^{-1} to 2 g L^{-1}, the friction coefficient during wear test is reduced (Figure 6.20) and the extent of shear fracture damage is greatly reduced (Figure 6.23).

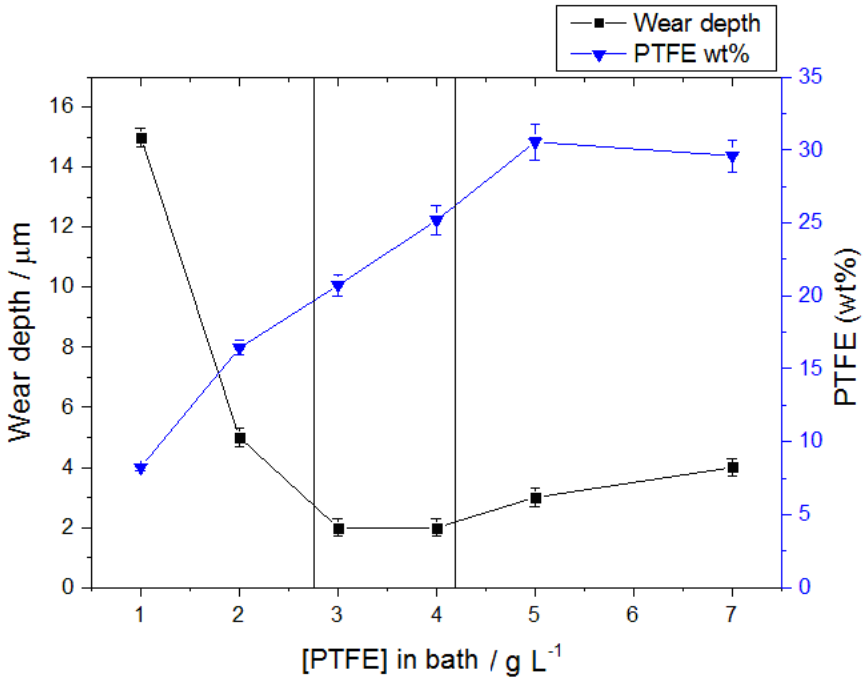

Figure 6.24 Effect of PTFE content in Ni-PTFE deposit on wear depth

The wear track cross section profiles are examined by optical microscope and different wear track depth are observed for the Ni-PTFE deposits (Figure 6.24). The most severe wear damage is seen for PTFE 1 g L^{-1} where the average wear depth is almost 30% of the coating thickness, which matched the observation of extensive wear seen under SEM. From PTFE 1 g L^{-1} to 4 g L^{-1}, the average wear depth is greatly reduced by higher PTFE contents. From PTFE 4 g L^{-1} to 7 g L^{-1}, average wear depth is suddenly increased by almost 50 % from 2 microns to 4 microns. Friction coefficient readings for these deposits also saw a 20-25% increase from PTFE 4 gL^{-1}, although no steep increase of friction

coefficient is observed. High PTFE content is thought to soften the nickel matrix to a certain extent that the roller counterpart could deform the contact area and penetrate more deeply into the wear track. The increased frictions are created by the deep ploughing movement of the roller to remove larger volumes of materials in front of its sliding direction, leading to more wear loss.

6.5 Summary and comments

The effect of MoS_2 particle concentration in bath on the structure and surface morphology of Ni-MoS_2 composite coating is studied. In general, increasing MoS_2 concentration in bath could lead to increased particle content in the coating up to a saturation point at around 20 g L^{-1}, but the coating deposit structure is too porous and fragile for practical tribological application over a wide MoS2 concentration range. For lower particle bath concentrations at or below 2 g L^{-1}, Ni-MoS_2 composite coating show improved friction reduction and wear resistance, which are related to suitable MoS_2 content and better surface coverage of the composite deposit. The optimal particle concentration in bath is narrowed down to 1 – 2 g L^{-1} for the best tribological performance of a single layer Ni-MoS_2 coating produced for this study. Therefore, process control over particle concentration in bath is viable for this application, although the recommended MoS_2 concentration is limited to a small range as a result of coating structural deterioration at higher particle contents.

In comparison, the friction and wear behaviour for Ni-PTFE samples are studied with changing PTFE bath concentrations. Higher PTFE bath concentrations could be applied for composite electrodeposition without compromising coating structural integrity. A balance between solid lubrication and wear resistance could be achieved by controlling PTFE content in the coating.

The major difference between Ni-PTFE deposits and Ni-MoS_2 deposits are coating morphology and structures. The compact structure of Ni-PTFE coatings allowed more precise micro characterisation of particle content levels via optical microscopy. Microhardness measurements also correlated coating mechanical property to the changing particle content. The Ni-PTFE coatings show a similar level of friction reduction to Ni-MoS_2 coatings, indicating a promising potential for continuous development of Ni-MoS_2 composite electrodeposition as an alternative self-lubricating surface coating technology.

The author notes here that the study for Ni-PTFE coatings is to provide a quick reference for comparing the morphology, friction and wear between Ni-PTFE coating and Ni-MoS_2 coating under similar test conditions as different test set up may give different friction data. There is no further attempt to optimise the PTFE coating in this study once satisfactory friction results are achieved. The aim is to measure particle conductivity and for the first time directly compare the surface morphology and cross section structures between Ni-MoS_2 and Ni-PTFE coatings when both demonstrate observable self-lubricating property. Ni-PTFE composite coatings have been widely applied

commercially via electroplating, e.g., on cylinder liners for performance engine designs, hence the urgency to look for differences in Ni-MoS_2 coatings to justify whether it could be a suitable candidate for alternative self-lubricating composite coating.

Chapter 7 Process control of bath agitation

Bath agitation is necessary during electroplating to provide electrolyte convection and main composite particle suspension without which the coating composition will become less uniform as the plating proceeds due to particle agglomeration and sedimentation. A common magnetic stirring process is adopted in this study due to its convenience in lab and consistency with most literature report so far. The purpose of this study is to determine if the effect of agitation speed can be manipulated to produce enhanced composite Ni-MoS_2 coatings in tribological tests.

7.1 Effect of bath agitation on Ni-MoS_2 coating composition and structure

Agitation is another important factor to be considered for electrodeposition, which controls mass transport for the convective–diffusion of suspended particles in the bath. A screening test is carried out for MoS_2 0.5 - 2.0 g L^{-1} with stirrer agitation from 100 – 1000 rpm (5 mm diameter, 15mm long, PTFE-coated stirring rod, CTAB 0.1 g L^{-1}, current density 5 A dm^{-2}, plating time 60 min). MoS_2 content (wt.%) on coating surface is obtained by EDS scan (Figure 7.1), which show an increase from 1 wt% to 17 wt% over 0 – 600 rpm, followed by a sharp decrease to 1 % at 1000 rpm. Cross section of the coatings from optical microscopy show coating structures containing various levels of particle inclusions in agreement with EDS analysis (Figure 7.2). At 100 rpm where minimum agitation is provided in a beaker, there is also a lack of effective convection flow to maintain particle suspension in bath, which led to some particle precipitation and agglomeration. From above 100 rpm to 600 rpm agitation speed, particle transport to the cathode surface is via convective-diffusion, which saw a combination of more effective diffusion and convection for increased particle inclusion rates. Particle suspension in bath is also improved over the increasing agitation speed, maintaining a sufficient concentration of dispersed particles and inhibiting the onset of particle agglomeration. From 800 rpm onwards, lower Mo wt.% in coating is oberved for higher agitation rates.

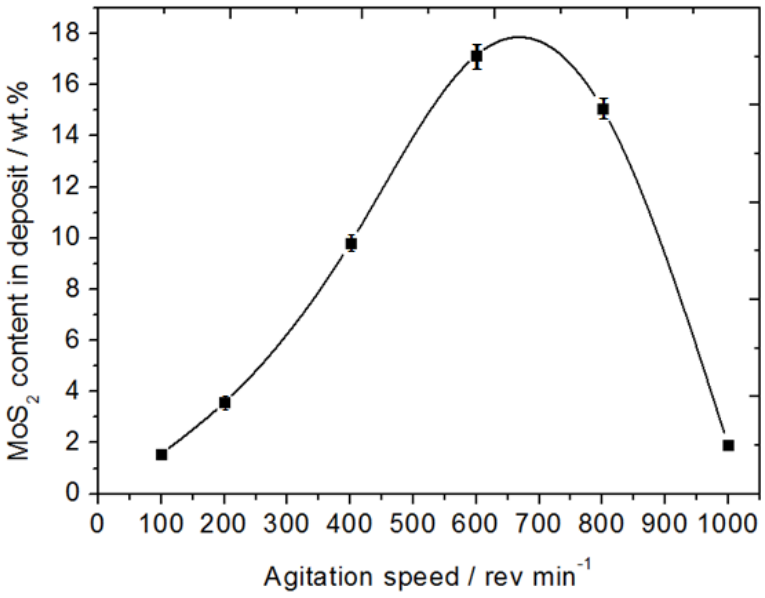

Figure 7.1 Effect of agitation speed on MoS_2 content in composite coating, MoS_2 2 g/L

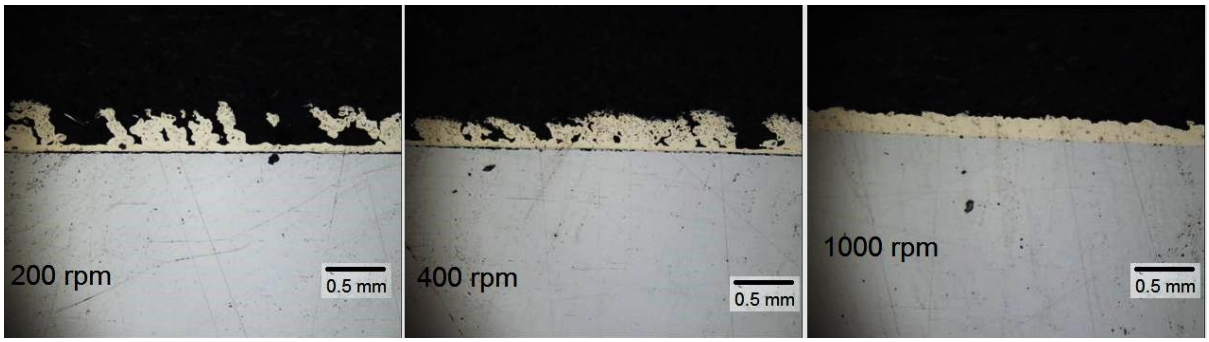

Figure 7.2 Cross section images of coatings from selected bath agitation rates

The observed relationship of codeposited particle content with agitation rate has also been described in another study[176], and it is observed that maximum particle codeposition could take place at a certain range of agitation rates, where particle covective-diffusion towards substrate is at its optimum conditions. Beyond this range, particle removal from cathode surface could take place more rapidly before inclusion could took place due to the vigorous hydrodynamic turbulance from excessive agitaion. Infact, for deposition at 1000 rpm, the particle level in the coating is barely detecable, and the coating cross section looked very similar to pure nickel coating. It has been proposed that a residence time is required for the particle to stay on surface of cathode in order for it to be incorporated into the growing metal matrix[60]. The shear turbulance from high speed agitation would increase both the particle removal speed as it exitsfrom cathode vicinity, preventing successful particle inclusion into the growing metal matrix.

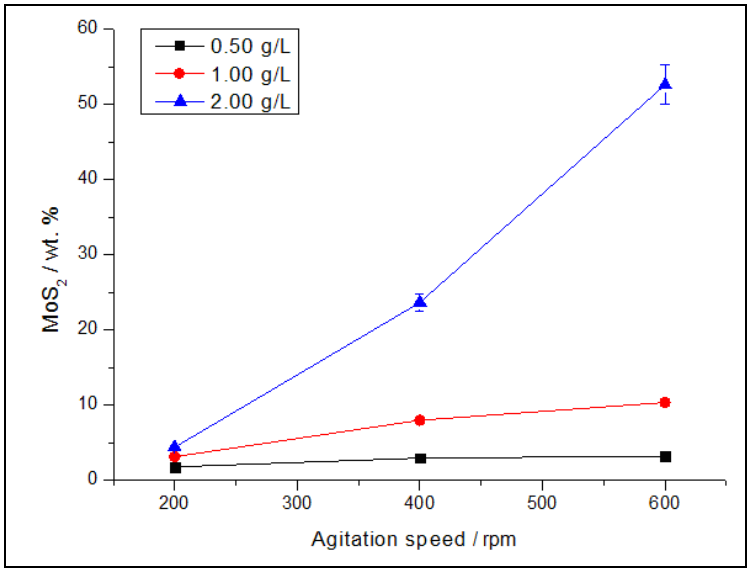

Figure 7.3 Effect of agitation speed on MoS_2 content (wt.%) in Ni-MoS_2 coatings, MoS_2 0.5 – 2 g/L

For Ni-MoS_2 coatings produced with MoS_2 bath concentrations at 0.50 g L^{-1}, 1.00 g L^{-1}, and 2.00 gL^{-1}, selected agitation speeds at 200, 400 and 600 rpm are studied to cover the main effective convective-diffusion region for particle mass transport. For lower MoS_2 concentrations, an increase for MoS_2 wt.%with increasing agitation speeds is observed Figure 7.3.

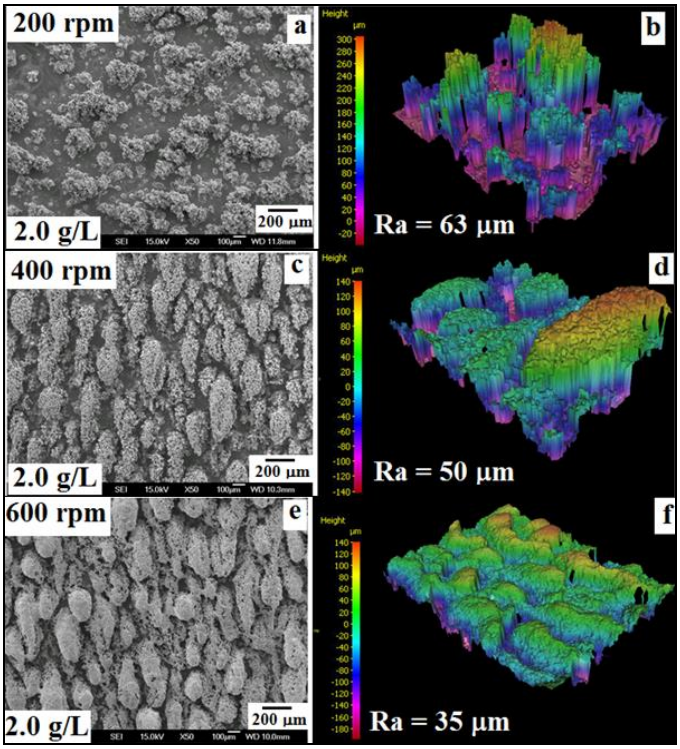

Figure 7.4 (a, c, e) SEM scan and (b, d, f) optical microscope scan of Ni- MoS_2 coating surfaces with MoS_2 bath concentrationsof 2.00 g L^{-1} for agitation speeds at 200 – 600 rpm.

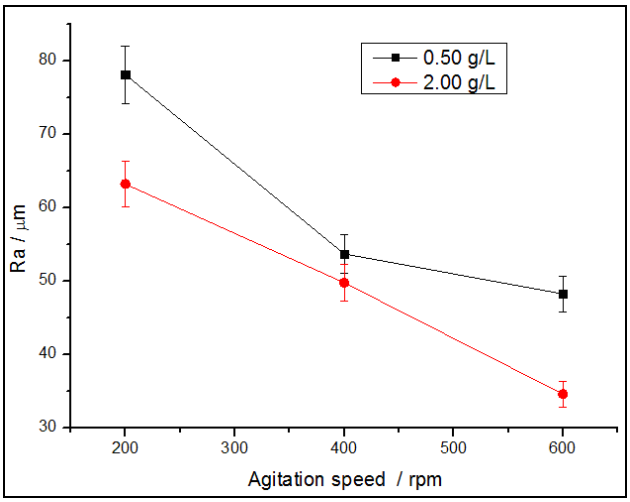

Figure 7.5 Influence of agitation speed on the average roughness (Ra) of Ni-MoS_2 coating surfaces

Ni-MoS_2 nodule numbers and sizes are found to increase with agitation speeds by SEM and optical microscope scans (Figure 7.4), which could be related to the improved MoS_2 incorporation into the coating. A gradual decrease of average surface roughness is observed over increasing agitation speeds (Figure 7.5). This could be due to less spacing between the nodules as they expand in sizes for more

surface coverage. Also, stronger hydrodynamic convections of the bath will serve to flatten the surface features of the nodules by removing loosely held protrusions. The advantage of applying agitation control is that it could achieve higher particle contents in the coating and reduce coating surface roughness in the meantime, whilst the higher particle bath concentration could also lead to higher particle contents in the coating but with more porous and fragile coating structure.

7.2 Effect of bath agitation on friction and wear of Ni-MoS_2 coatings

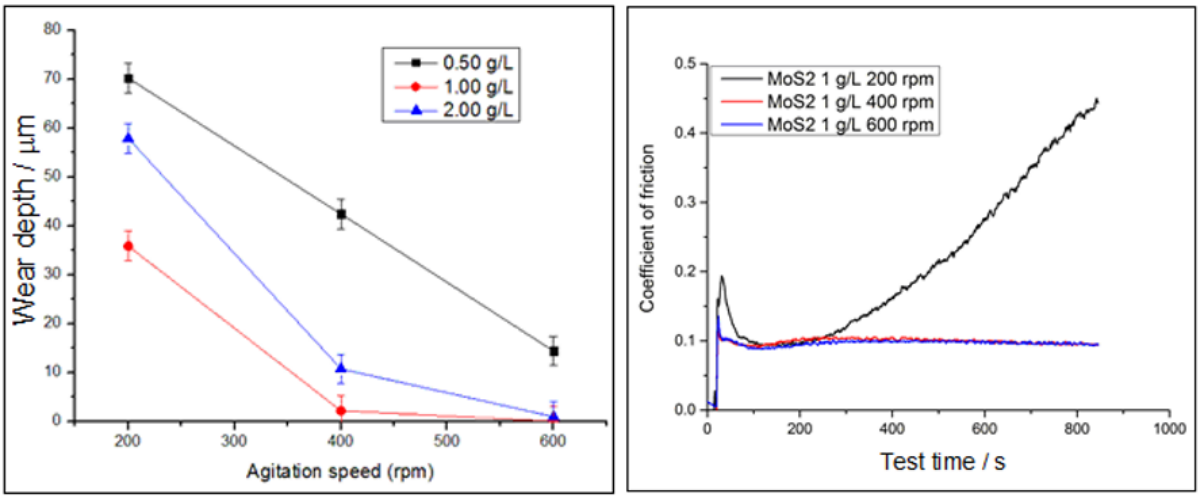

Figure 7.6 Effect of bath agitation speed on the wear and friction coefficient of Ni-MoS_2 deposits with selected particle bath concentrations (AISI-52100 bearing steel roller (diameter 6 mm, length 10 mm), load 20 N (roller, Hertzian contact pressure 0.16 GPa); sliding frequency 1 Hz; stroke length 10 mm.)

Friction and wear tests are carried out at same conditions as described for particle bath concentration study. Coefficient of friction is plotted against wear test time at each particle bath concentration level to reflect tribological behaviour of composite coatings (Figure 7.6).

At 200 rpm stirrer agitation, the friction coefficient of the coatings is around 0.1 right after the initial run-in period. A rapid increase of friction coefficient is observed for coatings with MoS_2 bath concentrations at 1.00 g L^{-1} after 100 s into the test time, and the tests are terminated at a cut-off point of 0.4 friction coefficient, when the coating is considered to have failed in providing sufficient self-lubrication.

At 400 rpm and 600 rpm stirrer agitation, the friction coefficient of Ni-MoS_2 coatings remained at around 0.1 after the run-in period until end of tests.

Table 7.1 Effect of bath agitation speed on wear depth (cross section profile) of Ni-MoS_2 deposits

[MoS_2] / g L^{-1}	Agitation / Rpm	Wear track cross section profile (Load 20 N, roller, Hertzian contact pressure *c.a.* 0.16 GPa, test time 900 s, 1 Hz, stroke length 10 mm)
1.0	200	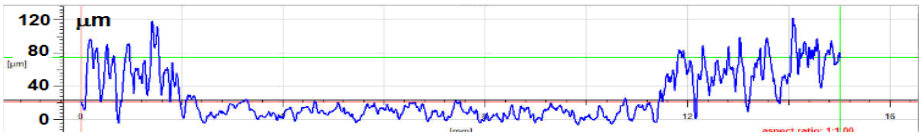
1.0	400	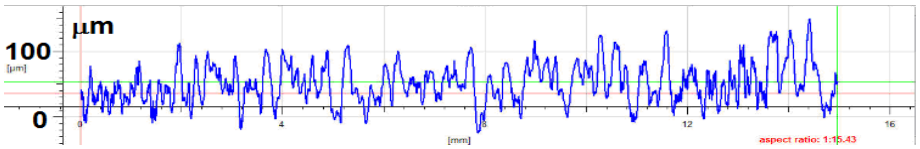
1.0	600	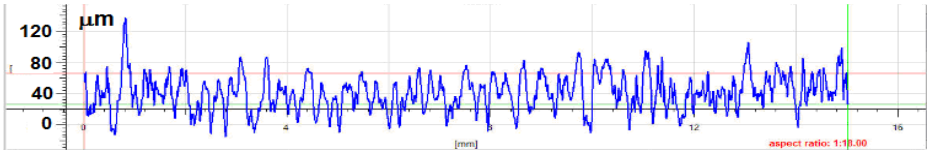

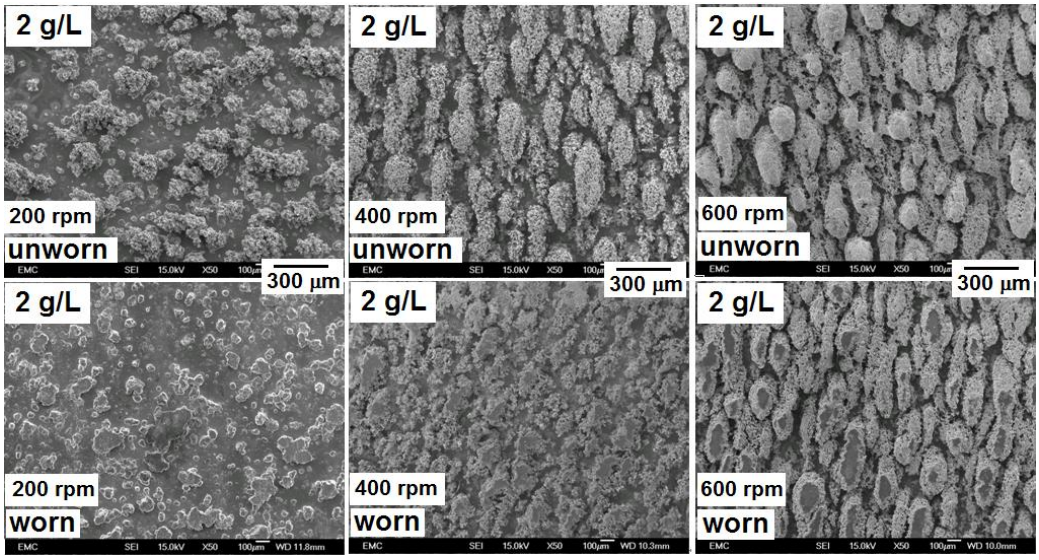

Figure 7.7 SEM scans of Ni-MoS_2 deposit before/after wear with baht agitation variations

Wear depth is further reduced by higher agitation speeds in bath and is least pronounced for MoS_2 1 and 2 g L^{-1} at 600 rpm (Figure 7.6). These are confirmed by wear track scan under optical microscope (Table 7.1) and SEM (Figure 7.7). Low agitation speed for Ni-MoS_2 deposit led to lower MoS_2 content and less coating surface coverage. The nodules are subjected to localised wear that could lead to concentrated load and higher contact pressures, resulting in extensive abrasive wear that saw high

removal rates of the surface features. In contrast, improved surface features could be found in Ni-MoS_2 deposits with higher agitation speeds, which produced uniform surface coverage with more abundant MoS_2 contents, hence small extent of abrasive wear is only observed on top of the coating.

7.3 Development of gradient composite deposits via agitation control

7.3.1 Gradient Ni-MoS_2 composite coating via agitation control

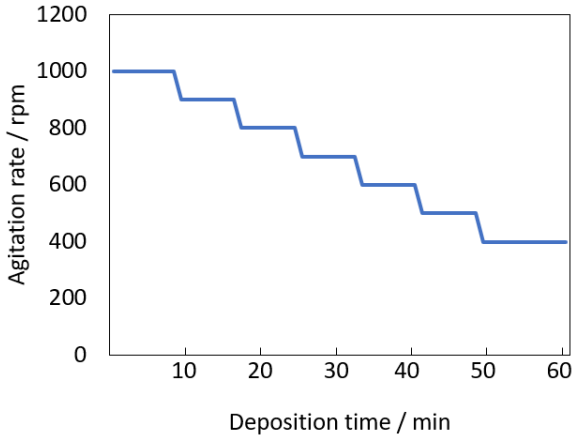

Figure 7.8 Process control for stepped agitation rate during Ni-MoS_2 composite electrodeposition (MoS_2 4.0 g L^{-1}, CTAB 0.2 g L^{-1}, saccharin 2 g L^{-1}, current density 5 A dm^{-2}, plating time 60 min)

A gradient deposit with varying composition throughout the coating thickness may offer several advantages, especially in terms of its tribological performances. This strategy is applied in some applications where an adherent film is required to improve bonding with the substrate, and low particle content is desired in the initial layer of the coating. The changing composition of the coating layers could also see more tribological functions being addressed by the top layer where the coatings meet the counterparts, and the lower layers of the coating would play more structural reinforcement roles to improve the overall load bearing capacity of the composite coating.

A sample gradient layer coating is produced from a bath containing higher particle concentration at 4 g L^{-1} MoS_2, allowing a wider range of changing MoS_2 content in the composite deposit, which is realised by the simple method of controlling bath agitation speed while other process parameters are kept constant. The agitation rate is started from 1000 rpm and stepped down by 100 rpm every 8 minutes until 400 rpm is reached and held for a total plating time of 60 minutes at 5 A dm^{-2} (Figure

7.8). The initial high agitation speed is designed to give a strong hydrodynamic environment that would lower the MoS_2 content in the deposit layer covering the substrate. Although same could be achieved by low or no agitation, the idle time would be too long and could lead to particle agglomeration or precipitation. The following decrease of agitation speed towards the optimum range for particle codeposition would then lead to a gradual increase of MoS_2 content towards the surface of the final deposit. A reference of a single layer Ni-MoS_2 composite deposit with MoS_2 4 g L^{-1} in bath is also produced with agitation speed at 400 rpm for 60 min.

There are other ways of controlling the particle content in the deposit, such as changing current density, particle concentrations in the bath and so on. In comparison with other methods, changing the agitation rate is easy to control and did not require altering the bath composition or slowing down the deposition rate of the coating, hence it could be a most facile way of process control to produce layered composite coating.

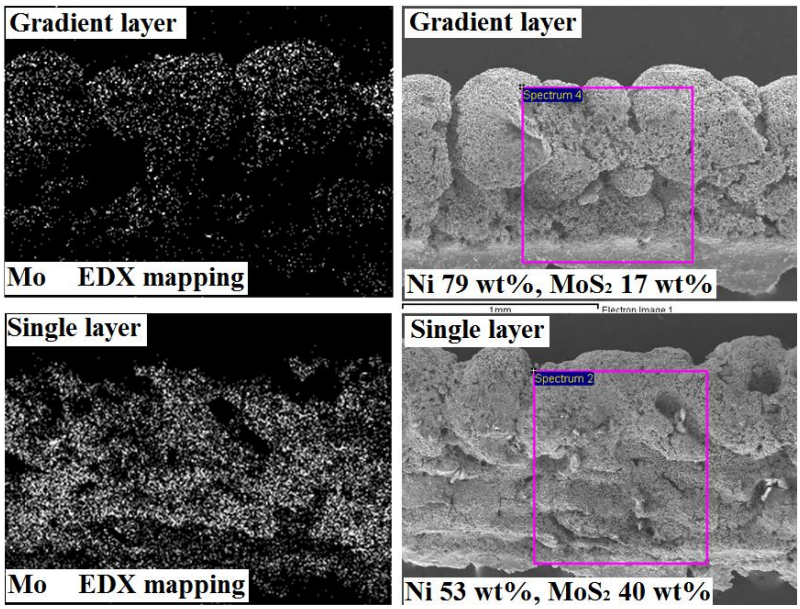

Figure 7.9 EDS mapping and SEM for cross section of gradient and single layer Ni-MoS_2 deposit

EDS mapping show that MoS_2 content in the gradient deposit is found to change from very low content near the substrate (image bottom) to relatively high content on the coating surface (image top, Figure 7.9). In contrast, MoS_2 content is uniformly distributed in the single layer Ni-MoS_2 deposit. Overall MoS_2 content throughout the thickness is 17 wt.% for the gradient deposit, and 40 wt.% for the single layer deposit. These observations indicated that it is successful to change MoS_2 distribution in the deposit via control of the agitation conditions.

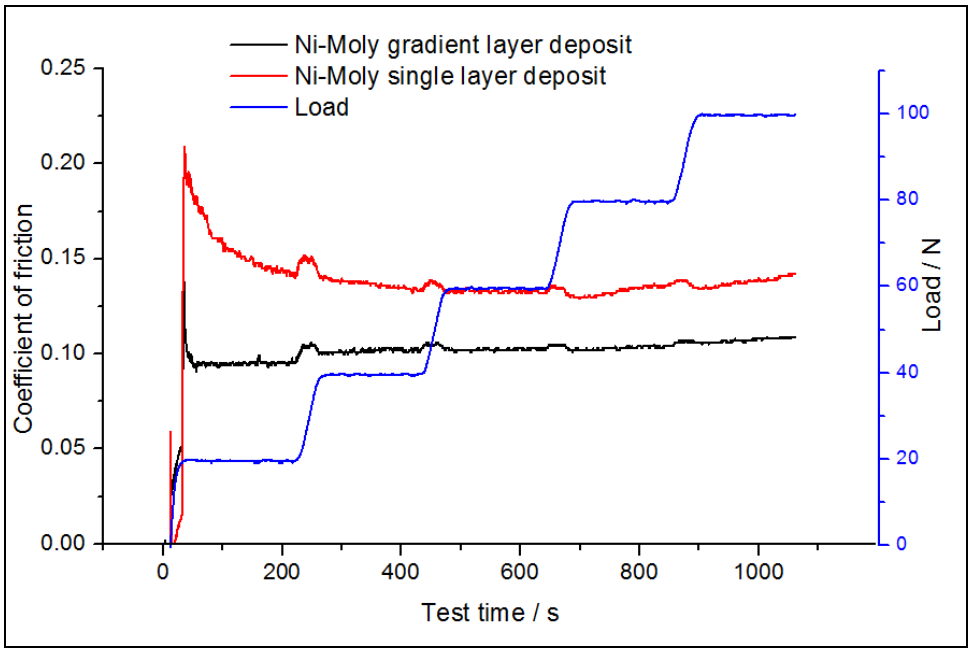

Figure 7.10 Coefficient of friction of Ni-MoS_2 deposits in load ramp test (load 20 – 100 N, AISI-52100 bearing steel roller (diameter 6 mm, length 10 mm); sliding frequency 1 Hz; stroke length 10 mm.)

Friction and wear tests are carried on the deposits with load ramping from 20 N to 100 N (Figure 7.10). The single layer deposit show coefficient of friction between 0.12 and 0.15, which is higher than those of coatings from baths containing optimised MoS_2 concentrations at lower levels. This is expected as higher particle contents in the coating would result in more porous and fragile structures, reducing the tribological performance of a single layer coating.

However, coefficient of friction for the gradient deposit is stabilised at about 0.1 with only a slight increase under the increasing load. The small friction coefficient of the gradient deposit is attributed to the high nickel content layers beneath the deposit surface which provided a strong support for the solid lubricant film. The flow of MoS_2 particles is restricted to the contact area followed by effective shearing between the wear counterparts to achieve optimum lubrication. For the single layer deposit, high MoS_2 content throughout the thickness reduced the hardness of the deposit, and a larger contact area is created with less contact pressure for shearing of MoS_2 particles. The formation of a MoS_2 lubricant film is less effective and removal of MoS_2 particles took place due to the roller counterpart ploughing deep into the deposit. The coefficient of friction for the single layer deposit is reduced to minimum by increasing the load from 20 N to 60 N, when a larger contact pressure could be achieved.

The gradient Ni-MoS_2 deposit is shown to be superior in terms of load bearing and solid lubrication compared to the single layer coating.

Chapter 8 Process control of MoS_2 Particle dispersion in bath preparation before electrodeposition

8.1 Introduction

A major challenge for electrodeposited Ni-MoS_2 composite coatings is that MoS_2 particles are hydrophobic and tend to form large agglomerates in the aqueous nickel-plating bath. This prevents a uniform particle suspension being achieved and may negatively affect particle incorporation into the nickel matrix, resulting in an increased particle concentration being required. Unstable particle dispersion can also result in fragile and porous deposits, which are prone to suffer from abrasive wear and corrosion. Studies for composite electrodeposition have often used magnetic stirring with surfactants for particle dispersion due to the convenience of the technique for an easy set-up[60]. However, magnetic stirring can be time-consuming with reports quoting a stirring time for MoS_2 particle dispersion overnight[173], which is impractical for industrial application. Furthermore, its effectiveness in particle dispersion remains unclear. From the literature survey summarised in Table 1, some of the composite coatings showing the lowest coefficient of friction reported are produced from particle dispersions via less conventional methods, such as ultrasonication of the electrolyte[182] or high-energy reaction ball milling of particulates before suspension in the bath[174]. Studies on different composite coatings have pointed out that magnetic stirring may not disperse other types of particles (TiO_2, SiC, WS_2, BN) effectively[126,183,184]. Defects such as non-uniform particle distribution and porous coating structures as a result of particle agglomeration can significantly lower the tribological performance of the composite coatings. Therefore, it is very important to identify facile and effective particle dispersion methods other than magnetic stirring for successful electrodeposition of composite coatings.

Ultrasonication has been frequently reported as a means for particle dispersion both before and during composite electrodeposition, which is summarised in a review[142]. The ultrasonic source may be a custom-made transducer for industrial trials, and an ultrasonic bath or probe for small bench operations. The outcome of ultrasonication may be influenced by ultrasonic bath/probe set-up, sample position, ultrasound frequency and power density at the sample surface, etc. Under suitable conditions, ultrasonication may provide a more effective particle dispersion than magnetic stirring, enabling more uniform composite coatings to be achieved. The drawbacks of ultrasonication may include noise pollution and heating of the bath. Adequate ear protection must be provided when working in the presence of strong ultrasonic sources and an additional cooling system for heat management may add to the cost of the operation.

Table 8.1 Summary of the Ni-MoS_2 composite coatings from literature

Composite coating	Deposition technique	MoS_2 particle size / μm	Particle concentration / g dm^{-3}	Particle dispersion method	Particle content in the coating	Coefficient of friction (dry)	Reference
Ni-MoS_2	direct current plating	1.44, 5.15	5 - 30	magnetic stirring	up to 14.3 wt% by EDX	0.40 - 0.72	187
Ni-Co-MoS_2	direct current plating	0.01	1	magnetic stirring	not reported	0.16 -0.23	119
Ni-P-MoS_2	direct current plating	1 – 4	3 - 20	ultrasonic bath	2 - 7.9 wt% by EDX	0.05 - 0.45	186
Ni-W-MoS_2	reverse pulse plating	3	0 - 2	magnetic stirring	0 - 45 at% by EDX	0.1 - 0.4	121
Ni-MoS_2-Graphite	brush plating	0.3	30	High-energy reaction ball milling	not reported	0.05-0.25	174
Ni-P-MoS_2	electroless plating	4	2.4	magnetic stirring	not reported	0.27-0.78	185

An alternative mechanical agitation method to aid particle dispersion during bath preparation is high-shear mixing. High-shear mixing is often used to produce bulk mixtures of normally immiscible components, such as pigments in paint coatings. Such mixing has shown the ability to achieve very stable dispersions that would otherwise be difficult by commonly used stirring procedures. A high-shear mixer generates large fluid velocity differences, hence shear, around a high-speed rotor blade. The mixing head also contains a stator with a close-clearance gap from the rotor, forming an extremely high-shear zone for materials exiting the rotor. Important parameters for high-shear mixing operations are mixing speed and time. A study on the effect of high-shear mixing speed and time on GNP/epoxy composites[188] found that a high mixing speed (9000 rev min^{-1}) and a long shear-mixing time (2 h) could reduce the size of particle agglomerates by almost 70% compared to mixing at lower speeds (1000 - 7000 rev min^{-1}). The potential for applying high-shear mixing to particle dispersion in composite electrodeposition is promising but has never been systematically studied. This study pioneers in using high-shear mixing as an alternative agitation method for particle dispersion in electrodeposition of robust and self-lubricating Ni-MoS_2 composite coatings.

8.1.1 Mechanism of high Shear mixing

High shear mixers generate very high shear forces between different parts of the mixture in opposite parallel directions to incorporate them together[188, 189]. They are characterised by a high-speed rotor blade capable of speeds up to 20,000 – 10,000 rpm which exerts a powerful suction, drawing liquid and solid materials upwards into the centre of the work head. The materials are driven by centrifugal force towards the periphery of the work head where they are subjected to a milling action in the precision-machined clearance between the ends of the rotor blades and the inner wall of the stator (*c.a.* 100 microns). This is followed by intense hydraulic shear as the materials are forced, at high velocity, out through the perforations in the stator and circulated into the main body of the mix. High shear mixer blades undergo very little wear when placed in soft mixtures, the only cost of the process comes from the energy consumption to drive the high-speed motor for the blade. Depending on the size of the mixer, bench top ones operate a blade head of as small as 1 cm in diameter which can be easily powered by a room socket. The work heads are interchangeable at low costs and can vary in shape to process different volumes of mixtures. The high-shear mixer in this study is designed for a multiple pass of materials through the rotor-stator array during turbulent mixing, creating a higher number of shear events that may result in a very narrow particle-size distribution.

The resulting coating from high-shear dispersed particles also show one of the lowest coefficients of dry friction reported for electrodeposited Ni-MoS_2 composite coatings. The aim of this work is to study the effectiveness of high-shear mixing for MoS_2 particle dispersion *prior* to composite electrodeposition when compared to magnetic stirring. A modified Watts nickel bath containing wetting and levelling additives is used. Surface microstructures and cross-sectional analysis of the

composite coatings are presented. Tribological properties of the composite coatings in terms of friction and wear are also investigated.

8.2 Experimental details

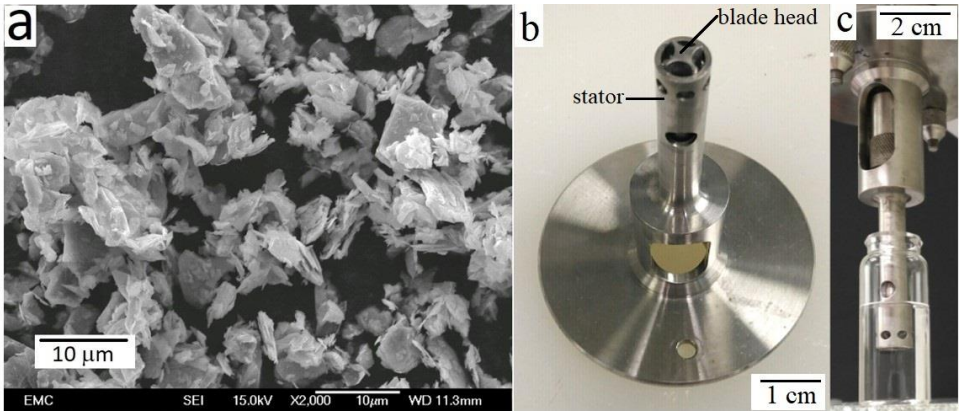

Figure 8.1. (a) SEM image of the as-received MoS_2 particles, (b) high-shear mixer blade, (c) arrangement for high-shear mixing

This study employs a Watts nickel bath for the electrodeposition of Ni-MoS_2 composite coatings. Prior to composite electrodeposition, as received MoS_2 particles (Figure 8.1 a) and surfactants are carefully weighed added into a glass vial with 10 mL Watts nickel bath. The contents in the glass vial are subjected to magnetic stirring (PTFE-coated cylindrical stirring bar, diam. 3 mm, L 8 mm, 2000 rev min^{-1}) or high-shear mixing (Silverson® L4RT high-shear mixer with a 1 cm 'Mini-Micro' stainless steel work head rotating at 8000 rev min^{-1} inside a stator, as shown in Figure 8.1 (b) and (c). The electrodeposition

Particle dispersions prepared by high-shear mixing and magnetic stirring are analysed by dynamic light scattering and laser doppler micro-electrophoresis for particle size distribution and zeta potential respectively in a Zetasizer Nano ZS system (Malvern Instruments Ltd.). A mixture of MoS_2 particles (2 g dm^{-3}) in the Watts bath (10 mL) together with appropriate additives is subjected to a controlled mechanical agitation for a set time. Particle-size distribution measurement is carried immediately after mixing. Particle dispersions are then diluted to 80 mL with Watts nickel electrolyte in a 100 mL cylindrical beaker for electrodeposition.

8.3 Visual appearance of particle dispersions

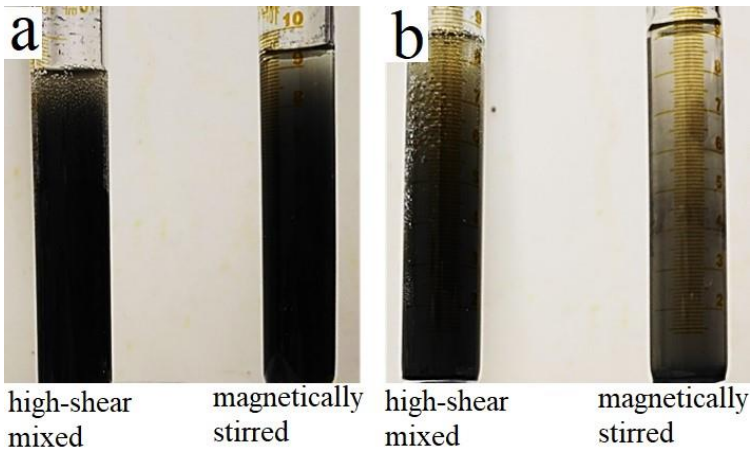

Figure 8.2. MoS_2 particle dispersion in deionised water (a) shortly after mixing, (b) 8 h after mixing.

Particle dispersions in deionised water (MoS_2 2 g dm^{-3}, CTAB 0.1 g dm^{-3}, vol. 10 mL) are prepared via magnetic stirring (2000 rev min^{-1}, 30 min) and high-shear mixing (8000 rev min^{-1}, 30 min) in 20 mL cylindrical glass vials. The choice of water as the dispersant is due to the dark green colour of Watts nickel bath interfering with visual inspection. The mixtures are transferred into 10 mL measuring cylinders after mixing and are allowed to settle undisturbed for visual inspection of particle dispersion stability (Figure 8.2). Shortly after dispersing, the mixtures are dense and dark with no difference in visual appearance. After standing still for overnight (*ca.*8 h), the dispersion using magnetic stirring turned into a much clearer mixture with thick particle sediments at the bottom, indicating a higher particle precipitation rate. The dispersion via high-shear mixing is more uniform and stable, showing a darker colour and smaller extent of particle precipitation.

8.4 Particle size distribution and zeta potential in dispersions

Particle dispersions in a Watts nickel bath are analysed by a Zetasizer Nano ZS (Malvern Instruments). The refractive index for MoS_2 particles and a Watts nickel bath are chosen from existing data in the software. In the case of the Watts nickel bath, the effect of individual components at the given concentrations are added separately to the profile refractive index of water to make up the complex refractive index of the bath.

Figure 8.3 (a) shows the relationship between particle Z-average size and high-shear mixing speed each with a mixing time for 1 h. A particle Z-average size of 1715 nm is found at a high-shear mixing speed of 3000 rev min^{-1}, indicating the presence of large particle agglomerates. The particle Z-average size decreased by almost 50% as the high-shear mixing speed increased from 3000 rev min^{-1} to 7000 rev min^{-1}. There is a small trend of further decrease of particle Z-average size for mixing speeds higher than 7000 rev min^{-1}, but the changes are relatively small compared to those at lower mixing speeds. For magnetic stirring, the maximum stirring speed available from the stirring plate (2000 rev min^{-1}) is applied to achieve a satisfactory particle dispersion. The Zetasizer only measures particle agglomerate sizes less than 10 □m in diameter and magnetic stirring at lower stirring speeds would simply not produce a uniform solid-liquid mixture or result in large agglomerates outside the measuring range of the available instrument.

Figure 8.3 (b) shows the relationship between particle Z-average size and duration of agitation via magnetic stirring and high-shear mixing. During the first 25 min into mixing, particle Z-average size in the dispersion via high-shear mixing saw a steep decline from 1900 nm to 1332 nm, and reached a stabilised value around 1180 nm after 100 min. In dispersions via magnetic stirring, the particle Z-average size is eventually reduced from 1996 nm to only 1518 nm, which took a longer period of about 100 min. This indicates that high-shear mixing is more effective in breaking down particle agglomerations to smaller sizes over a much shorter period than magnetic stirring.

Figure 8.3 (c) shows the particle zeta potential measurement of particle dispersions during mixing. Particle dispersion via high-shear mixing show a positive zeta potential of around 31 – 32 mV, which is slightly higher than 30.5 – 31.5 mV for particle dispersion produced via magnetic stirring. There is more fluctuation at the beginning of mixing, but further mixing seemed to have little influence on particle zeta potential. The positive zeta potential indicated that MoS2 particle dispersions are moderately stable in the Watts nickel bath. During electrodeposition, continuous agitation is essential to maintain the stability of particle dispersion.

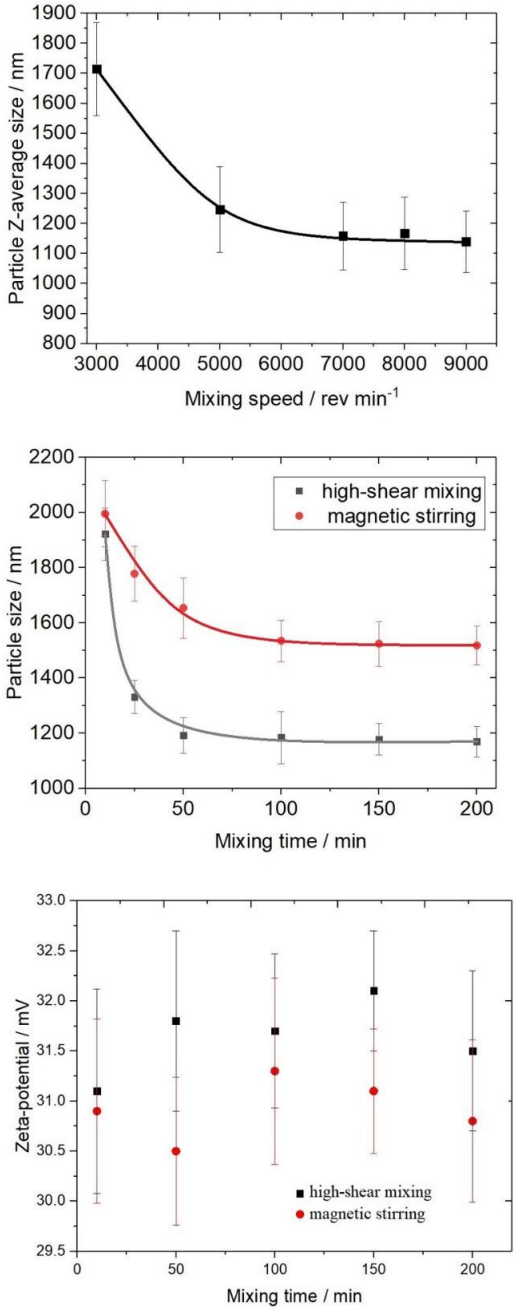

Figure 8.3. MoS_2 particle Z-average size as a function of: (a) high-shear mixing speed for 1 h, and (b) high-shear mixing time at 8000 rev min^{-1} compared with magnetic stirring at 2000 rev min^{-1}; (c) effect of mixing time on particle zetapotential measurement

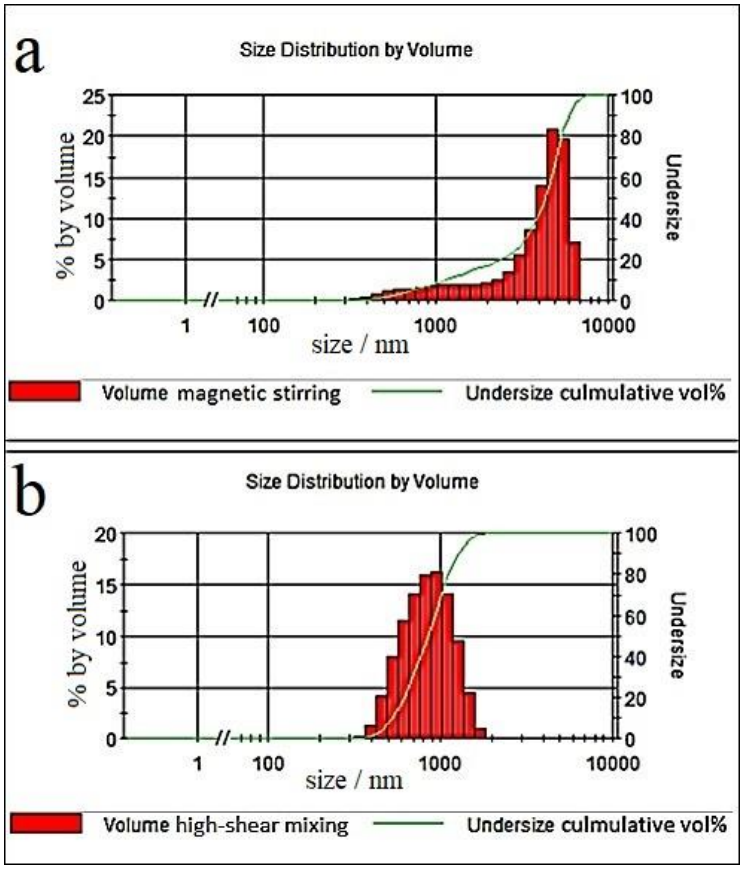

Figure 8.4. MoS_2 particle-size distribution in deionised water after: (a) magnetic stirring, 2000 rev min^{-1}, 3 h, and (b) high-shear mixing, 8000 rev min^{-1}, 3 h.

Figure 8.4 shows the optimum particle-size distribution measurement of MoS_2 particle dispersions under the two different methods studied: magnetic stirring (2000 rev min^{-1}, 3 h) and high-shear mixing (8000 rev min^{-1}, 3 h). Particle-size distribution in the dispersion via magnetic stirring show large particle agglomerates of up to 7 μm in diameter. High-shear mixing produced a narrow particle-size distribution with a Gaussian-alike curve ranging from 0.2 μm to 1.9 μm. The middle particle size of the distribution is around 0.9 μm, which is very close to the particle size given by the manufacturer (1 – 2 μm). The notable improvement of particle dispersion by reducing agglomerate sizes has also been reported in literature for the high-shear mixing method[188,189].

8.5 Structure and surface morphology of Ni-MoS_2 composite coatings

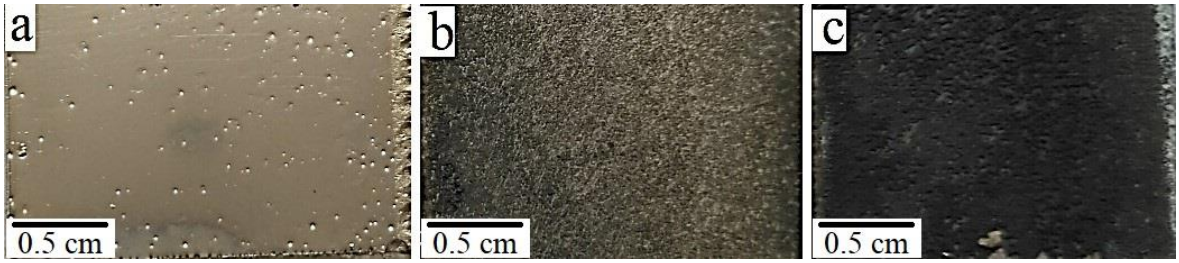

Figure 8.5. Examples of (a) pure nickel, (b) Ni-MoS_2 coating via particle dispersion from high-shear mixing (8000 rev min^{-1}, 3 h) and (c) Ni-MoS_2 coating via particle dispersion from magnetic stirring (2000 rev min^{-1}, 3 h)

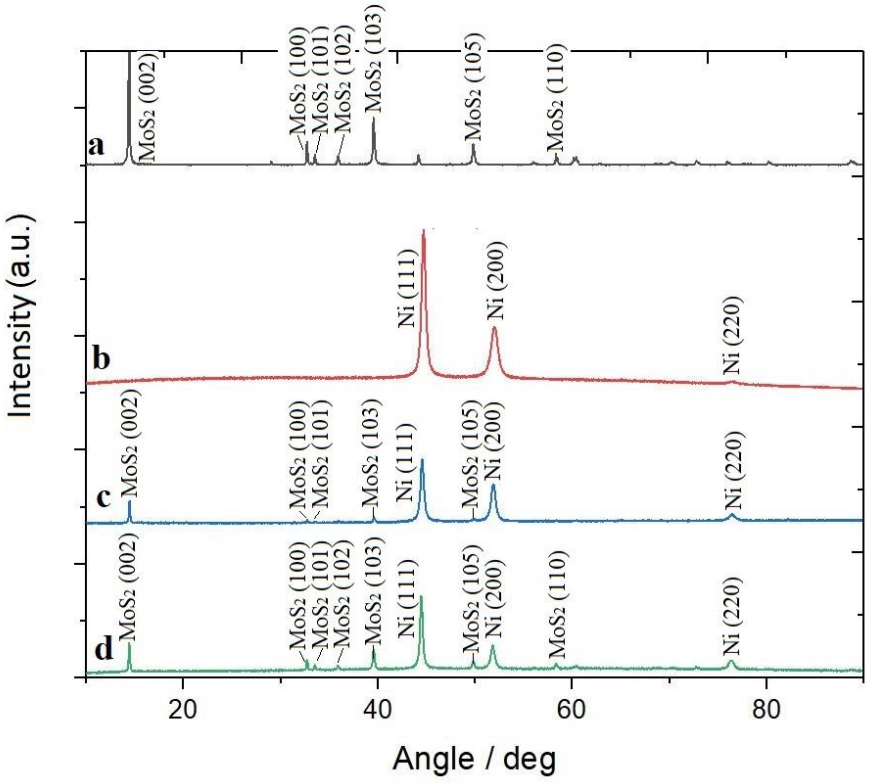

Figure 8.6 XRD patterns of: (a) MoS_2 powder, (b) pure Ni coating, (c) Ni-MoS_2 composite coating from particle dispersion via high-shear mixing and (d) Ni-MoS2 composite coating from particle dispersion via magnetically stirring.

Electrodeposition was carried out from a modified Watts nickel bath (MoS_2 2 g L^{-1}, CTAB 0.1 g L^{-1}, current density 5 A dm^{-2}, magnetic stirring 400 rpm, plating time 60 min, saccharin 2 g L^{-1}).

Figure 8.5 shows the examples of pure nickel and Ni-MoS_2 composite coatings deposited on mild steel substrates with particle dispersions via high-shear mixing (8000 rev min^{-1}, 3 h) and magnetic stirring (2000 rev min^{-1}, 3 h). The reference nickel deposit is bright and smooth, showing a metallic gloss under room light. Ni-MoS_2 composite coating using particle dispersion via high-shear mixing is dull and light grey. A darker deposit is produced using particle dispersion via magnetic stirring.

Figure 8.6 shows the XRD patterns of MOS_2 powder and the composite coatings. The MoS_2 peaks are present in both composite coatings but are more intense in Ni-MoS_2 composite coating with particle dispersion via magnetically stirring, indicating a higher MoS_2 particle content. Ni (111) and Ni (200) peaks are sharpened in composite coatings indicating an increase in crystallite sizes. The crystallite size calculated according to Debye-Scherrer equation is 10 nm for Ni coating, 20.8 nm for Ni-MoS_2 composite coating from a bath with particle dispersion via magnetically stirring and 27.8 nm for Ni-MoS_2 composite coating from a bath with particle dispersion via high-shear mixing.

Nanoindentation measurements on the coatings show that microhardness of the coatings is 5.6 GPa for Ni coating, 4.92 GPa for the Ni-MoS_2 composite coating from a bath with particle dispersion via magnetically stirring and 4.62 GPa for the Ni-MoS_2 composite coating from a bath with particle dispersion via high-shear mixing. The hardness value is consistent with XRD measurements and indicated that an increase in crystallite size reduced the microhardness of the coating.

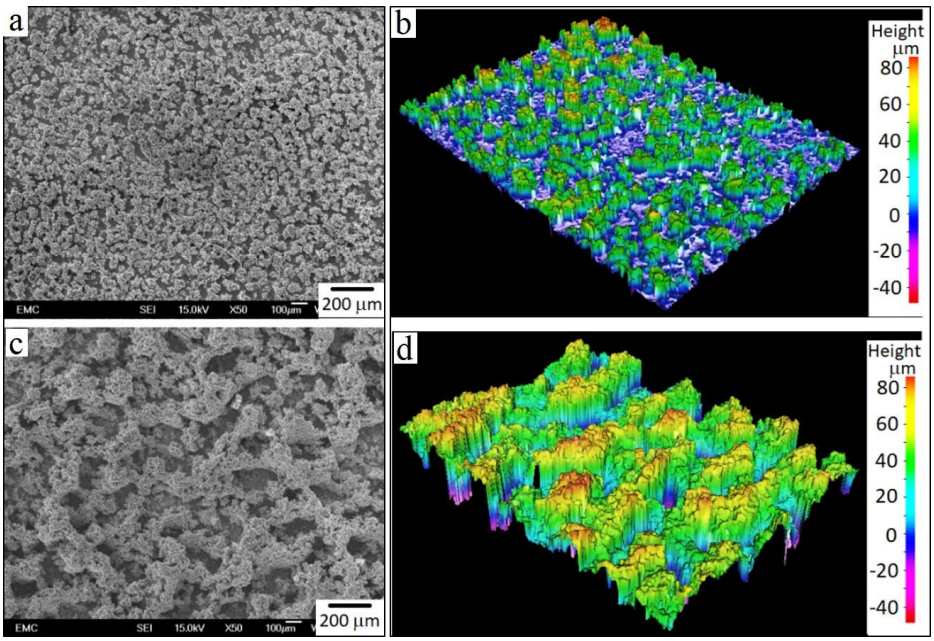

Figure 8.7 SEM and 3D optical images of (a), (b): Ni-MoS_2 coating via particle dispersion from high-shear mixing; (c), (d): Ni-MoS_2 coating via particle dispersion from magnetic stirring.

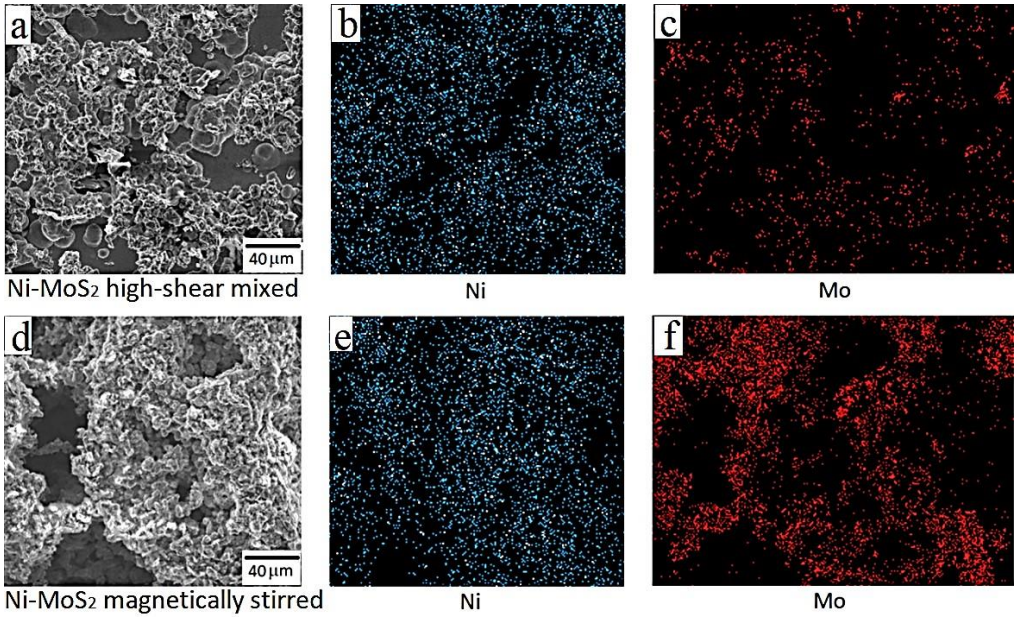

Figure 8.8 EDX mapping of (a), (b) and (c): Ni-MoS_2 coating via particle dispersion from high-shear mixing; (c), (d) and (e): Ni-MoS_2 coating from a bath involving particle dispersion by magnetic stirring.

SEM surveys revealed microscopic surface roughness features on Ni-MoS_2 composite coatings. Ni-MoS_2 composite coating using particle dispersion via high-shear mixing show small and densely packed nodular structures in Figure 8.7 (a), with a MoS_2 surface content of 8.7 wt.% as reported by EDX analysis (Figure 8.8, a – c). Ni-MoS_2 composite coating using particle dispersion via magnetic stirring show large, porous structures in Figure 8.7 (c) with a higher MoS_2 content of 30 wt.% by EDX. Elemental mapping show higher amount of MoS_2 contents in protrusion structures on coating surfaces as shown in Figure 8.8 (d – f).

Optical microscopic scans show 3D surface structures of Ni-MoS_2 composite coatings in Figure 8.7 (b, d). Surface roughness is measured by S_a value (average height of selected area), with S_a = 18.48 ± 2.58 µm for Ni-MoS_2 composite coating using particle dispersion via high-shear mixing as shown, and S_a = 49.80 ± 3.23 µm for Ni-MoS_2 composite coating using particle dispersion via magnetic stirring.

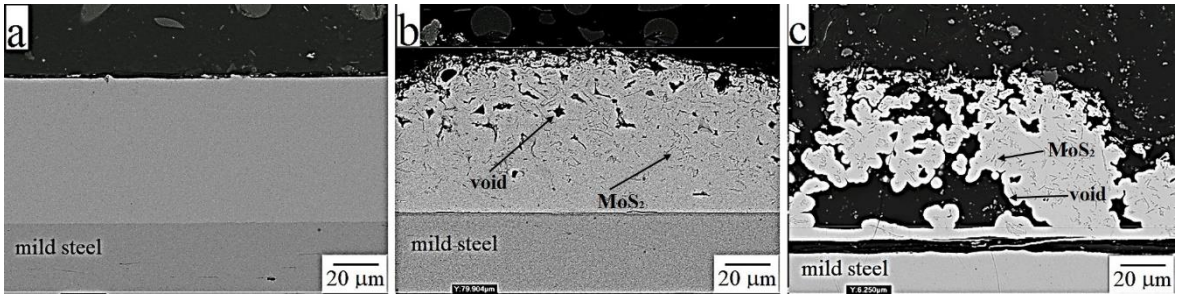

Figure 8.9 Cross-sectional BEI images of coatings on mild steel substrates: (a) Watts nickel coating, (b) Ni-MoS_2 coating via particle dispersion from high-shear mixing and (c) Ni-MoS_2 coating from a bath in which particle dispersion is achieved by magnetic stirring.

The surface roughness measurement is a reflection of the porosity of the coating structure, which agreed with SEM observations and is further explained by cross-sectional BEI scans of the deposits in Figure 8.9. Under same electrodeposition conditions, pure nickel coating show the highest level of compactness and smoothness, with a thickness of about 75 µm. A compact layer close to the mild steel substrate is found for Ni-MoS_2 composite coating using particle dispersion via high-shear mixing. The MoS_2 content increased as the thickness of the coating increased, which is covered by a thin porous top layer of around 20 µm as shown. Ni-MoS_2 composite coating using particle dispersion via magnetic stirring revealed extensive porosities throughout the coating structure, with some cavities of over 50 µm. The thickness of the porous layers is found to correlate well with surface roughness measurements by optical microscopy.

It has been observed that metal deposition can occur on both incorporated conductive particles and the electrode surface. Under same deposition conditions, a more conductive particle could lead to a more porous composite coating structure[109]. Simulation work by Celis *et al.*[181] show a higher current density distribution on the incorporated conductive particles on the surface of the cathode, leading to a localised acceleration of metal deposition that leads to dendritic or nodular structure growth. In Figure 8.9 (c) it could be clearly seen that the protruding structures resulted from the growth of nickel around incorporated MoS_2 particles, forming protruding structures both small and large, which is a clear indication that MoS_2 particles are conductive during electrodeposition. A non-uniform dispersion of conductive particles in bath could further increase the porosity of the coating, by introducing porosities from within large particle agglomerates as well as accelerating the growth of protrusions.

The above results show the effect of particle dispersion stability on the composition and structure of the composite coatings. To achieve compact coating structures and uniform particle content distributions, stable particle dispersions are generally desired. Choosing vigorous mechanical

agitations can avoid particle agglomerates in the bath that may otherwise lead to a porous and fragile composite coating.

8.6 Non-lubricated wear tests of Ni-MoS_2 composite coatings

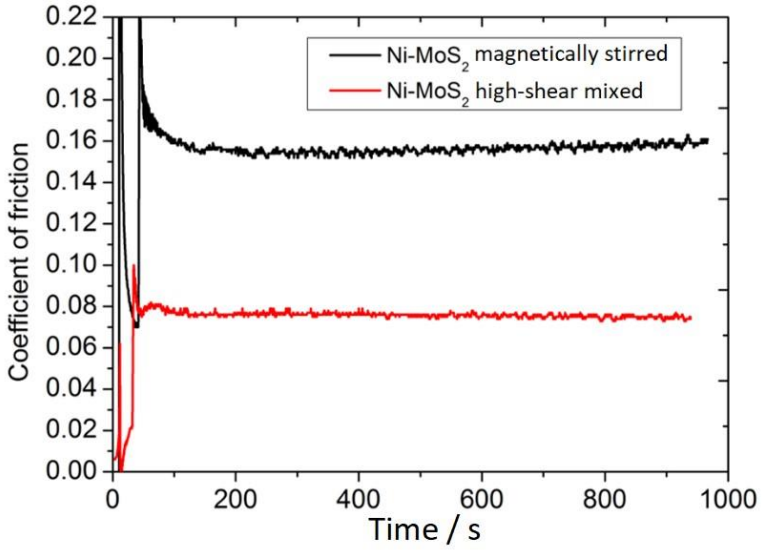

Figure 8.10 Coefficient of friction as a function of test time for Ni-MoS_2 composite coatings. (20 N, 1 Hz)

Non-lubricated roller-on-plate tests are performed to evaluate the friction properties of the electrodeposited composite coatings. Counterpart AISI-52100 bearing steel roller (diameter 6 mm, length 10 mm), load 20 N (roller, Hertzian contact pressure 0.16 GPa); sliding frequency 1 Hz; stroke length 10 mm. The coefficient of friction for Ni-MoS_2 composite coatings is presented as a function of test time in Figure 8.10. Ni-MoS_2 composite coating using particle dispersion via high-shear mixing show over 50% reduction in running-in and steady-state coefficient of friction from those of Ni-MoS_2 composite coating using particle dispersion via magnetic stirring. The coefficient of friction for pure Ni coating is around 0.6. It is evident that the presence of MoS_2 particles significantly reduced dry sliding friction of the composite coating against the bearing steel counterpart.

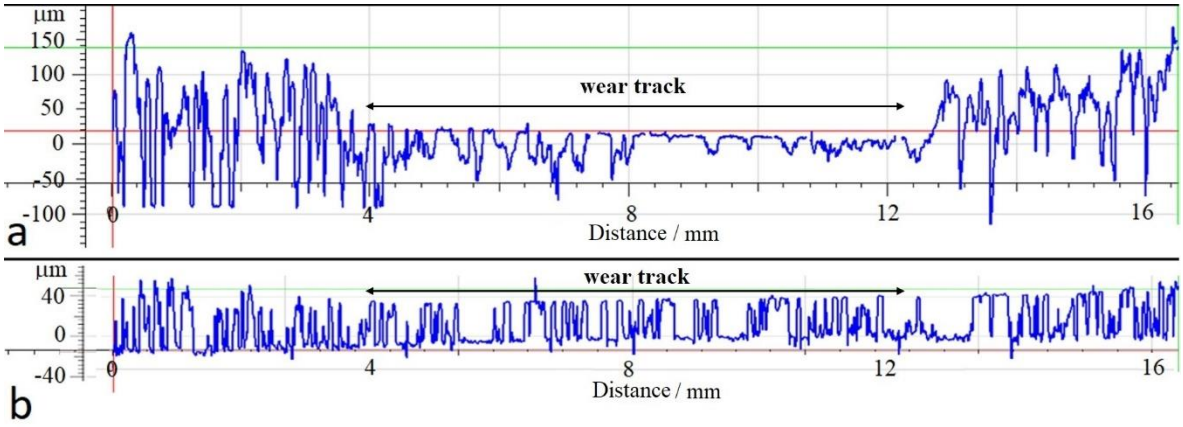

Figure 8.11 Wear track cross-sectional depth profile of (a) Ni-MoS_2 coating via particle dispersion from magnetic stirring and (b) Ni-MoS_2 coating via particle dispersion from high-shear mixing.

Wear track cross-sectional depth profile (Figure 8.11) show a small wear depth of about 12 µm for the Ni-MoS_2 composite coating using particle dispersion via high-shear mixing, whereas a wear depth of 120 µm is observed for the Ni-MoS_2 composite coating using particle dispersion via magnetic stirring.

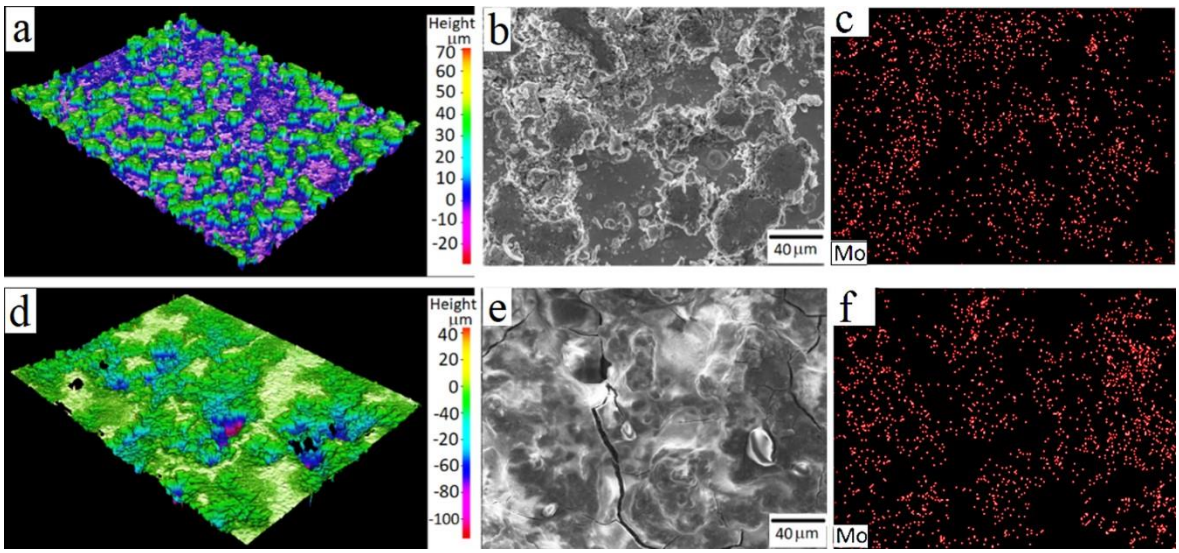

Figure 8.12. 3D optical scans and SEM images of (a), (b) and (c): wear track of Ni-MoS_2 coating via particle dispersion from high-shear mixing; (c), (d) and (e): wear track of Ni-MoS_2 coating from a bath in which particle dispersion is achieved by magnetic stirring.

3D optical scans and SEM of the wear track surfaces show that surface roughness features for Ni-MoS_2 composite coating using particle dispersion via high-shear mixing underwent polishing wear, with the top nodular structures being slightly flattened in Figure 8.12 (a) and (b). Surface roughness features for Ni-MoS_2 composite coating using particle dispersion via magnetic stirring are largely removed from the wear track, and a large amount of wear debris are found outside the wear track, showing extensive abrasive wear in Figure 8.12 (d) and (e).

EDX mapping show a uniform distribution of Mo over both wear track surfaces compared to the coating surfaces before wear in Figure 8.12 (c) and (f). This is due to the MoS_2 particles being sheared across the wear track, forming local tribofilms that contributed to the low friction in the wear test. Little wear is observed on the roller counterparts, however presence of MoS_2 content over contact areas is found, indicating a transfer of tribofilm to the roller counterpart.

In order to achieve maximum lubricity, MoS_2 particles need to be sheared into tribo-films with the weakly bonded MoS_2 intermolecular planes aligning parallel with the wear track[190,191]. The formation of the tribo-film separates the sliding surfaces, which not only provides a layer of easily sheared solid lubricant, but also reduces direct wear between the coating and bearing steel, hence the reduction in friction and wear. A compact and uniform coating provides a firm support for the MoS_2 particles to allow an effective shear to take place, so that a low-friction tribo-film may readily develop. This can be seen in the tribological performances of Ni-MoS_2 composite coating using particle dispersion via high-shear mixing. The high coefficient of friction for Ni-MoS_2 composite coating from a bath involving particle dispersion via magnetic stirring can be attributed to the energy consumption in removals of the MoS_2 rich but fragile surface roughness features under the load, which is shown from the deep wear and cracking on the wear track. The porosity of the composite coating makes a less effective pathway for MoS_2 tribo-film formation in spite of a higher content of MoS_2 in the coating.

For Ni-MoS_2 composite coatings, enhanced self-lubrication and wear resistance would tend to favour a compact coating structure with a uniform particle content distribution, which has been shown to result from a stable particle dispersion via effective means of mechanical agitation, such as high-shear mixing. Moreover, it has also been shown that particle content in the composite coating alone should not be regarded as the only criteria for assessing coating quality. In this study, a Ni-MoS_2 composite coating with a moderate but well-dispersed MoS_2 particle content (8.7 wt.%) show better tribological performance than the one with a much higher but agglomerated MoS_2 content (30 wt.%). If the content of the solid lubricant particle is too low, it may sometimes lead to insufficient friction reduction. A much higher particle content, however, may result from large particle agglomerates in a porous and friable coating structure, resulting in excessive wear and increased friction for Ni-MoS_2 composite coatings. The particle distribution and content in a tribological coating must be carefully controlled to meet the demand of target functionality without compromising durability.

In comparison with the previous chapter where magnetic stirring is studied for bath agitation during electrodeposition, it is important not to confuse bath agitation with particle dispersion. Although particle dispersion in this study is carried out with high shear mixing for effectively breaking down particle agglomerates during the preparation of solution *before* commencing electroplating, shear mixing is not suitable for maintaining particle suspension during electroplating due to its high energy turbulent flow which may disrupt particle distribution on coating surface. Also, the shear mixer blade geometry in this study is relatively small which could not be adapted for providing adequate bath agitation in larger containers for electroplating purposes.

8.7 Comparison with Güler's study on Ni-MoS_2 coatings

Güler et al. carried out studies on electroplating Ni-MoS_2 coating from a Watts nickel bath and published their results as early as in 2013[187]. The method and focus of her study are very similar to this work hence is used in comparison for further results discussion.

Güler quoted high particle concentrations in her study ranging from 10 – 30 g L^{-1}, which produced a coating with MoS_2 content of up to 5 – 10 wt% or 7 – 14 vol%. Compared to this study, Güler's particle concentration in bath is over 10 times higher but achieved less than half of the maximum particle content in the coating. A low particle concentration in bath is favoured due to the ease of maintaining particle dispersion and avoid particle agglomeration. Güler carried out tribology tests on a pin-on-disc tribometer using 6 mm diameter 100Cr6 steel balls and 1N load corresponding to a contact pressure of 0.44 GPa, and recorded friction coefficients of 0.4 – 0.6 for Ni-MoS_2 composite coating, which had a 50% reduction from pure Nickel coating in her test. The friction coefficient in this study are around 0.1 with a roller-on-disc contact pressure of 0.12 GPa (load 20N), showing over 80% reduction against pure Ni coating. Although MoS_2 has been found to be a good solid lubricant under high load bearing conditions and the dry solid lubricant show a decrease in friction at higher loads, Güler's coatings exhibited high friction coefficient and wear that indicated either an insufficient level of MoS_2 in the coating to provide solid lubrication or over stressing the coating with high load that led to accelerated wear.

The major cause of this difference is in surfactant choice. Güler selected an anionic surfactant SDS while this study selected a cationic surfactant CTAB. Both surfactant molecules contain similar hydrocarbon chain for effective dispersion of hydrophobic MoS_2 particles in bath, however cationic surfactant has the added benefit of electrophoresis that could increase particle incorporation into the bath while anionic surfactant may have no such effect or even do the opposite. The comparison between this study and Güler's work agrees with the claims and is a useful source for comparing the effect of surfactant property on Ni-MoS_2 electrodeposition. Güler claimed that CTAB has detrimental effect on coating structure however similar effects are also observed for SDS both in coating cross

section SEM from Güler's work and during the initial trial on surfactants in this study. Güler also used additional commercial additives including carrier, leveller, brightener, and wetting agent as a combined system to produce satisfactory coatings, which are not recorded for their composition and not available for this study.

Moreover, Güler only quoted long hours of mechanical agitation for particle dispersion, without any assisting means such as ultrasonication and in this study, high shear mixing. Mechanical agitation for bath preparation may be an ineffective way to break down particle agglomeration even in the presence of additional additives. The agglomerated particles could reduce the particle incorporation rate and lower particle content in the coating while also causing larger defects in the coating layer leading to high wear and friction.

8.8 Summary and comments

The effect of electrolyte agitation method on the stability of particle dispersions and the properties of resulting electrodeposited Ni-MoS_2 composite coatings has been studied.

High-shear mixing produced a particle dispersion with narrow particle-size distributions of 0.2 – 1.9 μm compared to 2 – 7 μm by magnetic stirring. It is shown to be a facile and effective way to achieve stable particle dispersions in the bath whereas magnetic stirring is much less effective in breaking down large particle agglomerates, leading to an unstable particle dispersion that quickly precipitates. The effective speed of high-shear mixing for particle dispersion should be higher than 7000 rev min^{-1} for the type of blade head employed in this study, which reduced particle agglomerate sizes from 1700 nm to 1150 nm within 1h at 8000 rev min^{-1}.

Particle dispersion stability exhibited a significant influence on the structure and tribological performance of the resulting Ni-MoS_2 composite coatings. A uniform MoS_2 particle dispersion in bath via high-shear mixing led to a compact Ni-MoS_2 coating, which show a ~50% reduction in coefficient of friction and ~90% reduction of wear in unlubricated wear tests against bearing steel when compared with a porous Ni-MoS_2 coating from an unstable particle dispersion via magnetic stirring.

High shear mixing is also found to be particularly effective in dispersing soft PTFE nanoparticles for benchmark Ni-PTFE coatings produced in this study.

Chapter 9 Conclusions

In this work, Ni-MoS_2 composite coatings are successfully deposited from a modified Watts Nickel Bath. They are found to be self-lubricating, and their wear resistance are influenced by surface morphology and particle contents. This study has covered most of the process factors involved in traditional DC electroplating process (current density, wetting surfactant, brightener additive, particle concentration, bath agitation, particle dispersion) to comprehensively evaluate the feasibility and potentials for DC electrodeposited Ni-MoS_2 composite coating.

The highlights of this study are as follows:

1. First direct comparison between conductive MoS_2 and inert PTFE particles under similar plating and tribological testing conditions to illustrate the effect of particle conductivity on coating morphology and structure. Despite the structural defects, Ni-MoS_2 coatings could achieve relative high particle content level in coating and achieve similar if not lower friction coefficient of c.a. 0.1 compared with Ni-PTFE coatings.

2. Successful demonstration of controlling MoS_2 particle content in coating via bath agitation speed which leads to a facile method of producing gradient Ni-MoS_2 coating with increasing particle content from substrate to the coating surface by stepping the agitation rate during electrodeposition. This process is easy to adapt for commercial plating facilities and the gradient coating holds potential for enhanced wear resistance and load bearing capabilities.

3. A detailed study on high shear mixing for effective MoS_2 particle dispersion in bath preparation before electroplating. High shear mixer successfully reduced particle agglomeration from 10 microns to 1 micron as analysed by particle size distribution in a Zetasizer. The resulting bath demonstrated higher suspension stability during electroplating that produced Ni-MoS_2 coatings with more uniform structures, lower friction and lower wear compared to particle dispersion by magnetic stirring.

Despite the improvements made in this study, there are still some issues surrounding the electrodeposition of composite Ni-MoS_2 coatings:

1. Due to the inherent conductivity of MoS_2 particles, surface roughness features could only be controlled but not eliminated in coatings via electrodeposition.

2. Coating porosity is still significantly higher than Ni-PTFE coatings, and although the lowest friction coefficient of both Ni-MoS_2 and Ni-PTFE coatings are around 0.1, higher wear rates are found for the more porous Ni-MoS_2 coatings.

3. The rapid onset of roughness features limits the overall plating time or coating thickness suitable for its deposition. MoS_2 Particle concentration in bath is kept at very low levels which may limit the range of available coating compositions.

The difficulty in controlling the surface morphology and structure of Ni-MoS_2 coatings via electrodeposition may explain the reason why it is less seen in commercial application today than traditional Ni-PTFE coatings. This study has explored most processing factors for traditional DC electroplating process and could not identify a strategy to eliminate porosity from electrodeposited Ni-MoS_2 coating. This may deter any interest in industrial application for producing wear / friction resistant coatings, as such coatings are usually operated under harsh conditions and need to show high reliability.

However, some points discussed in the highlights above are still applicable for studies on alternative particle materials via composite deposition. The author would like to call for emphasis on effective particle dispersion and monitoring its stability during future research in composite electroplating to ensure an optimum coating composition and performance.

Chapter 10 Future work

For Ni-MoS_2 composite deposits, the primary focus is to control the porous and nodular growth of nickel deposited on the conductive MoS_2 particles. A number of methods are proposed below based on understanding of the process parameters and electrodeposition mechanisms:

a) Mechanical agitation is shown to improve particle codeposition and suppress roughness feature growth. Quantitative electrolyte flow conditions should be applied to composite deposition studies for example, using a flow cell. Other mechanical agitation methods such as brush plating and ultrasound assisted deposition are of further interest in controlling particle incorporation and deposit surface morphologies. New electrodeposition bath set-ups are needed with special designs for the additional techniques.

b) The formula of composite electrodeposition could be reinforced by hybrid particle inclusions. For example, the codeposition of both PTFE and MoS_2 particles alongside nickel may inhibit surface roughness growth by PTFE adsorption onto MoS_2 particles for blocking and insulation. Additional structural reinforcement inclusions such as ceramic particles may offer strengthened coatings for enhanced mechanical and tribological properties,

The goal is to facilitate the development of convenient electrodeposition techniques with advanced process parameter controls to achieve multifunctional composite deposits that are robust enough to meet future tribological challenges with minimum increase in production cost and complexity.

List of publications

1. Simulations of fluid flow, mass transport and current distribution in a parallel plate flow cell during nickel electrodeposition, Tzayam Pérez, Luis F. Arenas, Daniel Villalobos-Lara, Nan Zhou, Shuncai Wang, Frank C. Walsh, José L. Nava, Carlos Ponce de León, Journal of Electroanalytical Chemistry, June 2020

2. The Electrodeposition of Composite Coatings: Diversity, Applications and Challenges, Frank C. Walsh, Shuncai Wang, Nan Zhou. Current Opinion in Electrochemistry, February 2020.

3. Effective particle dispersion via high-shear mixing of the electrolyte for electroplating a nickel-molybdenum disulphide composite, S. C. Wang, N. Zhou, F. C. Walsh. Electrochimica Acta, Volume 283, 2018, Pages 568-577 (Adapted from Chapter 5 of this thesis).

4. Diverse electrodeposits from a Watts nickel acid sulphate bath, S. C. Wang, N. Zhou, F. C. Walsh. Transactions of the Institute of Materials Finishing, 2016, vol. 94, pp. 274-282.

List of References

1. Jost, H. P. Tribology — Origin and future. *Wear* **136**, 1–17 (1990).

2. Scott, D. Tribology in perspective. *Tribology Series* **8**, 1–11 (1983).

3. Holmberg, K. & Erdemir, A. Influence of tribology on global energy consumption, costs and emissions. *Friction* **5**, 263–284 (2017).

4. Wood, R. J. K. 1 - Understanding surface wear in engineering materials. in *Surface Coatings for Protection Against Wear* (ed. Mellor, B. G.) 1–57 (Woodhead Publishing, 2006).

5. Wood, R. J. K. Multifunctional materials for tribological applications. 1–376 (2015).

6. Bartz, W. J. Solid Lubricant. **17**, 421–432 (1971).

7. Walsh, F. *et al.* The formation of nanostructured surfaces by electrochemical techniques: A range of emerging surface finishes - Part 1: Achieving nanostructured surfaces by electrochemical techniques. *Transactions of the IMF* **93**, 209-224 (2015).

8. You, Y. H., Gu, C. D., Wang, X. L. & Tu, J. P. Electrochemical preparation and characterization of Ni-PTFE composite coatings from a non-aqueous solution without additives. *International Journal of Electrochemical Science* **7**, 12440–12455 (2012).

9. Szeptycka, B. & Gajewska-Midzialek, A. The influence of the structure of the nanocomposite Ni-PTFE coatings on the corrosion properties. *Reviews on Advanced Materials Science* **14**, 135–140 (2007).

10. Sharma, A. & Singh, A. K. Corrosion and wear resistance study of Ni-P and Ni-P-PTFE nanocomposite coatings. *Central European Journal of Engineering* **1**, 234–243 (2011).

11. Hampshire, W. TYPICAL PROPERTIES of PTFE. 9–11 (2011).

12. Berçot, P., Pea-Muoz, E. & Pagetti, J. Electrolytic composite Ni-PTFE coatings: An adaptation of Guglielmi's model for the phenomena of incorporation. *Surface and Coatings Technology* **157**, 282–289 (2002).

13. Tang, A., Wang, M., Huang, W. & Wang, X. Composition design of Ni-nano-Al_2O_3-PTFE coatings and their tribological characteristics. *Surface and Coatings Technology* **282**, 121–128 (2015).

14. Suiyuan, C. *et al.* Synthesis of Ni-P-PTFE-nano-Al_2O_3 composite plating coating on 45 steel by electroless plating. *Journal of Composite Materials* **46**, 1405–1416 (2012).

15. Zhang, Y. Z., Wu, Y. Y., Sun, K. N. & Yao, M. Characterization of electroless Ni-P-PTFE composite deposits. *Journal of Materials Science Letters* **17**, 119–122 (1998).

16. Wang, F., Arai, S. & Endo, M. Electrochemical preparation and characterization of nickel/ultra-dispersed PTFE composite films from aqueous solution. *Materials Transactions* **45**, 1311–1316 (2004).

17. Assoul, M., Pena-Munoz, E., Roizard, X. & Zahouani, H. A tribological study of electrolytic nickel-PTFE composite coatings. *Journal of Synthetic Lubrication* **15**, 107–116 (1998).

18. Wu, Y., Liu, H., Shen, B., Liu, L. & Hu, W. The friction and wear of electroless Ni-P matrix with PTFE and/or SiC particles composite. *Tribology International* **39**, 553–559 (2006).

19. Huang, Y. S., Zeng, X. T., Annergren, I. & Liu, F. M. Development of electroless NiP-PTFE-SiC composite coating. *Surface and Coatings Technology* **167**, 207–211 (2003).

20. Ramalho, A. & Miranda, J. C. Friction and wear of electroless NiP and NiP + PTFE coatings. *Wear* **259**, 828–834 (2005).

21. Pena-Munoz, E., Berçot, P., Grosjean, A., Rezrazi, M. & Pagetti, J. Electrolytic and electroless coatings of Ni-PTFE composites: Study of some characteristics. *Surface and Coatings Technology* **107**, 85–93 (1998).

22. Liew, K. W., Kong, H. J., Low, K. O., Kok, C. K. & Lee, D. The effect of heat treatment duration on mechanical and tribological characteristics of Ni-P-PTFE coating on low carbon high tensile steel. *Materials and Design* **62**, 430–442 (2014).

23. Wu, Y., Liu, L., Shen, B. & Hu, W. Study of self-lubricant Ni-P-PTFE-SiC composite coating. *Journal of Materials Science* **40**, 5057–5059 (2005).

24. Tang, A., Wang, M., Huang, W. & Wang, X. Composition design of Ni-nano-Al_2O_3-PTFE coatings and their tribological characteristics. *Surface and Coatings Technology* **282**, 121–128 (2015).

25. Bagi, S. D. & Aswath, P. B. Mechanism of friction and wear in MoS_2 and ZDDP/F-PTFE greases under spectrum loading conditions. *Lubricants* **3**, 687–711 (2015).

25. Sierra Rayne & Kaya Forest, Perfluoroalkyl sulfonic and carboxylic acids: A critical review of physicochemical properties, levels and patterns in waters and istewaters, and treatment methods, *Journal of Environmental Science and Health Part A*, **44:12**, 1145-1199 (2009)

26. Miyoshi, K. & NASA. Solid lubrication fundamentals and applications - Introduction and background. (1998).

27. Lee-Prudhoe, I., Starkey, M. S. & Sayles, R. S. Observations of Frictional Behaviour of MoS_2 and Dependence on Surface Roughness Orientation. in *Tribology for Energy Conservation* (eds. Dowson, D. et al.) **34**, 129–137 (Elsevier, 1998).

28. Wang, S., An, C. & Yuan, J. Synthetic fabrication of nanoscale MoS_2-based transition metal sulfides. *Materials* **3**, 401–433 (2010).

29. Pflüger, E. & Savan, A. Modern Solid Lubricants, Especially Based on MoS_2. *Vakuum in Forschung und Praxis* **11**, 236–240 (1999).

30. Berdinsky, A. S. *et al.* Research on annealing temperature in the process of MoS_2 nanostructure synthesis from nanoscale powder. *Proceedings - 6th Russian-Korean International Symposium on Science and Technology, KORUS 2002* 402–405 (2002).

31. Serpini, E. *et al.* The role of humidity and oxygen on MoS_2 thin films deposited by RF PVD magnetron sputtering. *Surface and Coatings Technology* **319**, 345–352 (2017).

32. Gradt, T. & Schneider, T. Tribological performance of MoS_2 coatings in various environments. *Lubricants* **4**, (2016).

33. Steinmann, P. & Spalvins, T. Influence of the deposition conditions on radiofrequency magnetron sputtered MoS_2 films. *NASA TEchnical Paper* (1990).

34. Bolster, R. N. Ion-Beam-Assisted Deposition of MoS_2 and Other Low-Friction Films. (1992).

35. Savan, A., Pflüger, E., Voumard, P., Schröer, A. & Paul, M. S. Modern solid lubrication: Recent developments and applications of MoS_2. *Lubrication Science* **12**, 185–203 (2000).

36. Crichton, T. Coatings – the basis of the UK's manufacturing economy. *Transactions of the IMF* **95**, 235–236 (2017).

37. Abys, J. Modern Electroplating, Fifth Edition. in 327–368 (2011).

38. ECHA (European Chemicals Agency). ANNEX XVII TO REACH – Conditions of restriction. 63–65 (2010).

39. ECHA (European Chemicals Agency). *Analysis of Alternatives, Functional chrome plating, Public Version*. (2015)

40. Gabe, D. R. Watts of Watts Nickel fame. *Transactions of the IMF* **94**, 236 (2016).

41. Yli-Pentti, A. 4.11 - Electroplating and Electroless Plating. in *Comprehensive Materials Processing* (eds. Hashmi, S., Batalha, G. F., Tyne, C. J. van & Yilbas, B.) 277–306 (Elsevier, 2014).

42. Hart, A. C. The Anodic Passivation and Dissolution of Non-Activated Nickel in Nickel Sulphate/Chloride Electrolytes. *Transactions of the IMF* **51**, 69–76 (1973).

43. Abyaneh, M. Y. & Hashemi-Pour, M. The Effect of the Concentration of Boric Acid on the Kinetics of Electrocrystallization of Nickel. *Transactions of the IMF* **72**, 23–26 (1994).

44. Laban, N. R. Problems in High Current Density Nickel and Chromium Deposition. *Transactions of the IMF* **6**, 159–166 (1930).

45. O'Sullivan, J. B. Studies in the Electro-Deposition of Nickel. Part I. The Effect of PH and of Various Buffering Agents; The Presence of Oxygen in the Deposits. *Transactions of the IMF* **5**, 37–48 (1929).

46. Saltonstall, R. B. Bright Nickel Plating—A Review of Progress. *Transactions of the IMF* **31**, 223–242 (1954).

47. Kalantary, M. R. & Gabe, D. R. Vibratory agitation for electrodeposition: I Characterization of agitation. *Transactions of the IMF* **67**, 24–27 (1989).

48. Gabe, D. R. Hull and his cell. *Transactions of the IMF* **85**, 285–286 (2007).

49. Dennis, J. K. & Such, T. E. Bright nickel electroplating. *Nickel and Chromium Plating* 96–131 (1993).

50. Crouch, P. C. & Hendrickson, M. v. Effect of Brightener Systems on the Cathode and Anode Efficiencies of Nickel Plating Solutions. *Transactions of the IMF* **61**, 133–140 (1983).

51. Ramazan, K., Esma, S. & Belkıs, U. Statistical optimisation of organic additives for maximum brightness and brightener analysis in a nickel electroplating bath. *Transactions of the IMF* **93**, 89–96 (2015).

52. Kendrick, R. J. The Effects of Some Aromatic Sulphonic Acids on the Stress, Structure, and Composition of Electrodeposited Nickel. *Transactions of the IMF* **40**, 19–27 (1963).

53. Abyaneh, M. Y., Berkem, M. & Fleischmann, M. The Electrocrystallisation of Nickel: The Effects of Additives. *Transactions of the IMF* **60**, 114–119 (1982).

54. Kruglikov, S. S., Kudriavtsev, N. T., Antonov, A. Ya. & Dribinski, A. v. A Study of Levelling in Nickel and Copper Plating Solutions. *Transactions of the IMF* **42**, 129–137 (1964).

55. Watson, S. A. & Edwards, J. An Investigation of the Mechanism of Levelling in Electrodeposition. *Transactions of the IMF* **34**, 167–198 (1956).

56. Bertorklle, E., Bellobono, I. R. & Bordonall, C. Bright Nickel and Levelling Power. *Transactions of the IMF* **35**, 231–250 (1957).

57. Szmid, K., Zak, T. & Kwiatkowski, Zb. Rapid Quantitative Methods for the Determination of Brighteners, Levellers and Anti-Pitting Agents in Nickel Electroplating Baths. *Transactions of the IMF* **36**, 17–21 (1959).

58. Silman, H. Wetting Agents—Their Use in Electroplating and Allied Processes. *Transactions of the IMF* **19**, 131–146 (1943).

59. Such, T. E. Practical Bright Nickel Plating. *Transactions of the IMF* **32**, 26–42 (1954).

60. Walsh, F. C. & de Leon, C. P. A review of the electrodeposition of metal matrix composite coatings by inclusion of particles in a metal layer: an established and diversifying technology. *Transactions of the IMF* **92**, 83–98 (2014).

61. Donovan, P. D. & Watson-Adams, B. R. Formation of composite materials by electrodeposition: Metals and Materials Vol 3, No 11, pp 443–450 (November 1969). *Composites* **1**, 185 (1970).

62. Larson, C. Electrodeposited gold composites. *Composites* **7**, 9–11 (1976).

63. Electrodeposited composite coatings: Kedward, E. C. Cobalt, No 3 (July–Sept 1973) pp 53–59. *Composites* **5**, 132 (1974).

64. Improvements in and relating to electrodeposition of composite materials: Kedward, E. C., Kiernan, B. and Cottrell, C. L. M. (Bristol Aerojet Ltd) UK Patent Specification, 1,224,166 (3 March 1971). *Composites* **2**, 196 (1971).

65. Hirshhorn, J. S. & Daver, E. M. Wear and friction studies of nickel/tungsten-carbide/graphite composites: Powder Metallurgy, Vol 12, no 24, pp 519–537 (1969). *Composites* **1**, 185 (1970).

66. Baker, A. A., Martin, A. & Bache, R. J. Carbon-fibre-metal-matrix composites: fabrication by electrodeposition. *Composites* **2**, 154–160 (1971).

67. Kedward, E. C., Wright, K. W. & Tennett, A. A. B. The development of electrodeposited composites for use as wear control coatings on aero engines. *Tribology* **7**, 221–227 (1974).

68. Robertson, A., Erb, U. & Palumbo, G. Practical applications for electrodeposited nanocrystalline materials. *Nanostructured Materials* **12**, 1035–1040 (1999).

69. Möller, A. & Hahn, H. Synthesis and characterization of nanocrystalline Ni/ZrO_2 composite coatings. *Nanostructured Materials* **12**, 259–262 (1999).

70. Joshi, P. B. *et al.* Powder metallurgical silver–metal oxide electrical contacts by an electroless coating process. *Advanced Powder Technology* **7**, 121–130 (1996).

71. Rudolphi, Å. K. & Jacobson, S. Gross plastic fretting mechanical deterioration of silver coated electrical contacts. *Wear* **201**, 244–254 (1996).

72. Miao, H. J. & Piron, D. L. Composite-coating electrodes for hydrogen evolution reaction. *Electrochimica Acta* **38**, 1079–1085 (1993).

73. Fan, C. & Piron, D. L. Electrodeposition as a means of producing large-surface electrodes required in water electrolysis. *Surface and Coatings Technology* **73**, 91–97 (1995).

74. Dávila, M., Elizalde, M. P., González, M., Pérez, M. A. & Silva, R. Morphological and electrochemical characterization of Ni–polyvinylchloride composites. *Electrochimica Acta* **44**, 1307–1316 (1998).

75. Rajeshwar, K. & de Tacconi, N. R. Electrodeposition and characterization of nanocrystalline semiconductor films. in *Semiconductor Nanoclusters - Physical, Chemical, and Catalytic Aspects* **103**, 321–351 (Elsevier, 1997).

76. Sikder, A. K., Misra, D. S., Singhbal, D. & Chakravorty, S. Surface engineering of metal–diamond composite coatings on steel substrates using chemical vapour deposition and electroplating routes. *Surface and Coatings Technology* **114**, 230–234 (1999).

77. Kim, S. K. & Yoo, H. J. Formation of bilayer Ni–SiC composite coatings by electrodeposition. *Surface and Coatings Technology* **108–109**, 564–569 (1998).

78. Sofer, Y., Yarnitzky, Y. & Dirnfeld, S. F. Evaluation and uses of composite Ni-Co matrix coatings with diamonds on steel applied by electrodeposition. *Surface and Coatings Technology* **42**, 227–236 (1990).

79. Zhitomirsky, I. Cathodic electrophoretic deposition of diamond particles. *Materials Letters* **37**, 72–78 (1998).

80. Guglielmi, N. Kinetics of the Deposition of Inert Particles from Electrolytic Baths. *Journal of The Electrochemical Society* **119**, 1009–1012 (1972).

81. Kariapper, A. M. J. & Foster, J. Further Studies on the Mechanism of Formation of Electrodeposited Composite Coatings. *Transactions of the IMF* **52**, 87–91 (1974).

82. Celis, J. P., Roos, J. R. & Buelens, C. A Mathematical Model for the Electrolytic Codeposition of Particles with a Metallic Matrix. *Journal of The Electrochemical Society* **134**, 1402–1408 (1987).

83. Low, C. T. J., Wills, R. G. A. & Walsh, F. Electrodeposition of composite coatings containing nanoparticles in a metal deposit. *Surface and Coatings Technology* **201**, 371–383 (2006).

84. Huang, W., Zhao, Y. & Wang, X. Preparing a high-particle-content Ni/diamond composite coating with strong abrasive ability. *Surface and Coatings Technology* **235**, 489–494 (2013).

85. Pompei, E., Magagnin, L., Lecis, N. & Cavallotti, P. L. Electrodeposition of nickel–BN composite coatings. *Electrochimica Acta* **54**, 2571–2574 (2009).

86. Benea, L. *et al.* Fretting and wear behaviors of Ni/nano-WC composite coatings in dry and wet conditions. *Materials & Design (1980-2015)* **65**, 550–558 (2015).

87. Surender, M., Basu, B. & Balasubramaniam, R. Wear characterization of electrodeposited Ni–WC composite coatings. *Tribology International* **37**, 743–749 (2004).

88. Ogihara, H., Wang, H. & Saji, T. Electrodeposition of Ni–B/SiC composite films with high hardness and wear resistance. *Applied Surface Science* **296**, 108–113 (2014).

89. Jin, P., Sun, C., Zhou, C., Shi, L. & Liu, C. Effect of SiC particle size on structures and properties of Ni–SiC nanocomposites deposited by magnetic pulse electrodeposition technology. *Ceramics International* **45**, 20155–20164 (2019).

90. Jenczyk, P. *et al.* Application of SiC particles coated with a protective Ni layer for production of Ni/SiC co-electrodeposited composite coatings with enhanced tribological properties. *Ceramics International* (2019).

91. Xu, M. *et al.* Fabrication of Ni-SiC superhydrophilic surface by magnetic field-assisted scanning electrodeposition. *Journal of Alloys and Compounds* **799**, 224–230 (2019).

92. Zhou, Y., Xie, F. Q., Wu, X. Q., Zhao, W. D. & Chen, X. A novel plating apparatus for electrodeposition of Ni-SiC composite coatings using circulating-solution co-deposition technique. *Journal of Alloys and Compounds* **699**, 366–377 (2017).

93. Jiang, W. *et al.* Preparation of Ni-SiC composite coatings by magnetic field-enhanced jet electrodeposition. *Journal of Alloys and Compounds* **762**, 115–124 (2018).

94. Isekar, N. P., Latha, S. M., Ramakrishna, M., Rao, D. S. & Sundararajan, G. Pulsed electrodeposition and mechanical properties of Ni-W/SiC nano-composite coatings. *Materials & Design* **112**, 140–150 (2016).

95. Jiang, W., Shen, L., Xu, M., Wang, Z. & Tian, Z. Mechanical properties and corrosion resistance of Ni-Co-SiC composite coatings by magnetic field-induced jet electrodeposition. *Journal of Alloys and Compounds* **791**, 847–855 (2019).

96. Shafiee, Z., Bahrololoom, M. E. & Hashemi, B. Electrodeposition of nanocrystalline Ni/Ni–Al_2O_3 nanocomposite modulated multilayer coatings. *Materials & Design* **108**, 19–26 (2016).

97. Alizadeh, M. & Safaei, H. Characterization of Ni-Cu matrix, Al_2O_3 reinforced nano-composite coatings prepared by electrodeposition. *Applied Surface Science* **456**, 195–203 (2018).

98. Li, B., Zhang, W., Huan, Y. & Dong, J. Synthesis and characterization of Ni-B/Al_2O_3 nanocomposite coating by electrodeposition using trimethylamine borane as boron precursor. *Surface and Coatings Technology* **337**, 186–197 (2018).

99. Jiang, S. W., Yang, L., Pang, J. N., Lin, H. & Wang, Z. Q. Electrodeposition of Ni-Al_2O_3 composite coatings with combined addition of SDS and HPB surfactants. *Surface and Coatings Technology* **286**, 197–205 (2016).

100. Alizadeh, M. & Cheshmpish, A. Electrodeposition of Ni-Mo/Al_2O_3 nano-composite coatings at various deposition current densities. *Applied Surface Science* **466**, 433–440 (2019).

101. Kartal, M., Buyukbayram, I., Alp, A. & Akbulut, H. Production of pulse electrodeposited Ni-TiC nanocomposite coatings. *Materials Today: Proceedings* **4**, 6982–6989 (2017).

102. Mai, Y. J. *et al.* Self-lubricating Ti3C2 nanosheets/copper composite coatings. *Journal of Alloys and Compounds* **770**, 1–5 (2019).

103. Karbasi, M., Yazdian, N. & Vahidian, A. Development of electro-co-deposited Ni–TiC nano-particle reinforced nanocomposite coatings. *Surface and Coatings Technology* **207**, 587–593 (2012).

104. Shi, T. *et al.* Microstructure and wear resistance of in-situ TiC surface composite coating on copper matrix synthesized by SHS and Vacuum-Expendable Pattern Casting. *Surface and Coatings Technology* **324**, 288–297 (2017).

105. Singh, D. K. & Singh, V. B. Electrodeposition and characterization of Ni–TiC composite using N-methylformamide bath. *Materials Science and Engineering: A* **532**, 493–499 (2012).

106. Garcia, I., Fransaer, J. & Celis, J.-P. Electrodeposition and sliding wear resistance of nickel composite coatings containing micron and submicron SiC particles. *Surface and Coatings Technology* **148**, 171–178 (2001).

107. Li, M., Ding, W., Li, B. & Xu, J. Morphological evolution and grinding performance of vitrified bonded microcrystal alumina abrasive wheel dressed with a single-grit diamond. *Ceramics International* **45**, 19669–19678 (2019).

108. Petrov, I. *et al.* Nickel galvanic coatings co-deposited with fractions of detonation nanodiamond. *Diamond and Related Materials* **15**, 2035–2038 (2006).

109. Stankovic, V. D. & Gojo, M. Electrodeposited composite coatings of copper with inert, semiconductive and conductive particles. *Surface and Coatings Technology* **81**, 225–232 (1996).

110. Zhang, B. Chapter 9 - Electrical Properties of Nanometer Materials. in *Physical Fundamentals of Nanomaterials* (ed. Zhang, B.) 337–385 (William Andrew Publishing, 2018).

111. Taherian, R. 1 - The Theory of Electrical Conductivity*. in *Electrical Conductivity in Polymer-Based Composites*, 1–18 (William Andrew Publishing, 2019).

112. Afshar, A. *et al.* Electrodeposition of graphite-bronze composite coatings and study of electroplating characteristics. *Surface and Coatings Technology* **187**, 3548–3553 (2011).

113. Cui, G., Bi, Q., Zhu, S., Yang, J. & Liu, W. Tribological properties of bronze–graphite composites under sea water condition. *Tribology International* **53**, 76–86 (2012).

114. Balaji, R., Pushpavanam, M., Kumar, K. Y. & Subramanian, K. Electrodeposition of bronze–PTFE composite coatings and study on their tribological characteristics. *Surface and Coatings Technology* **201**, 3205–3211 (2006).

115. Iacovetta, D., Tam, J. & Erb, U. Synthesis, structure, and properties of superhydrophobic nickel–PTFE nanocomposite coatings made by electrodeposition. *Surface and Coatings Technology* **279**, 134–141 (2015).

116. Sangeetha, S., Kalaignan, G. P. & Anthuvan, J. T. Pulse electrodeposition of self-lubricating Ni–W/PTFE nanocomposite coatings on mild steel surface. *Applied Surface Science* **359**, 412–419 (2015).

117. Rezrazi, M., Doche, M. L., Berçot, P. & Hihn, J. Y. Au–PTFE composite coatings elaborated under ultrasonic stirring. *Surface and Coatings Technology* **192**, 124–130 (2005).

118. Tam, J., Jiao, Z., Lau, J. C. F. & Erb, U. Wear stability of superhydrophobic nano Ni-PTFE electrodeposits. *Wear* **374–375**, 1–4 (2017).

119. Shi, L., Sun, C. & Liu, W. Electrodeposited nickel–cobalt composite coating containing MoS_2. *Applied Surface Science* **254**, 6880–6885 (2008).

120. Furlan, K. P., de Mello, J. D. B. & Klein, A. N. Self-lubricating composites containing MoS_2: A review. *Tribology International* **120**, 280–298 (2018).

121. Cardinal, M. F., Castro, P. A., Baxi, J., Liang, H. & Williams, F. J. Characterization and frictional behaviour of nanostructured Ni–W–MoS_2 composite coatings. *Surface and Coatings Technology* **204**, 85–90 (2009).

122. He, Y., Wang, S., Sun, W., Reed, P. A. S. & Walsh, F. C. Synthesis and Properties of Electrodeposited Ni–Co/WS2 Nanocomposite Coatings. *Coatings* **9**, (2019).

123. Roy, D. *et al.* Pulse current co-deposition of Ni-WS_2 nano-composite film for solid lubrication. *Materials and Manufacturing Processes* **32**, 365–372 (2017).

124. Ünal, E. & Karahan, İ. H. Effects of ultrasonic agitation prior to deposition and additives in the bath on electrodeposited Ni-B/hBN composite coatings. *Journal of Alloys and Compounds* **763**, 329–341 (2018).

125. Ünal, E. & Karahan, İ. H. Production and characterization of electrodeposited Ni-B/hBN composite coatings. *Surface and Coatings Technology* **333**, 125–137 (2018).

126. Tudela, I., Zhang, Y., Pal, M., Kerr, I. & Cobley, A. J. Ultrasound-assisted electrodeposition of thin nickel-based composite coatings with lubricant particles. *Surface and Coatings Technology* **276**, 89–105 (2015).

127. Aruna, S. T., Arunima, S., Latha, S. & Grips, V. K. W. Preparation of Oil-Encapsulated Microcapsules and Tribological Property of Ni Composite Coating. *Materials and Manufacturing Processes* **31**, 107–111 (2016).

128. GhalayaniEsfahani, A. & Ghorbani, mohammad. Electrophoretic Deposition of Ni/SiO_2 Nanocomposite Coating: Fabrication Process and Tribological and Corrosion Properties. *Journal of Nano Research* **26**, 45–51 (2013).

129. Szczygieł, B. & Kołodziej, M. Composite Ni/Al2O3 coatings and their corrosion resistance. *Electrochimica Acta* **50**, 4188–4195 (2005).

130. Shao, W., Nabb, D., Renevier, N. & Sherrington, I. Mechanical and corrosion resistance properties of TiO2 nanoparticles reinforced Ni coating by electrodeposition. *Journal of Physics Conference Series* **40**, 12043 (2012).

131. Ha, H. T., Anh, C. T., Ha, N. T. & Cao, D. T. Co-deposition and microstructure of Ni-nano SiC coating on metal. *Journal of Physics: Conference Series* **187**, 12083 (2009).

132. Das, S., Banthia, S., Patra, A., Sengupta, S. & Singh, S. B. Novel bilayer ZnNi/NiCoSiC nanocomposite coating with exceptional corrosion and wear properties by pulse electrodeposition. *Journal of Alloys and Compounds* **738**, 394–404 (2018).

133. Liu, L. & Xu, J. A study of the erosion–corrosion behavior of nano-Cr_2O_3 particles reinforced Ni-based composite alloying layer in aqueous slurry environment. *Vacuum* **85**, 687–700 (2011).

134. Mohan Reddy, R., Praveen, B. M., Praveen Kumar, C. M. & Venkatesha, T. v. Ni--Si3N4: Electrodeposition, properties and corrosion behavior. *Surface Engineering and Applied Electrochemistry* **53**, 258–264 (2017).

135. Losiewicz, B., Budniok, A., Lasia, A. & Lagiewka, E. Composite Ni-P+TiO_2 electrocoatings for hydrogen evolution reaction in alkaline solutions. *Polish Journal of Chemistry* **78**, 1457–1476 (2004).

136. Chen, Z., Ma, Z., Song, J., Wang, L. & Shao, G. A novel approach for the preparation of Ni–CeO_2 composite cathodes with enhanced electrocatalytic activity. *RSC Adv.* **6**, 60806–60814 (2016).

137. Liu, B. *et al.* Nickel–Cobalt Diselenide 3D Mesoporous Nanosheet Networks Supported on Ni Foam: An All-pH Highly Efficient Integrated Electrocatalyst for Hydrogen Evolution. *Advanced Materials* **29**, 1606521 (2017).

138. Zhang, S., Li, G. L., Wang, H. D., Xu, B. S. & Ma, G. Z. Impact of Nanometer Graphite Addition on the Anti-deliquescence and Tribological Properties of Ni/MoS2 Lubricating Coating. *Physics Procedia* **50**, 199–205 (2013).

139. Baudonnet, L., Grossiord, J. -L. & Rodriguez, F. Effect of Dispersion Stirring Speed on the Particle Size Distribution and Rheological Properties of Three Carbomers. *Journal of Dispersion Science and Technology* **25**, 183–192 (2004).

140. Pradhan, S., Hedberg, J., Blomberg, E., Wold, S. & Odnevall Wallinder, I. Effect of sonication on particle dispersion, administered dose and metal release of non-functionalized, non-inert metal nanoparticles. *Journal of nanoparticle research: an interdisciplinary forum for nanoscale science and technology* **18**, 285 (2016).

141. Akpan, E. I., Shen, X., Wetzel, B. & Friedrich, K. 2 - Design and Synthesis of Polymer Nanocomposites. in *Polymer Composites with Functionalized Nanoparticles*, 47–83 (Elsevier, 2019).

142. Tudela, I., Zhang, Y., Pal, M., Kerr, I. & Cobley, A. J. Ultrasound-assisted electrodeposition of composite coatings with particles. *Surface and Coatings Technology* **259**, 363–373 (2014).

143. Ignacio Tudela, Andrew J. Cobley, Yi Zhang, Tribological performance of novel nickel-based composite coatings with lubricant particles. *Friction,* volume **7**, 169–180 (2019).

144. Walsh, F. C., Low, C. T. J. & Bello, J. O. Influence of surfactants on electrodeposition of a Ni-nanoparticulate SiC composite coating. *Transactions of the IMF* **93**, 147–156 (2015).

145. Atkin, R., Craig, V. S. J., Wanless, E. J. & Biggs, S. Mechanism of cationic surfactant adsorption at the solid–aqueous interface. *Advances in Colloid and Interface Science* **103**, 219–304 (2003).

146. Nwosu, N., Davidson, A., Hindle, C. & Barker, M. On the Influence of Surfactant Incorporation during Electroless Nickel Plating. *Industrial & Engineering Chemistry Research* **51**, 5635–5644 (2012).

147. Helle, K. & Walsh, F. Electrodeposition of Composite Layers Consisting of Inert Inclusions in a Metal Matrix. *Transactions of the IMF* **75**, 53–58 (1997).

148. Walsh, F. C. *et al.* Plasma electrolytic oxidation (PEO) for production of anodised coatings on lightweight metal (Al, Mg, Ti) alloys. *Transactions of the IMF* **87**, 122–135 (2009).

149. Barati Darband, Gh., Aliofkhazraei, M., Hamghalam, P. & Valizade, N. Plasma electrolytic oxidation of magnesium and its alloys: Mechanism, properties and applications. *Journal of Magnesium and Alloys* **5**, 74–132 (2017).

150. Ren, L., Wang, T., Chen, Z., Li, Y. & Qian, L. Self-Lubricating PEO–PTFE Composite Coating on Titanium. *Metals* **9**, (2019).

151. Ghafaripoor, M., Raeissi, K., Santamaria, M. & Hakimizad, A. The corrosion and tribocorrosion resistance of PEO composite coatings containing α-Al2O3 particles on 7075 Al alloy. *Surface and Coatings Technology* **349**, 470–479 (2018).

152. Larson, C. & Farr, J. P. G. Recent advances in pulsed current electrodeposition: a brief review. *Transactions of the IMF* **88**, 237–242 (2010).

153. Larson, C. & Farr*, J. P. G. Current research and potential applications for pulsed current electrodeposition – a review. *Transactions of the IMF* **90**, 20–29 (2012).

154. Kamnerdkhag, P., Free, M. L., Shah, A. A. & Rodchanarowan, A. The effects of duty cycles on pulsed current electrodeposition of $ZnNiAl_2O_3$ composite on steel substrate: Microstructures, hardness and corrosion resistance. *International Journal of Hydrogen Energy* **42**, 20783–20790 (2017).

155. Allahkaram, S. R., Golroh, S. & Mohammadalipour, M. Properties of Al_2O_3 nano-particle reinforced copper matrix composite coatings prepared by pulse and direct current electroplating. *Materials & Design* **32**, 4478–4484 (2011).

156. Torres, H., Rodríguez Ripoll, M. & Prakash, B. Tribological behaviour of self-lubricating materials at high temperatures. *International Materials Reviews* **63**, 309–340 (2018).

157. Sliney, H. E. Solid lubricant materials for high temperatures—a review. *Tribology International* **15**, 303–315 (1982).

158. Bi, Q. High Temperature Self-Lubricating Materials. in (ed. Zhu, S.) Ch. 7 (IntechOpen, 2013). doi:10.5772/55645

159. Kim, K. & Korsunsky, A. Fretting Damage of Ni—MoS_2 Coatings: Friction Coefficient and Accumulated Dissipated Energy Evolutions. *Proceedings of the Institution of Mechanical Engineers. Part J, Journal of Engineering Tribology* **224**, (2010).

160. Low, C. T. J. & Walsh, F. C. Self-lubricating Metal Composite Coatings by Electrodeposition or Electroless Deposition, Encyclopaedia of Tribology. in (eds. Wang, Q. J. & Chung, Y.-W.) 3025–3031 (Springer US, 2013). doi:10.1007/978-0-387-92897-5_1242

161. Miyoshi, K. Solid Lubricants and Coatings for Extreme Environments: State-of-the-Art Survey. (2019).

162. Erdemir, A. Solid lubricants and self-lubricating films. in *Modern Tribology Handbook: Volume One: Principles of Tribology* 787–825 (2000).

163. Wang, F., Arai, S. & Endo, M. Electrochemical Preparation and Characterization of Nickel/Ultra-Dispersed PTFE Composite Films from Aqueous Solution. *Materials Transactions,* **45**, 1311–1316 (2004).

164. Straffelini, G., Colombo, D. & Molinari, A. Surface durability of electroless Ni–P composite deposits. *Wear* **236**, 179–188 (1999).

165. Huang, Y. S., Zeng, X. T., Annergren, I. & Liu, F. M. Development of electroless NiP–PTFE–SiC composite coating. *Surface and Coatings Technology* **167**, 207–211 (2003).

166. Wu, Y., Liu, H., Shen, B., Liu, L. & Hu, W. The friction and wear of electroless Ni–P matrix with PTFE and/or SiC particles composite. *Tribology International* **39**, 553–559 (2006).

167. Chen, S. *et al.* Synthesis of Ni-P-PTFE-nano-Al2O3 composite plating coating on 45 steel by electroless plating. *Journal of Composite Materials - J Compos Mater* **46**, 1405–1416 (2012).

168. Tang, A., Wang, M., Huang, W. & Wang, X. Composition design of Ni–nano-Al_2O_3–PTFE coatings and their tribological characteristics. *Surface and Coatings Technology* **282**, 121–128 (2015).

169. Zhao, Q., Liu, Y., Müller-Steinhagen, H. & Liu, G. Graded Ni–P–PTFE coatings and their potential applications. *Surface and Coatings Technology* **155**, 279–284 (2002).

170. M. Ghouse, M. Vishwanathan and E.G. Ramachandran; "Friction and Wear Characteristics of Electrodeposited Nickel Graphite and Nickel-MoS_2 Composites", Metal Finishing, Vol. 78, August 1980, pp. 57-63. *Metal Finishing* **78**, 57–63 (1980).

171. Chang, Y. C., Chang, Y. Y. & Lin, C. I. Process aspects of the electrolytic codeposition of molybdenum disulfide with nickel. *Electrochimica Acta* **43**, 315–324 (1998).

172. Wang, L. M. Effect of surfactant BAS on MoS_2 codeposition behaviour. *Journal of Applied Electrochemistry* **38**, 245–249 (2008).

173. Huang, Z. & Xiong, D. MoS_2 coated with Al_2O_3 for Ni–MoS_2/Al_2O_3 composite coatings by pulse electrodeposition. *Surface and Coatings Technology* **202**, 3208–3214 (2008).

174. Ma, G. *et al.* Research on the microstructure and space tribology properties of electric-brush plated Ni/MoS2–C composite coating. *Surface and Coatings Technology* **221**, 142–149 (2013).

175. Wu, B., Yu, X., Zhang, B. & Xu, B. Preparation and characterization of graphite–nickel composite coatings by automatic brush plating. *Surface and Coatings Technology* **202**, 1975–1979 (2008).

176. Shourije, S. M. J. S. & Bahrololoom, M. E. Effect of current density, MoS2 content and bath agitation on tribological properties of electrodeposited nanostructured Ni-MoS2 composite coatings. *Tribology - Materials, Surfaces & Interfaces* **13**, 76–87 (2019).

177. Bari, G. Electrodeposition of Nickel. in *Modern Electroplating* 79–114 (2011).

178. Farrell, T. & Greig, D. The electrical resistivity of nickel and its alloys. *Journal of Physics C: Solid State Physics* **1**, 1359–1369 (1968).

179. El Beqqali, O. *et al.* Electrical properties of molybdenum disulfide MoS2. Experimental study and density functional calculation results. *Synthetic Metals* **90**, 165–172 (1997).

180. Tarzhanov, V. I., Zhugin, Yu. N. & Krupnikov, K. K. Electrical conductivity of polytetrafluoroethylene under shock-wave loading and rarefaction. *Journal of Applied Mechanics and Technical Physics* **38**, 826–832 (1997).

181. Celis, J. P., Roos, J. R., Buelens, C. & Fransaer, J. Mechanism of electrolytic composite plating: survey and trends. *Transactions of the IMF* **69**, 133–139 (1991).

182. He, Y., Wang, S. C., Walsh, F. C., Chiu, Y. L. & Reed, P. A. S. Self-lubricating Ni-P-MoS_2 composite coatings. *Surface and Coatings Technology* **307**, 926–934 (2016).

183. García-Lecina, E. *et al.* Codeposition of inorganic fullerene-like WS_2 nanoparticles in an electrodeposited nickel matrix under the influence of ultrasonic agitation. *Electrochimica Acta* **114**, 859–867 (2013).

184. Lampke, T., Dietrich, D., Leopold, A., Alisch, G. & Wielage, B. Cavitation erosion of electroplated nickel composite coatings. *Surface and Coatings Technology* **202**, 3967–3974 (2008).

185. Li, Z., Wang, J., Lu, J. & Meng, J. Tribological characteristics of electroless Ni–P–MoS_2 composite coatings at elevated temperatures. *Applied Surface Science* **264**, 516–521 (2013).

186. He, Y., Wang, S. C., Walsh, F. C., Chiu, Y. L. & Reed, P. A. S. Self-lubricating Ni-P-MoS_2 composite coatings. *Surface and Coatings Technology* **307**, 926–934 (2016).

187. Saraloğlu Güler, E., Konca, E. & Karakaya, I. Investigation of the tribological behaviour of electrocodeposited Ni-MoS2 composite coatings. *International Journal of Surface Science and Engineering* **11**, 418–432 (2017).

188. Pullicino, E., Zou, W., Gresil, M. & Soutis, C. The Effect of Shear Mixing Speed and Time on the Mechanical Properties of GNP/Epoxy Composites. *Applied Composite Materials* **24**, 301–311 (2017).

189. Benali, M., Gerbaud, V. & Hemati, M. Effect of operating conditions and physico–chemical properties on the wet granulation kinetics in high shear mixer. *Powder Technology* **190**, 160–169 (2009).

190. Chen, C.-S., Cian, H.-J., Yu, C.-H. & Huang, C.-W. Friction Coefficient Calculation and Mechanism Analysis for MoS_2 Nanoparticle from Molecular Dynamics Simulation. *Procedia Engineering* **79**, 617–621 (2014).

191. Wu, H. *et al.* An investigation on the lubrication mechanism of MoS_2 nano sheet in point contact: The manner of particle entering the contact area. *Tribology International* **107**, 48–55 (2017).

192. Rashidi, A. M. & Amadeh, A. The effect of saccharin addition and bath temperature on the grain size of nanocrystalline nickel coatings. *Surface and Coatings Technology* **204**, 353–358 (2009).

193. M. Priest, C.M. Taylor, Automobile engine tribology — approaching the surface, *Wear* **241**, 193–203 (2000)